JAERI-Tech
96-055

DESIGN OF DIVERTOR IMPURITY MONITORING SYSTEM FOR ITER

December 1996

Tatsuo SUGIE, Hiroaki OGAWA
Jun KATSUNUMA*, Mitsumasa MARUO*
Toshiro ANDO and Satoshi KASAI

日本原子力研究所
Japan Atomic Energy Research Institute

本レポートは，日本原子力研究所が不定期に公刊している研究報告書です。
入手の問合わせは，日本原子力研究所研究情報部研究情報課（〒319-11 茨城県那珂郡東海村）あて，お申し越しください。なお，このほかに財団法人原子力弘済会資料センター（〒319-11 茨城県那珂郡東海村日本原子力研究所内）で複写による実費頒布をおこなっております。

This report is issued irregularly.
Inquiries about availability of the reports should be addressed to Research Information Division, Department of Intellectual Resources, Japan Atomic Energy Research Institute, Tokai-mura, Naka-gun, Ibaraki-ken 319-11, Japan.

編集兼発行　日本原子力研究所
印　　刷　日立高速印刷株式会社

Design of Divertor Impurity Monitoring System for ITER

Tatsuo SUGIE, Hiroaki OGAWA, Jun KATSUNUMA *
Mitsumasa MARUO * , Toshiro ANDO +1 and Satoshi KASAI +2

Department of Fusion Plasma Reaearch
Naka Fusion Research Establishment
Japan Atomic Energy Research Institute
Naka-machi, Naka-gun, Ibaraki-ken

(Received November 15, 1996)

The divertor impurity monitoring system of ITER has been designed. The main objectives of this system are to identify impurity species and to measure two-dimensional distributions of particle influxes in the divertor plasmas. This system , which is one of the most important diagnostic systems for plasma control of ITER, is nominated for the start-up set of ITER diagnostics. The conceptual design, the optical design and the mechanical design are mainly carried out. In order to satisfy the required measurements, three deferent type of spectral systems are selected corresponding to each objectives. First is the spectral system for impurity species monitoring. Second is the spectral system for particle influx measurement with spatial and time resolution. Third is the spectral system with high dispersion for particle energy distribution measurement in the divertor. The divertor impurity monitoring system is composed of these three systems. The two-dimensional measurement in the divertor is carried out with two viewing fans intersected each other. These viewing fans are realized by metallic mirrors (made of molybdenum or copper) sitting in the divertor cassette.

This design work was carried out under the ITER EDA task agreement of design task D214, 215, 216, 238, 239
(Task Agreement number: S91 TD21 95-01-20FJ,Task number: G55 TD07).

+1 Department of ITER Project
+2 Department of Fusion Engineering Research
*Nikon Corporation

In the optical design, the optimization of the optical system from the divertor to the spectrometer are carried out by using ray trace analysis. As the result, it is difficult to satisfy the spatial resolution of 3 mm in the divertor region. About 10 mm resolution will be reasonable. In addition, the measurable limit, the neutron and γ -ray irradiation effect on the optical fiber, the remote handling concept and the space requirement are considered preliminarily. The necessary design works during EDA, and necessary R& D are also listed.

Keywords: ITER, ITER EDA, Divertor, Impurity, Monitoring System, Spectroscopy, Optical Design, First Mirror, Optical Fiber, Visible Ray

ITERにおけるダイバータ部不純物モニターシステムの設計

日本原子力研究所那珂研究所炉心プラズマ研究部
杉江　達夫・小川　宏明・勝沼　　淳*
丸尾　光正*・安東　俊郎*1・河西　　敏*2

（1996年11月15日受理）

ITERにおけるダイバータ部不純物モニターシステムの設計を行った。このシステムは、ダイバータ部での不純物粒子の同定、粒子流入束の二次元測定等を行うことを主な目的としており、ITERのプラズマ制御に欠かせない計測システムの一つとして、初期運転時計測器群（Start－up set）の中に入っている。今回は、システムの概念設計、光学設計、及び初期的な機械設計を主に行った。計測要求を満足するために、目的に合わせて三つの最適な分光系を選んだ。一つはダイバータ部での不純物の種類をモニターする分光系、二番目は粒子束の空間分布を高速測定する分光系、三番目は粒子の運動エネルギーを測定する高分散分光系である。これらの三つを合わせてひとつのシステムとした。また、ダイバータ部の二次元測定はダイバータカセット内部に金属（モリブデンあるいは銅）ミラーを設置し、互いに交差する視野から行える構造とした。光学設計では、ダイバータ部から分光器までの伝送光学系も含めて、光線追跡による解析を駆使して最適化を行ったが、ダイバータ部での3mmの空間分解能は難しく、10mm程度が限界であることが判明した。その他、機器のリモートハンドリング、ダイバータで発光するスペクトル線の強度の見積、測定限界の初期的評価、ニュートロン束に対する光ファイバーの使用限界の検討、占有空間の評価、ITERの工学設計活動期間中に設計を完了しなければならない項目、及び開発しなければならない技術の抽出を行った。

本設計はITER工学設計活動の一環として行ったものであり、設計タスクD214、215、216、238、239（TA numeber：S91 TD21 95－01－20 FJ、Task number：G55 TD07）に基づくものである。

＋1 ITER開発室
＋2 核融合工学部
＊ （株）ニコン

Contents

目　　次

1. Introduction

The impurity species monitor and two-dimensional measurements of particle influxes in the divertor plasma are very important for ITER plasma control as well as divertor plasma. The Divertor Impurity Monitoring System is expected to carry out these measurement and nominated for the start-up set of ITER diagnostics as one of the most important diagnostic systems for plasma control. As shown in the design description document (DDD) 5.5.E.04, the objective of the Divertor Impurity Monitoring System is to obtain spatially resolved measurements from the plasma in the divertor channel to identify and quantify the impurity species. The line averaged measurements, in the wave length range 200-1000 nm, have to be inverted using the magnetic configuration and the local plasma parameters in area considered. In other words,

- 200 nm - 1000 nm of wavelength range,
- 2- dimensional measurement in the poloidal plane

are required.

The more detailed requirements for parameter to be measured, parameter range, spatial resolution, time resolution and accuracy are summarized as shown in table 1-1[1].

In this report, the conceptual design, the optical design and the mechanical design of the Divertor Impurity Monitoring System are mainly carried out. In addition, the measurable limit, the neutron and γ-ray irradiation effect on the optical fiber, the remote handling concept and the space requirement are considered preliminary. The necessary design works during EDA, and necessary R & D are also listed.

Reference

[1] ITER EDA Design Description Document 5.5.E.04.

Table 1-1 Requirements for parameter to be measured, parameter range, spatial resolution, time resolution and accuracy [1].

12) Impurity Species Monitor

Parameter	Parameter range	Spatial res.	Time res.	Accuracy
Be influx	TBD	Several points	10 ms	10%(rel.)
C influx	TBD	TBD	10 ms	10%(rel.)
Cu influx	TBD	Several points	10 ms	10%(rel.)
Ne influx	TBD	TBD	10 ms	10%(rel.)

16) Key Divertor Parameters

Parameter	Parameter range	Spatial res.	Time res.	Accuracy
Max. surface plate temp.	200-2500°C	1 cm	1 ms	10%
Rad. power	≤ 0.4 GW	10 cm	1 ms	10%
	≤ 10^3 GW †	10 cm	0.1ms	30%
Plate Ablation	To be defined			
Gas pressure	≤ 0.1 Torr	Several points	5 ms	10%
'Ionization front' position	0-2 m	~10 cm	1 ms	10%

† *At thermal quench at a disruption.*

35) Impurity and D,T Influx in Divertor

Parameter	Parameter range	Spatial res.	Time res.	Accuracy
G_{Be}, G_W	10^{17} - 10^{22} at/sec	3mm	1ms	30%
G_D, G_T	10^{19} - 10^{25} at/sec	3mm	1ms	30%

37) Radiation Profile

Region	Rad. power range	Spatial res.	Time res.	Accuracy
Main plasma	0.01-1 MWm^{-3}	20cm	10ms	20%
X-point/MARFE	≤300 MWm^{-3}	20cm	10ms	20%
Divertor	≤100 MWm^{-3}	5cm	10ms	30%

2. Concept of design

2.1 Constitution of the system

In order to realize the requirements, it is better that the system should be composed of following three kind of spectrometers.

i) Spectrometers for species monitor (Visible Survey Spectrometer)
- Wavelength resolution: ~ 1 Å
- Time Rsolution: 10 ms
- Spatial Resolution 10 cm (on the divertor plate)

ii) Filter optical systems for influx measurement (Filter Spectrometer)
- Wavelength resolution: ~ 10 Å
- Time Rsolution: 1 ms
- Spatial Resolution 3 mm - 10 mm (on the divertor plate)

iii) High dispersion spectrometers for line shape measurement
- Wavelength resolution: ~ 0.1 Å
- Time Rsolution: 10 ms
- Spatial Resolution 10 cm (on the divertor plate)

2.2 Magnetic field and shielding for detector

Magnetic shield is necessary to the detector which has a image intensifier such as a micro channel plate (MCP). The divertor impurity monitoring system have been planned to use such detectors. It is necessary to shield the detector from the strong magnetic field induced by the poloidal coils. The permissible magnetic flux density of the detector, which already surrounded by the magnetic shield materials, is about 0.01 T (100 G).

If the detector is set in the divertor diagnostic shield block located in the divertor port as shown in Fig. 2.2-1, the estimated magnetic flux density at the detector will reach around 1 T [1].

2.2.1. Magnetic field induced by poloidal coils

The magnetic field induced by the poloidal coils calculated by Dr A.Portone (Naka JWS) is shown in Fig.2.2-2 along the major radius on Z=-5 and -6. The detector will be set somewhere along the line. If we set the detector in the diagnostic shield block located in the divertor port, the magnetic flux density is estimated around 1T at the position of the detector (Z=-5 ~ -6 m, R=13 ~ 14 m).

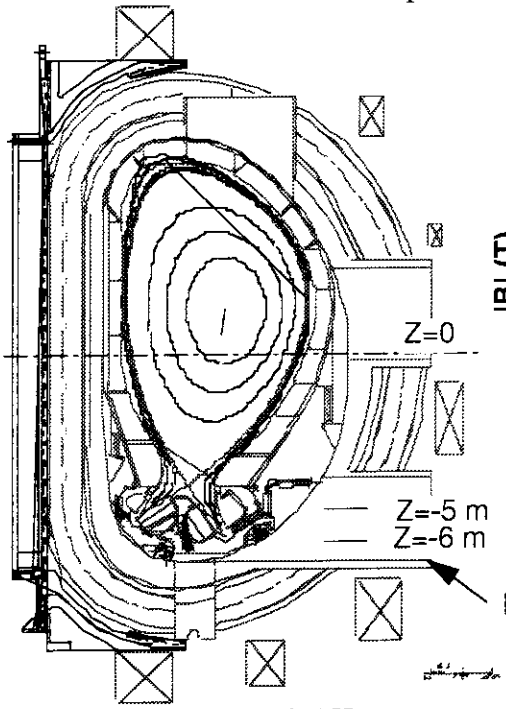

Fig. 2.2-1 Cross section of ITER

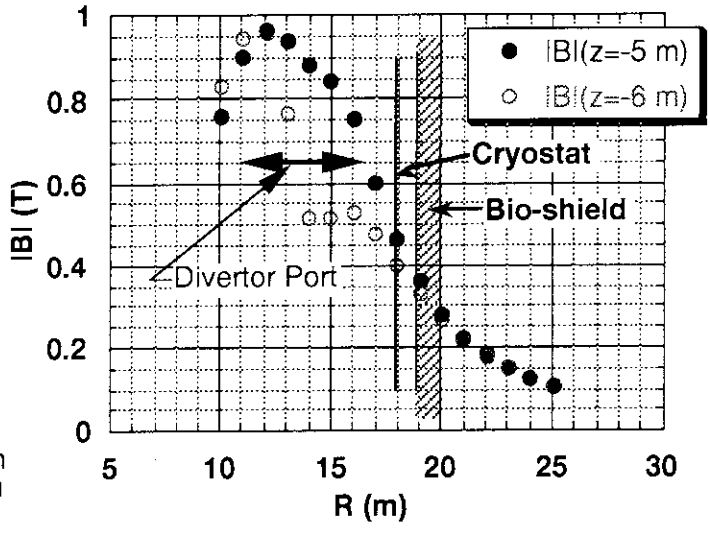

Fig. 2.2-2 Magnetic field induced by the poloidal coils.

2.2.2. Rough estimation of magnetic shield

Here, we consider single layer shielding, because we assume the detector is already surrounded by the shielding materials (such as iron and Mumetal) against the magnetic flux density of 100 G.

The magnetic flux density in a shielding material B_m should be less than the value of the saturation magnetic flux density B_{sat}.

$$B_m < B_{sat} \qquad (2.2\text{-}1)$$

If we use the cylindrical model and assume that the magnetic field lines in the region of twice diameter of shielding material come into the shielding material as shown in Fig.2.2-3, the magnetic flux density in a shielding material B_m is

$$B_m = B_{out} \times 2D / 2t$$
$$= B_{out} \times (D_{in}+2t) / t. \qquad (2.2\text{-}2)$$

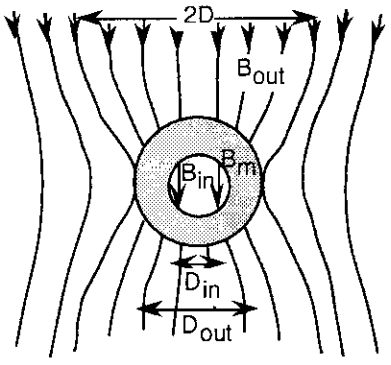

Fig. 2.2-3 Concept of magnetic shielding.

Here, B_{out} is the magnetic flux density of outer region of the shield, and D, D_{in}, and t are the outer diameter, inner diameter and thickness of the shield material.

From the equation (2.2-1) and (2.2-2), we can estimate the required thickness of shielding material as a function of B_{out}.

We assume;

i) shielding material:
soft iron Fe, which has a large value of the saturation magnetic field B_{sat} = 21.5 kG,

ii) inner diameter D_{in} = 15 cm, and 10 cm.

Table 2.2-1 The required thickness t of the shielding material.

D_{in} (cm)	B_{out} (kG)	t (cm)	D (cm)	t_{80} (cm)	D_{80} (cm)
15	10	100.0	215.0	no solution	no solution
15	8	21.8	58.6	100.0	215.0
15	6	9.5	33.9	17.3	49.6
15	4	4.4	23.9	6.5	28.0
15	2	1.7	18.4	2.3	19.5
15	1	0.8	16.5	1.0	17.0
10	10	66.7	143.3	no solution	no solution
10	8	14.5	39.1	66.7	143.3
10	6	6.3	22.6	11.5	33.1
10	4	3.0	15.9	4.3	18.7
10	2	1.1	12.3	1.5	13.0
10	1	0.5	11.0	0.7	11.3

The result is shown in table 2.2-1. In the table, t is the required thickness and t_{80} is the thickness in case we permit 80% of the saturation magnetic field, because of uncertainties.

From this table, the reasonable limit of B_{out} is expected around 4 -6 kG. This value is correspond to the position of the cryostat wall as shown in Fig. 2.2-2.

2.2.3. Inner magnetic flux density B_{in}

If we assume the spherical model, B_{in} is

$$B_{in} = (9/2) \times B_{out} / (\mu(1 - D_{in}^3/D^3)). \qquad (2.2\text{-}3)$$

The shielding factor S is

$$1/S = B_{in} / B_{out} = (9/2) / (\mu(1 - D_{in}^3/D^3)). \qquad (2.2\text{-}4)$$

(μ : permeability, 300 for soft iron)

The inner magnetic flux density B_{in} and the value 1/S is plotted in Fig. 2.2-3 and 4. From these figure, it is difficult to reduce the magnetic flux density of 1 T to less than 100 G. The reasonable limit of B_{out} is also expected around 4 -6 kG.

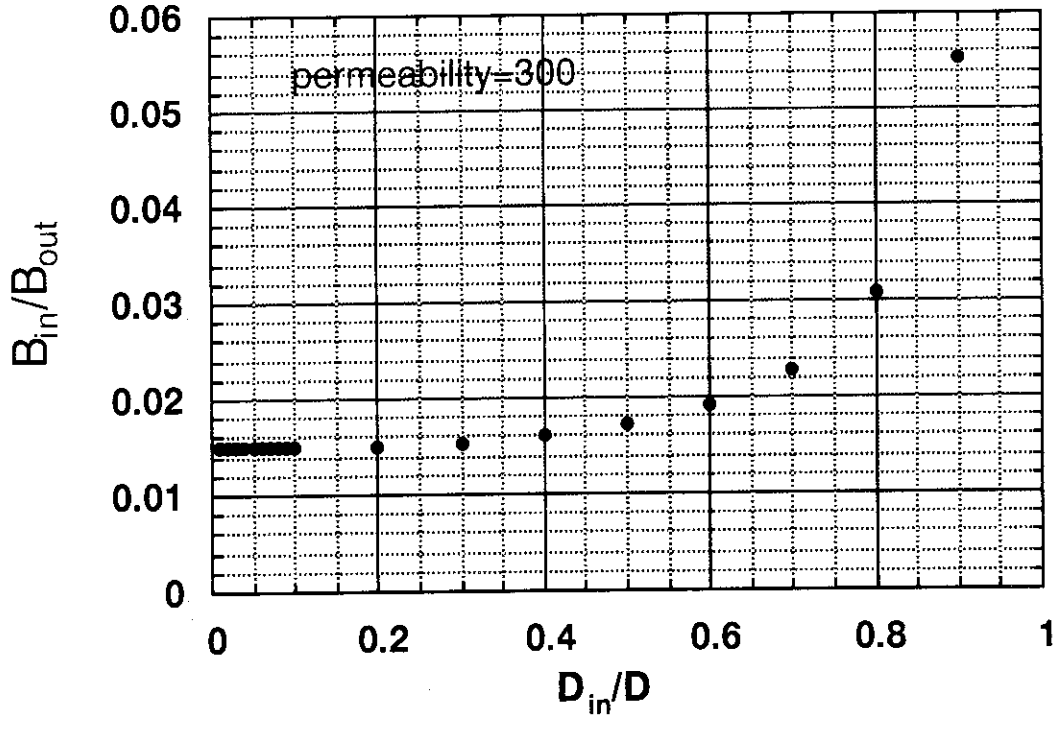

Fig. 2.2-3 Shielding characteristic: B_{in}/B_{out} vs D_{in}/D.

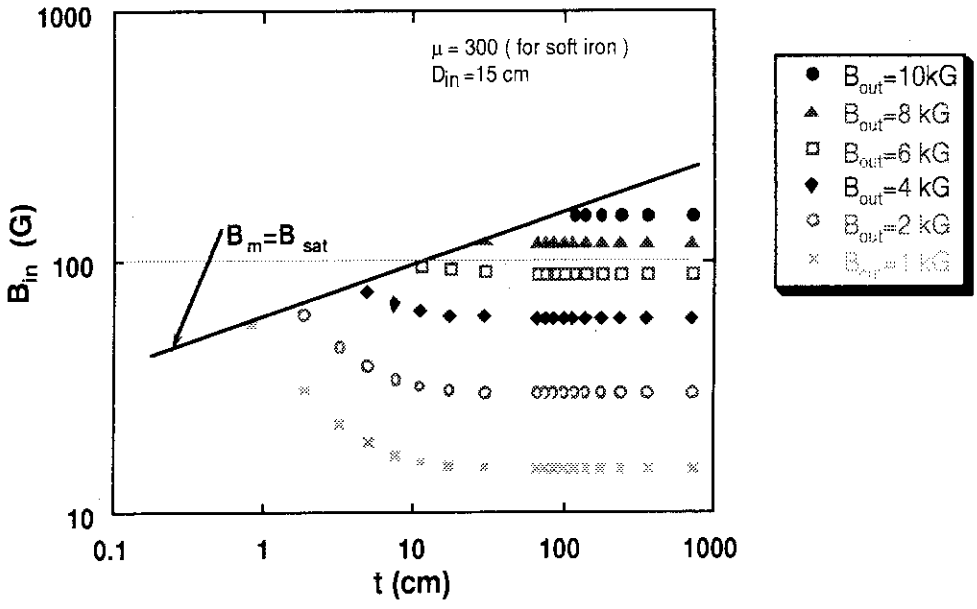

Fig. 2.2-4 Inner magnetic flux density Bin vs thickness t of shielding material.

2.2.4. Conclusion

From the results of section 2.2.2 and 2.2.3, it seems that there is no feasibility for setting the detector in the diagnostic shield block located in the divertor port. It is better to set the detector, at least, behind the cryostat from the magnetic shield's point of view.

Reference

[1]: Calculation by Dr A.Portone (Naka JWS).

2.3 Optical fiber

In order to relay optical images from the divertor to the spectrometer through the vacuum vessel, the cryostat and the biological shield, two methods are considered. One is a mirror optics and the other is a fiber optics. Here, the fiber optics will be examined from the just outside the divertor port to the spectrometers, so that the problem of the displacement of the optical axes due to the movement of the divertor port will be evaded. If we will use only mirrors, the optical system will become more complicated to against the movement. We will consider the mirror system from the divertor port to the spectrometer in the next phase.

It is necessary to consider the neutron and γ-ray irradiation effect on the optical fiber at the laying location. It will be discussed in section 3.9.

The transmissivities of the UV-fiber [1] of 10, 20 and 100 m long are shown in Fig. 2.3-1 as a function of the wavelength. From this figure, it is difficult to measure spectral lines below 500 nm through the long optical fiber. Therefore, spectrometers for the wavelength range of 200-500 nm should be located just behind the biological shield. On the other hand, it is better to set the spectrometers for over 500 nm in the diagnostic room from the accessibility and flexibility point of view. We will be able to change the spectrometers easily correspond to the change of the ITER experiment.

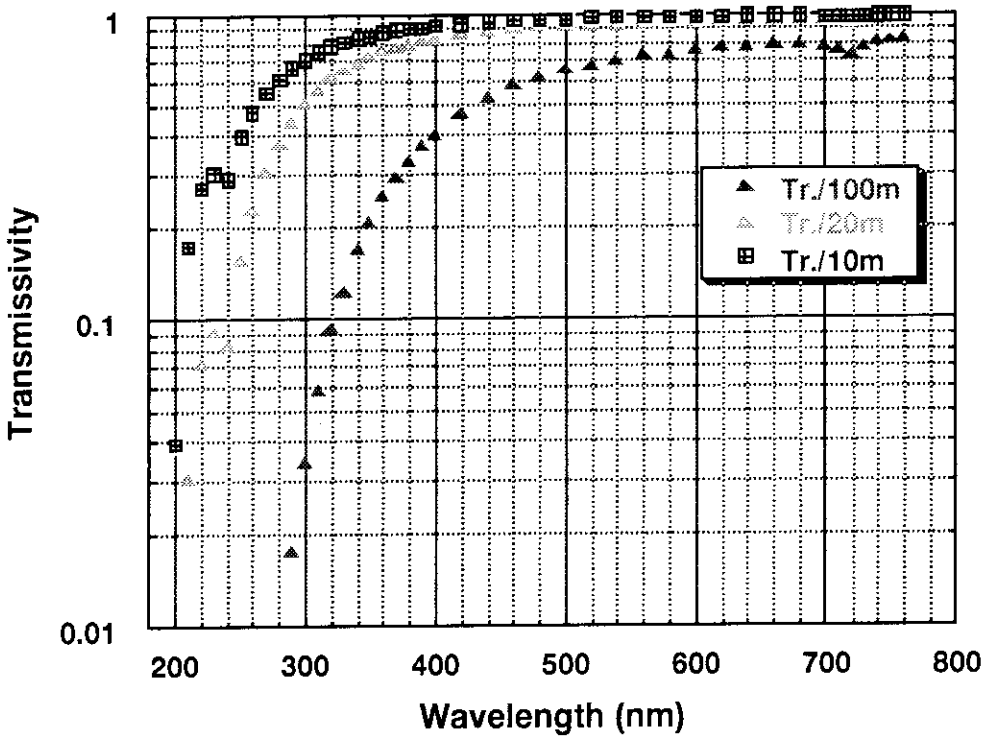

Fig. 2.3-1 The transmissivities of the UV-fiber of 10, 20 and 100 m long as a function of the wavelength.

Reference

[1] Data from Mitsubishi Cable Industries, LTD.

2.4 First mirror

In the strong field of neutron and γ-ray, it is impossible to use the optical component made by glass such as a lens, because of the degradation. The metallic mirror should be used as a first mirror. For the first mirror, copper mirror is listed as the ITER reference.

The reflectivity of molybdenum (Mo), copper (Cu) and aluminum (Al) are shown in Fig.2.4-1 vs wavelength. [1] In the region of 200 - 500 nm, the reflectivity of Mo is better than that of Cu. In the region of 500 - 1000 nm, Cu is better than Mo. The sputtering yield of Mo is about ten times as low as that of Cu. [2] Therefore, We consider both materials of Mo and Cu, as a first mirror at this moment.

Another serious problem is adhesion of the dust on the mirror surface. Unfortunately, the problem will be not considered here, because of the difficulties and no data.

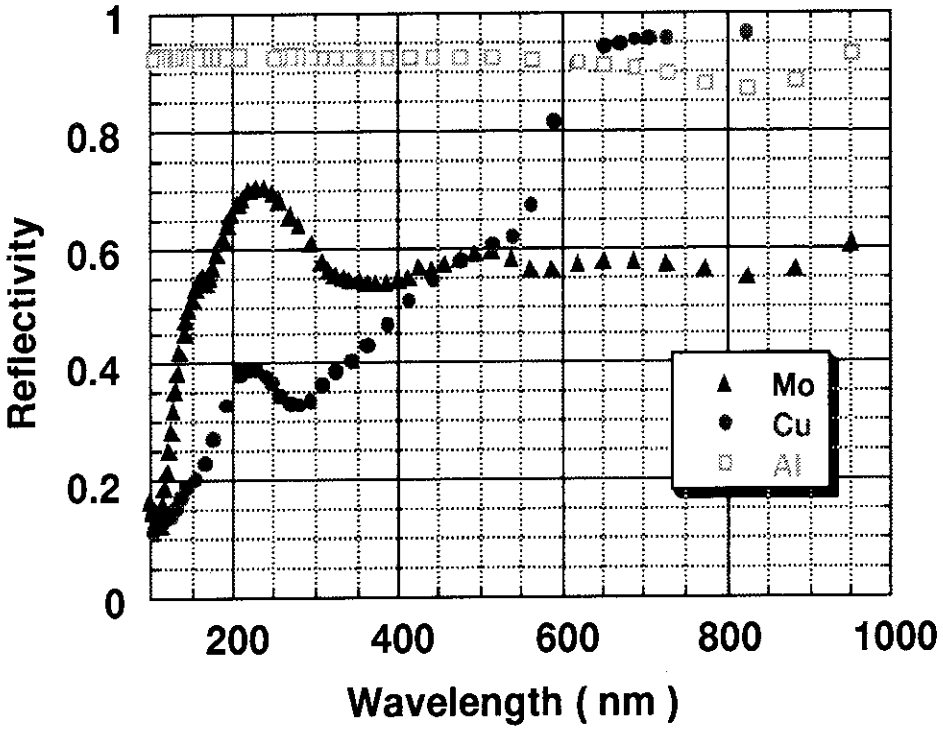

Fig.2.4-1 The reflectivity of molybdenum (Mo), copper (Cu) and aluminum (Al) vs wavelength.

Reference

[1] CRC Handbook of Chemistry and Physics.
[2] Y. Yamamura, H. Tawara, NIFS-DATA-23 (1995).

2.5 Conceptual arrangement of divertor impurity monitoring system

From the consideration in sections 2.1 - 2.4, the conceptual arrangement of the divertor impurity monitoring system is decided as shown in Fig. 2.5.-1.

The light beams from the deferent chord of the divertor plasma are relayed by the mirror optics in the diagnostic divertor cassette and enter the shield block sitting in the divertor port for remote handling. The beams reflected by the plane mirror in the shield block come into a collecting optics through a quartz window (first vacuum boundary) located on the side wall of the divertor port. After that, the lights focused on the deferent channels of the optical fiber array corresponding to the chord of the divertor plasma.

The lights entered the optical fiber bundles are guided to spectrometers through optical feed throughs (second vacuum boundary) on the cryostat. The lights are divided into the wavelength region of 200 - 500 nm and over 500 nm, and the light of the wavelength region of 200 - 500 nm enter the spectrometers set on the transport cask in the pit because it is difficult to measure spectral lines below 500 nm through the long optical fiber. The length of the optical fiber will be less than 10 m. The light of the wavelength region over 500 nm are guided to the spectrometers set in the diagnostic room by optical fiber bundles, so that the accessibility for the maintenance will be better. Furthermore, we will be able to change the spectrometers easily correspond to the change of the ITER experiment.

The transport cask will be able to remove easily together with the spectrometers and fibers before divertor maintenance. The detailed procedure is shown in section 4.4.

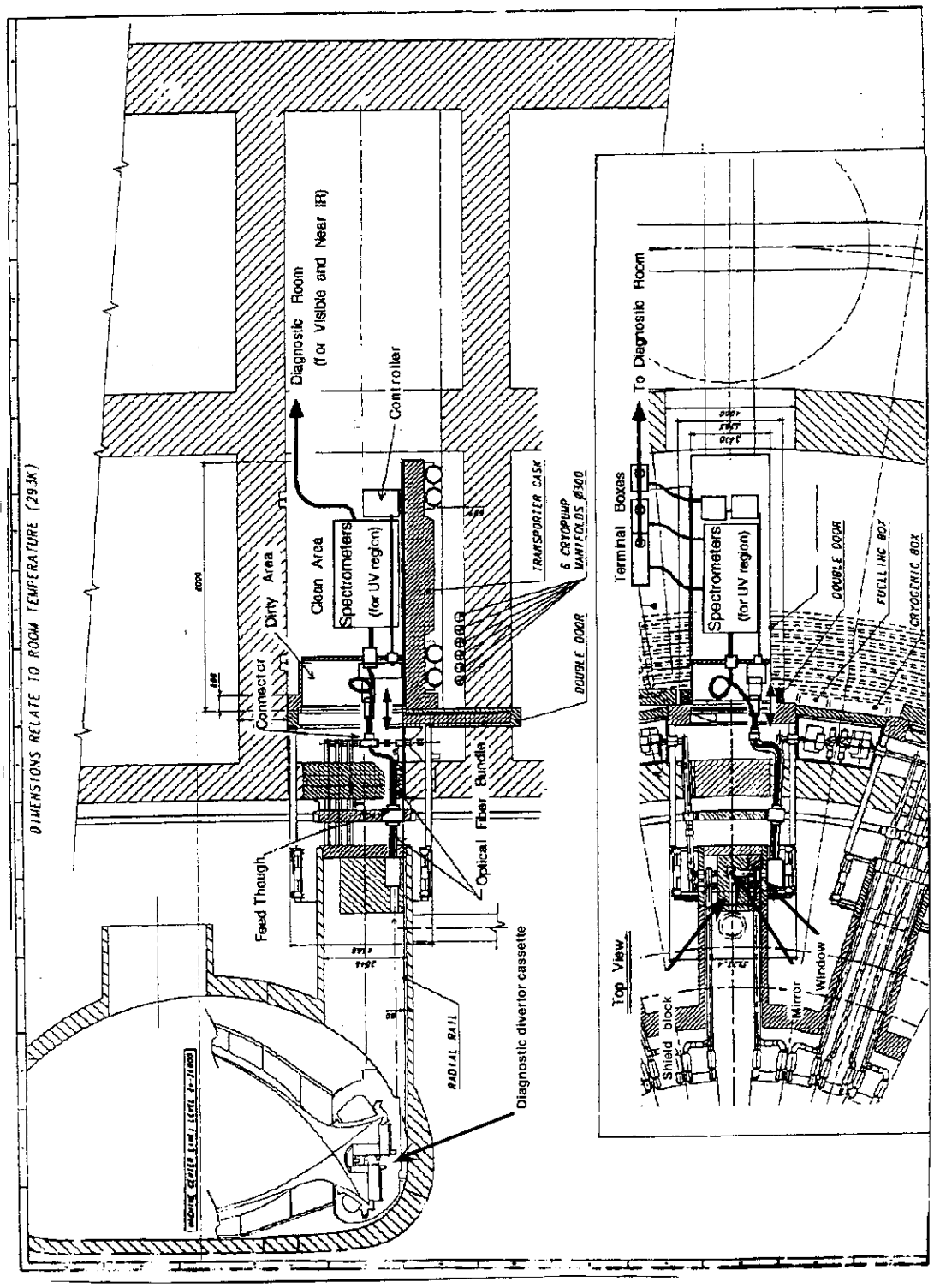

Fig. 2.5-1 Conceptual arrangement of Impurity Monitoring System.

3. Optical design

3.1 Design concept and viewing fans in the diagnostic divertor cassette

In order to realize the 2D measurement on the poloidal plane both in outer and inner divertor region we proposed four viewing fans as shown in Fig. 3.1-1. The detailed mechanical design is in progress at Garching JCT. This is a specially designed diagnostic cassette as one of the options.

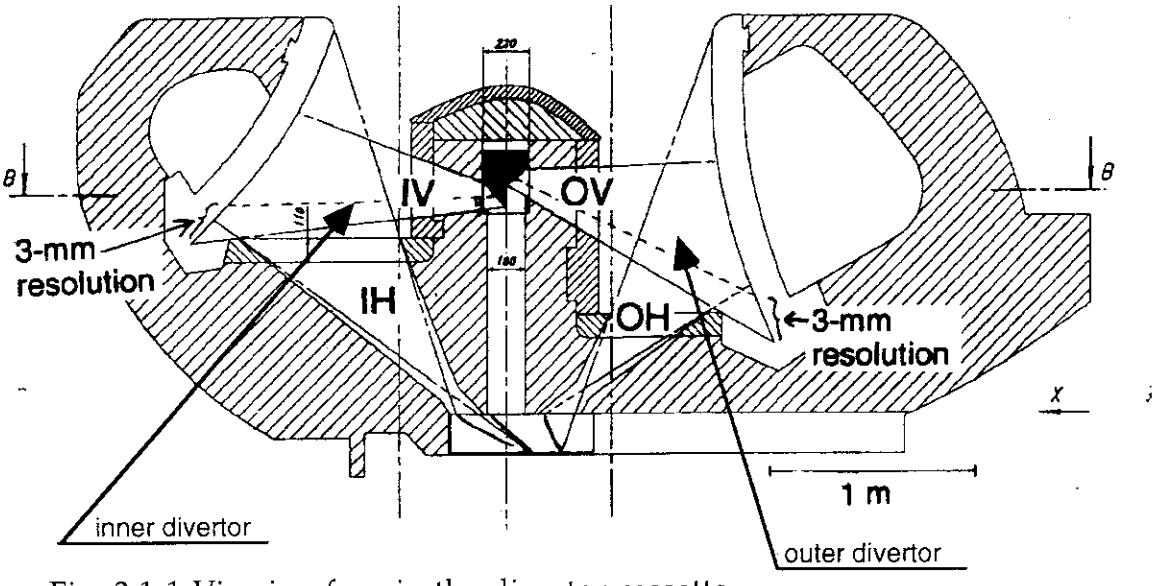

Fig. 3.1-1 Viewing fans in the divertor cassette.

The 2D measurements will be carried out with two viewing fans named OV and OH for outer divertor region, and IV and IH for inner one. The 3-mm spatial resolution was planed only in the bottom region of the divertor plates about 18 cm long along the poloidal direction. The planed spatial resolution of the other region was 1 cm. This was a target of optical design.

The numbers of viewing chords (channels) are listed in table 3.1-1 for each viewing fans. The breakdown (the number of chords for each spectrometer) of each viewing fan is also listed in it. The 2D measurements are carried out by the filter spectrometers. Here, VSS is a visible survey spectrometer, FS is a filter spectrometer and HDS is a high dispersion spectrometer.

The results of the optical design are shown in the following sections.

Table 3.1-1 Number of viewing chords (channels).

	IV	IH	OV	OH
VSS	10	0	10	0
FS(10 mm)	80	140	80	140
FS(3 mm)	60	0	60	0
HDS	10	0	10	0

3.2 Overview and detailed arrangement of optical penetration system

The overview of the optical penetration system is shown in Fig. 3.2-1. The light from the divertor region is reflected by mirrors in the divertor dome and enters a plane mirror 1 in a dog-leg tunnel. After that, the light is reflected by a plane mirror 2 through a quartz window and focused on fiber arrays by a mirror optics such as a off-axis Cassegrain type in order to avoid the chromatic aberration, because of the wide wavelength range (200-1000 nm).

The detailed mirror arrangements are shown in Fig. 3.2-2 ~ 3. The collecting and focusing optics is show in Fig. 3.2-4. In these figures, many abbreviations are used as the following meanings.

IV	: Viewing fan IV, Viewing area of IV
IH	: Viewing fan IH, Viewing area of IH
OV	: Viewing fan OV, Viewing area of OV
OH	: Viewing fan OH, Viewing area of OH
IV/COARSE	: Viewing area of IV for filter spectrometer with 10 mm spatial resolution
IV/FINE	: Viewing area of IV for filter spectrometer with 3 mm spatial resolution
IV/VSS-HDS	: Viewing area of IV for visible survey spectrometer and high dispersion spectrometer
OV/COARSE	: Viewing area of OV for filter spectrometer with 10 mm spatial resolution
OV/FINE	: Viewing area of OV for filter spectrometer with 3 mm spatial resolution
OV/VSS-HDS	: Viewing area of OV for visible survey spectrometer and high dispersion spectrometer

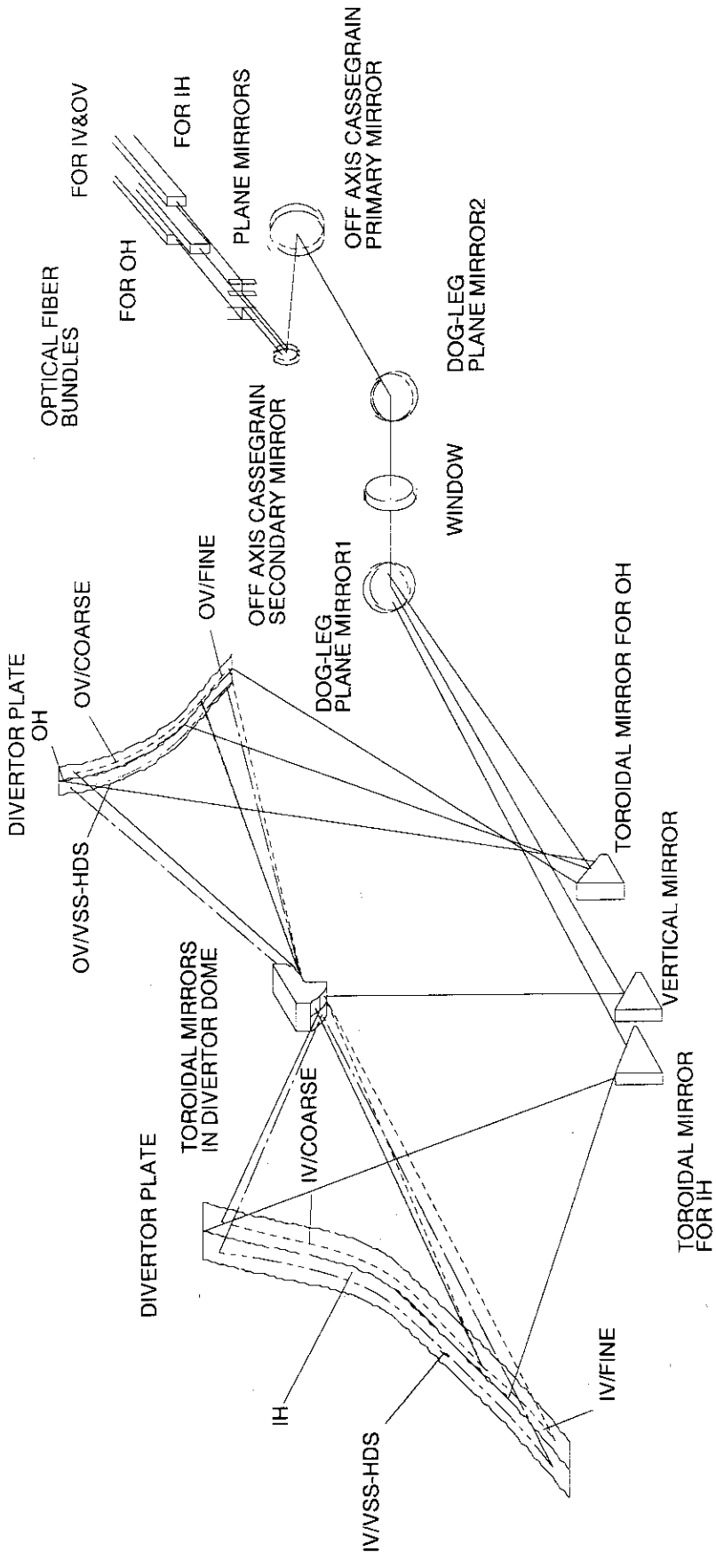

Fig. 3.2-1 Overview of the optical penetration system.

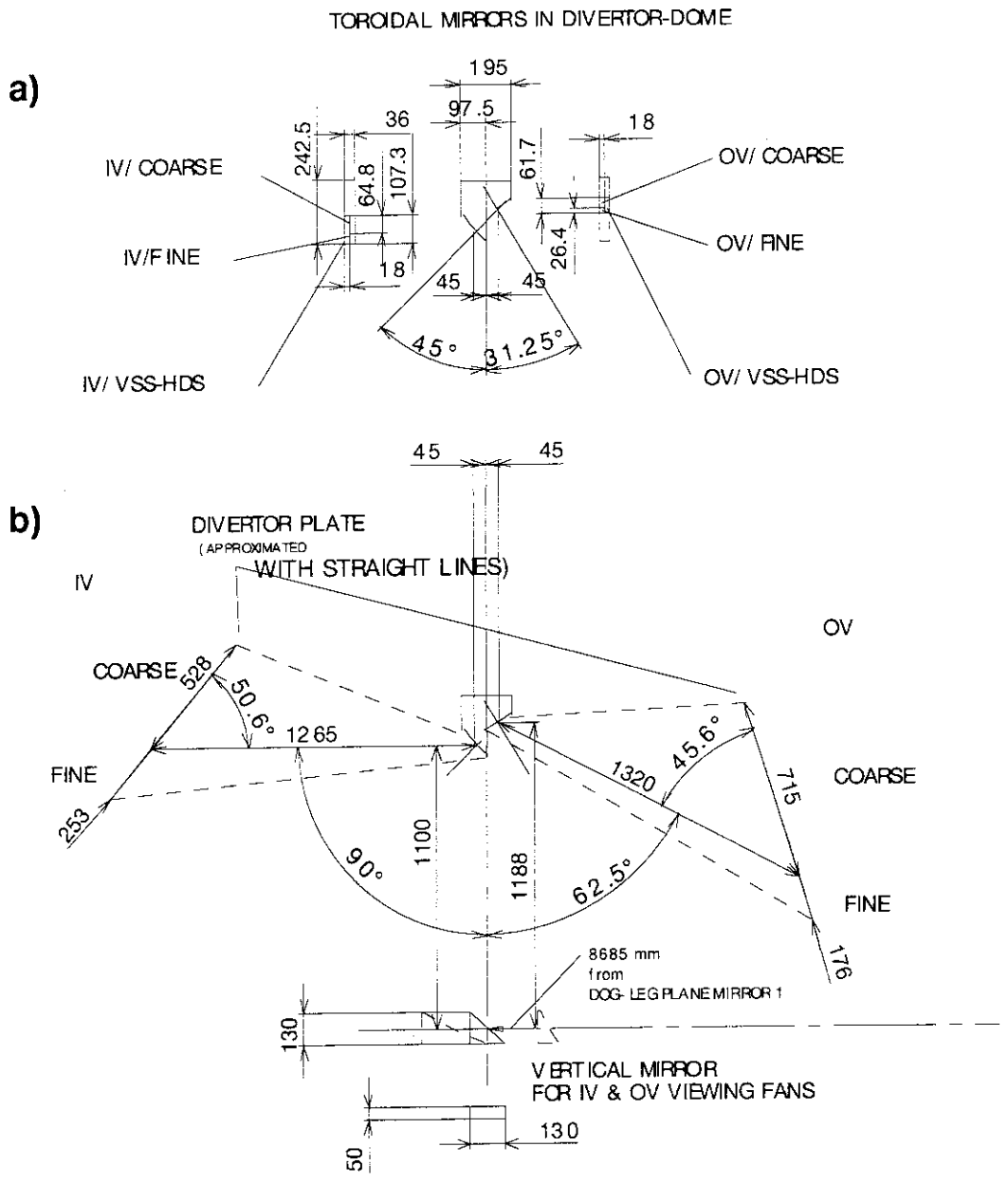

Fig. 3.2-2 a) Mirror arrangement for viewing fans of IV and OV. There are six toroidal mirror for IV/COARSE, IV/FINE, IV/VSS-HDS, OV/COARSE, OV/FINE and OV/VSS-HDS in the divertor dome.
b) Viewing fans for IV/COARSE, IV/FINE, OV/COARSEA and OV/FINE of the filter spectrometers. A plane mirror sits in the bottom of the divertor cassette.

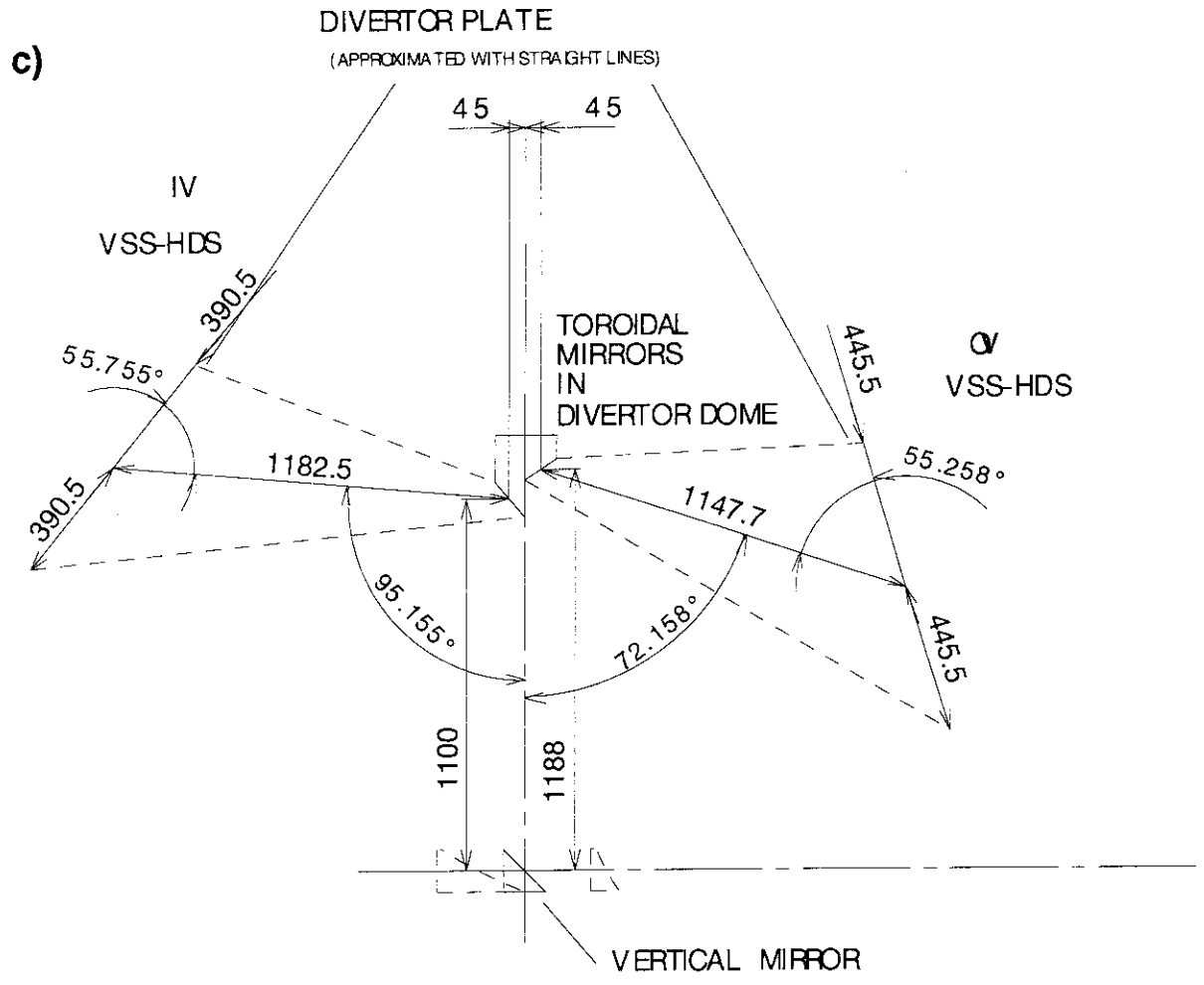

Fig. 3.2-2 c) Viewing fans of visible survey spectrometers (VSS) and high dispersion spectrometers (HDS) for inner and outer divertor region.

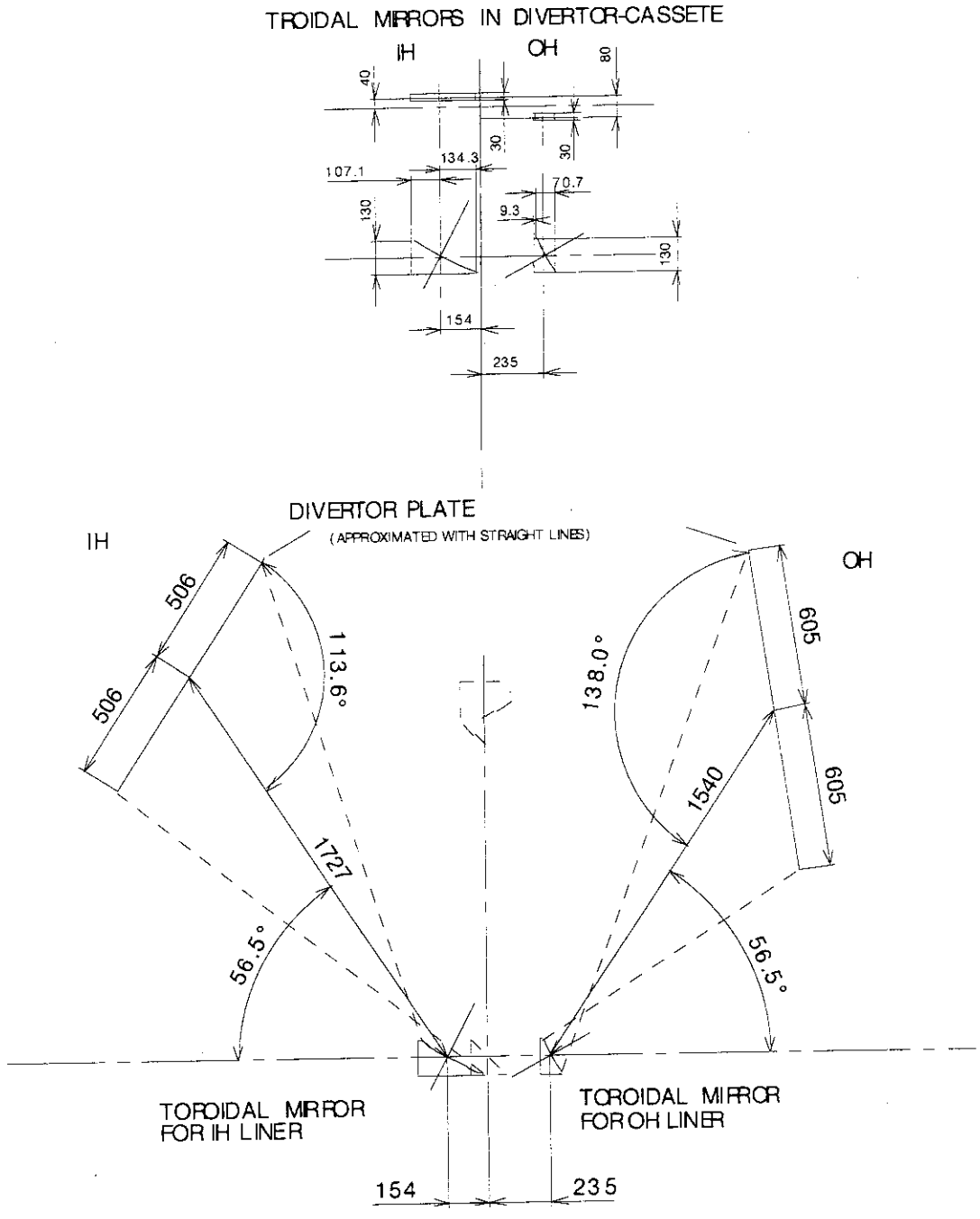

Fig. 3.2-3 Mirror arrangement and viewing fans of IH and OH for filter spectrometers. There are two toroidal mirrors in the bottom of the divertor cassette.

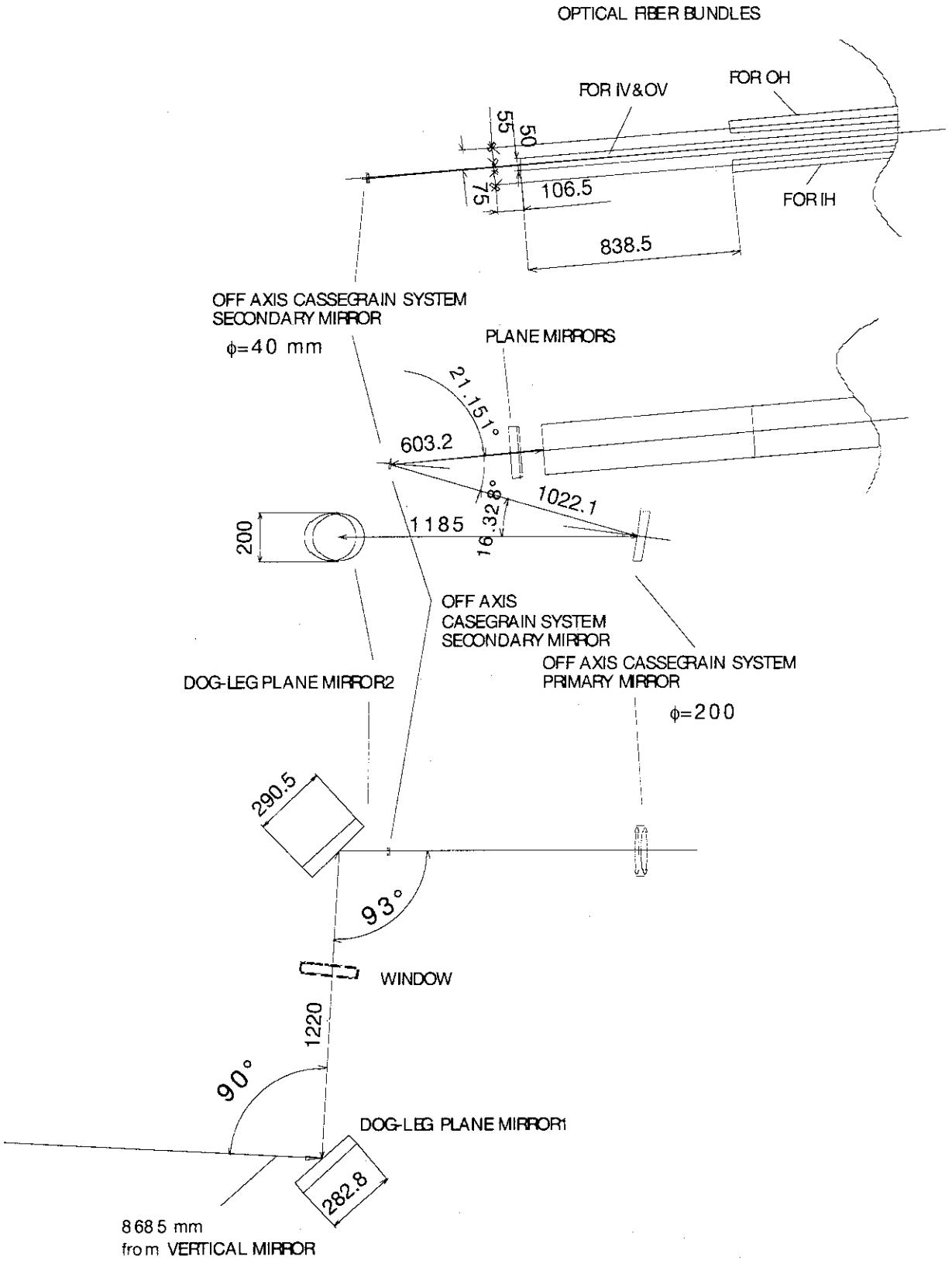

Fig. 3.2-4 Collecting and focusing system. The light reflected by a plane mirror 2 is focused on fiber arrays by a mirror optics such as a off-axis Cassegrain type in order to avoid the chromatic aberration, because of the wide wavelength range (200-1000 nm).

3.3 Fiber array

In order to increase the light coming into the fiber, a taper-type light guide is connected with each end of the fiber as shown in Fig. 3.3-1. The size of the light guide and the image area on the divertor plate are listed in table 3.3-1 for each viewing channel.

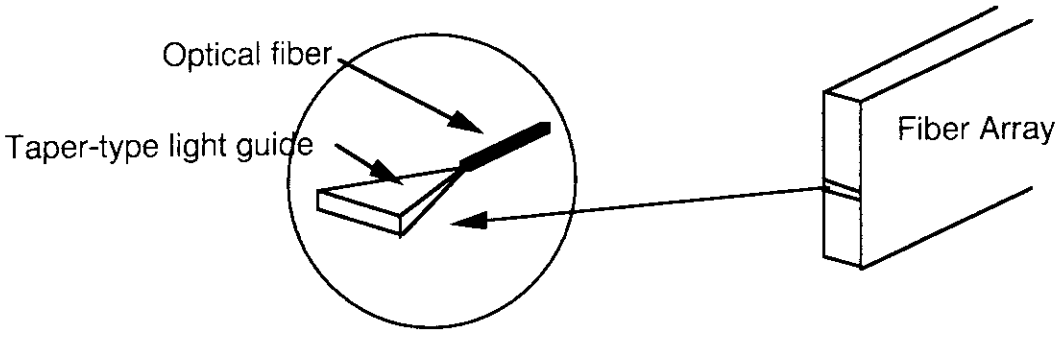

Fig. 3.3-1 Conceptual sketch of a taper-type light guide.

	Aperture Area of Light Guide	Image Area on the Divertor Plate		
		upper	middle	lower
FS: IV(FINE)	0.2 mm x 1.5 mm	2.5 mm x 14.2 mm	2.2 mm x 13.0 mm	2.1 mm x 12.0 mm
FS: IV(COARSE)	0.2 mm x 1.5 mm	5.1 mm x 32.5 mm	4.3 mm x 25.3 mm	4.3 mm x 25.3 mm
FS: OV(FINE)	0.2 mm x 1.5 mm	1.7 mm x 10.0 mm	1.8 mm x 10.5 mm	1.9 mm x 11.2 mm
FS: OV(COARSE)	0.2 mm x 1.5 mm	4.9 mm x 26.1 mm	5.6 mm x 33.5 mm	7.7 mm x 44.7 mm
FS: IH	0.4 mm x 2 mm	3.0 mm x 6.3 mm	2.0 mm x 9.2 mm	2.3 mm x 13.9 mm
FS: OH	0.4 mm x 2 mm	1.4 mm x 0.04 mm	2.3 mm x 0.3 mm	7.3 mm x 1.0 mm
VSS/HDS: IV	1 mm x 1.5 mm	20.2 mm x 24.7 mm	15.3 mm x 18.2 mm	13.3 mm x 13.5 mm
VSS/HDS: OV	1 mm x 1.5 mm	28.6 mm x 28.8 mm	20.3 mm x 20.2 mm	15.2 mm x 15.1 mm

Table 3.3-1 Size of the light guide and the image area on the divertor plate

upper : Image area of the upper part of the divertor plate.
middle : Image area of the middle part of the divertor plate.
lower : Image area of the lower part of the divertor plate.
FS : Filter spectrometer.
VSS/HDS : Visible survey spectrometer and high dispersion spectrometer
IV(FINE) : Viewing fan of IV with a target spatial resolution of 3 mm.
IV(COARSE) : Viewing fan of IV with a target spatial resolution of 10 mm.
OV(FINE) : Viewing fan of OV with a target spatial resolution of 3 mm.
OV(COARSE) : Viewing fan of OV with a target spatial resolution of 10 mm.

3.4 Ray trace analysis

The ray trace analysis has been carried out in order to get a optimum design of the optical penetration system. The results of each viewing fan are shown in Fig.3.4-1(a),(b) ~ Fig.3.4-8. These are the optimum results at this moment.

A ray is started from the center of a channel of the fiber array as shown in Fig. 3.4-1(b). The spot diagrams on the divertor plate for the upper, middle and lower part of the viewing fans are shown in these figures.

As the results, the following things become clear.

1) It is difficult to satisfy the 3-mm spatial resolution in the all region of the divertor.
2) In this design, the 10-mm spatial resolution is also difficult for all region of the divertor.

It seems that the above results are caused by to observe wide area of the divertor through the narrow channel of the divertor cassette. If we give up the 3-mm spatial resolution, it is expected that the spatial resolution of around 10 mm will be satisfied in the almost all region of the divertor. The optical penetration system will become more reliable, because it becomes more simple.

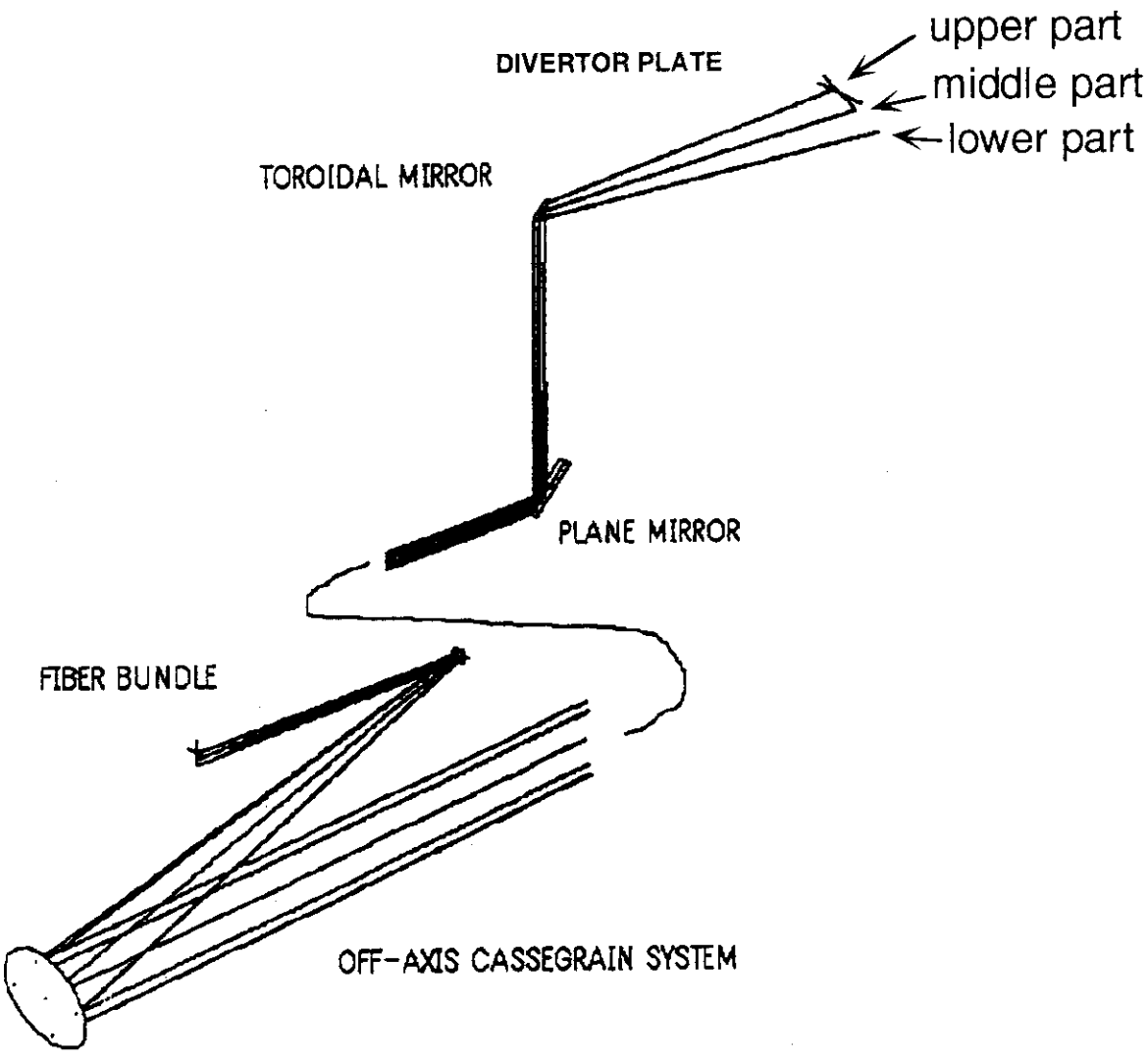

Fig.3.4-1(a) Ray trace for viewing fan IV (FINE): To simplify, rays started from only three deferent channels of the fiber array are drawn here. Those rays are focused on the upper, middle and lower part of the divertor plate.

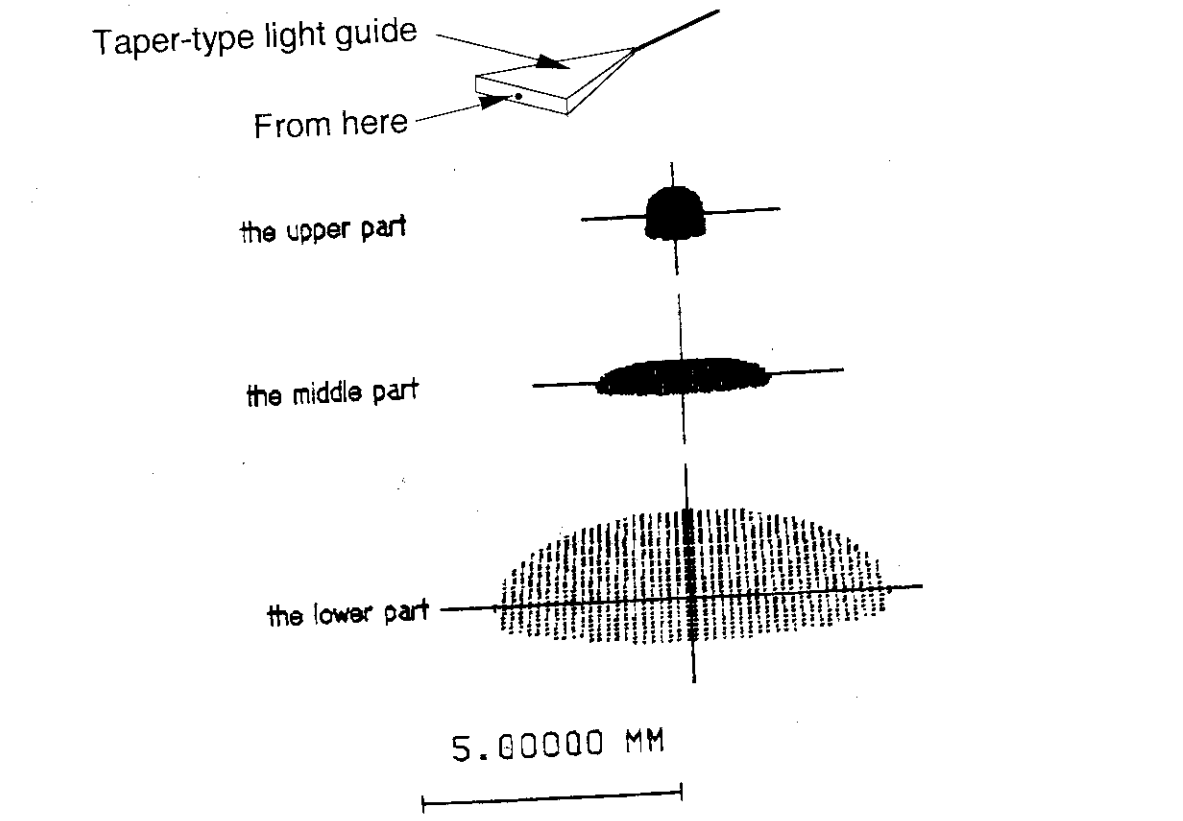

Fig.3.4-1(b) Spot diagrams for the viewing fan of IV (FINE): The rays are started from single point of each light guide and focused on the divertor plate. The 3-mm spatial resolution will be satisfied in the upper and middle part of the viewing fan. It is difficult in the lower part.

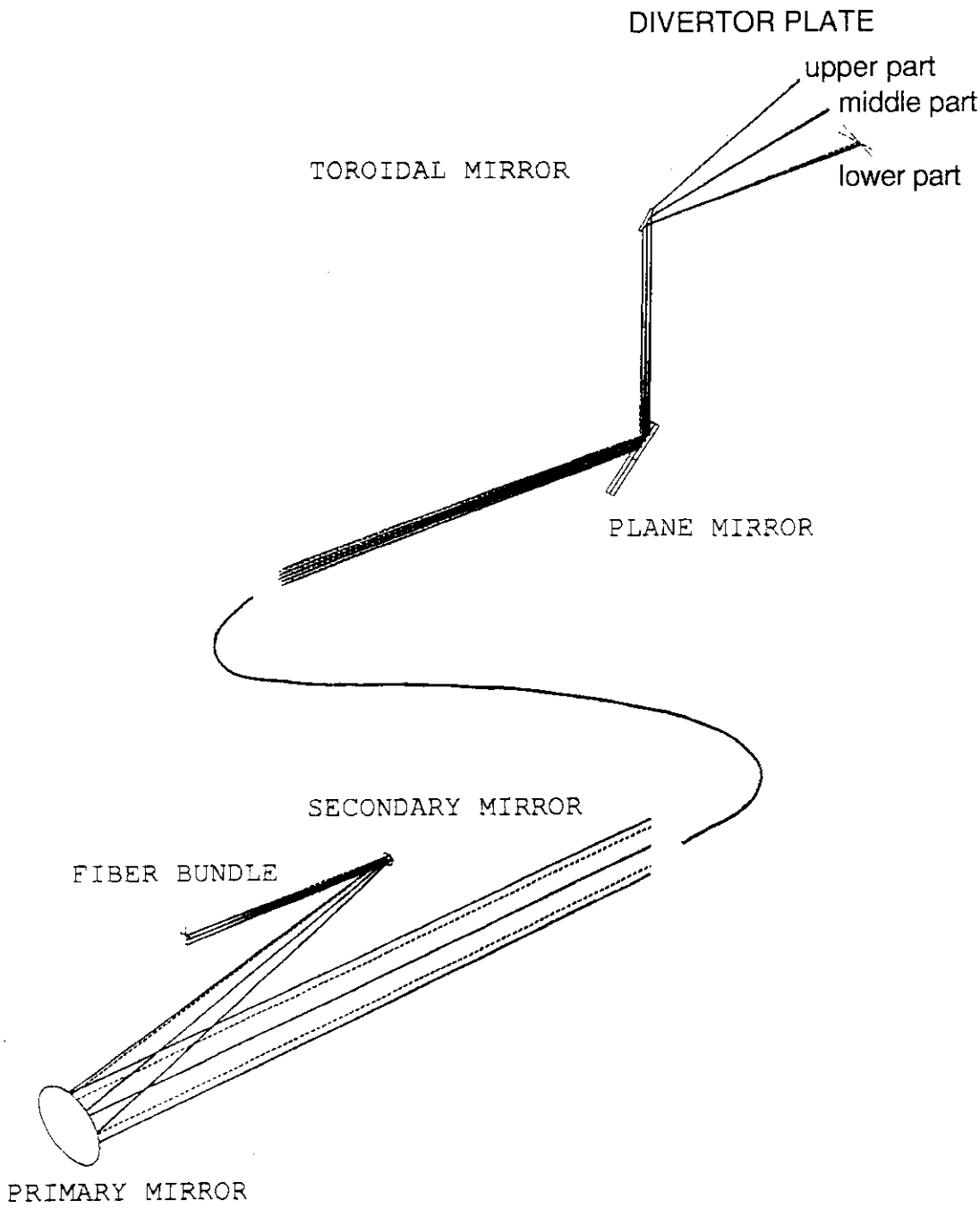

Fig.3.4-2(a) Ray trace for viewing fan IV (COARSE): To simplify, rays started from only three deferent channels of the fiber array are drawn here. Those rays are focused on the upper, middle and lower part of the divertor plate.

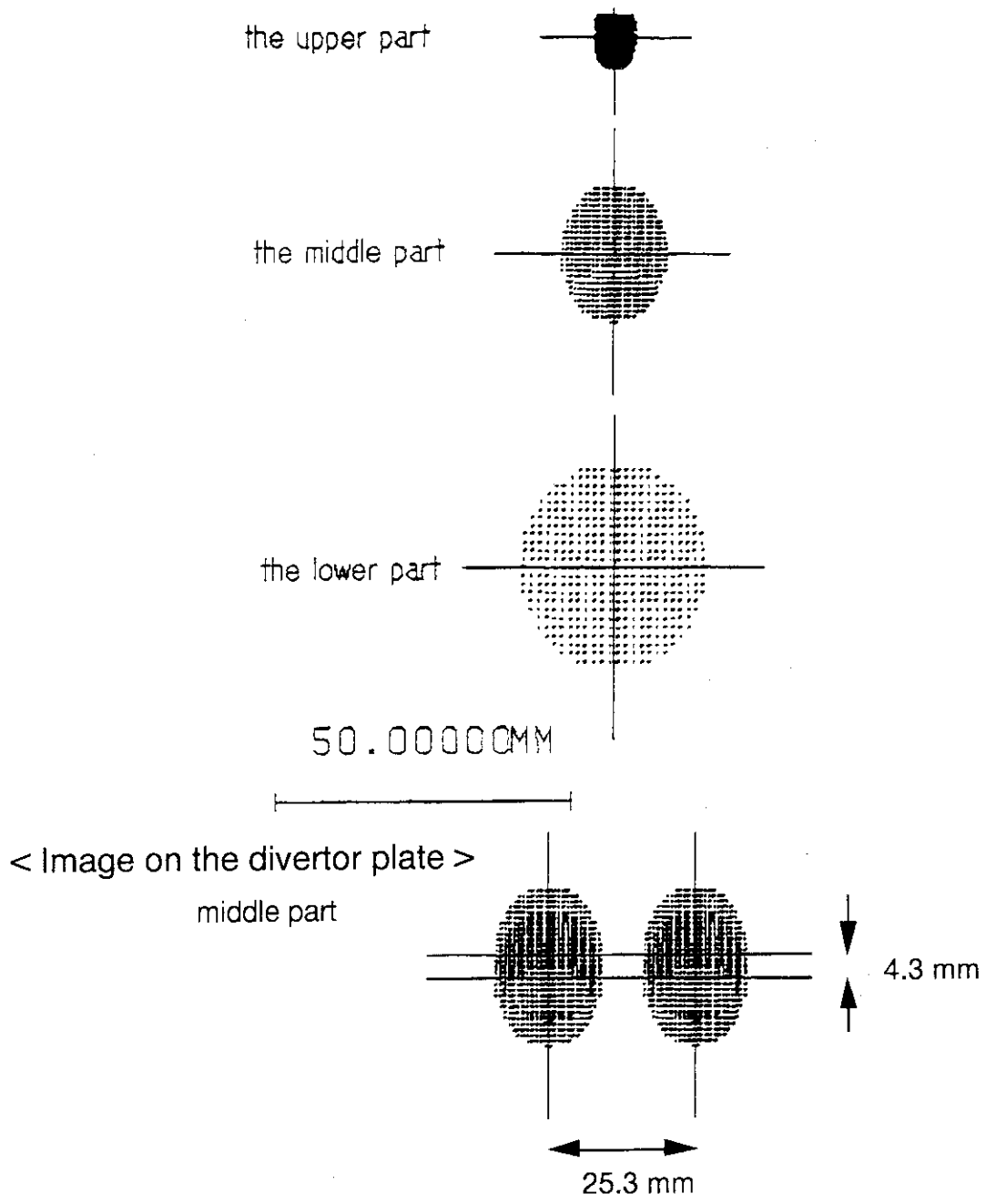

Fig.3.4-2(b) Spot diagrams for the viewing fan of IV (COARSE): The rays are started from single point of each light guide and focused on the divertor plate. The 10-mm spatial resolution will be satisfied in the upper part of the viewing fan. It is difficult in the middle and the lower part.

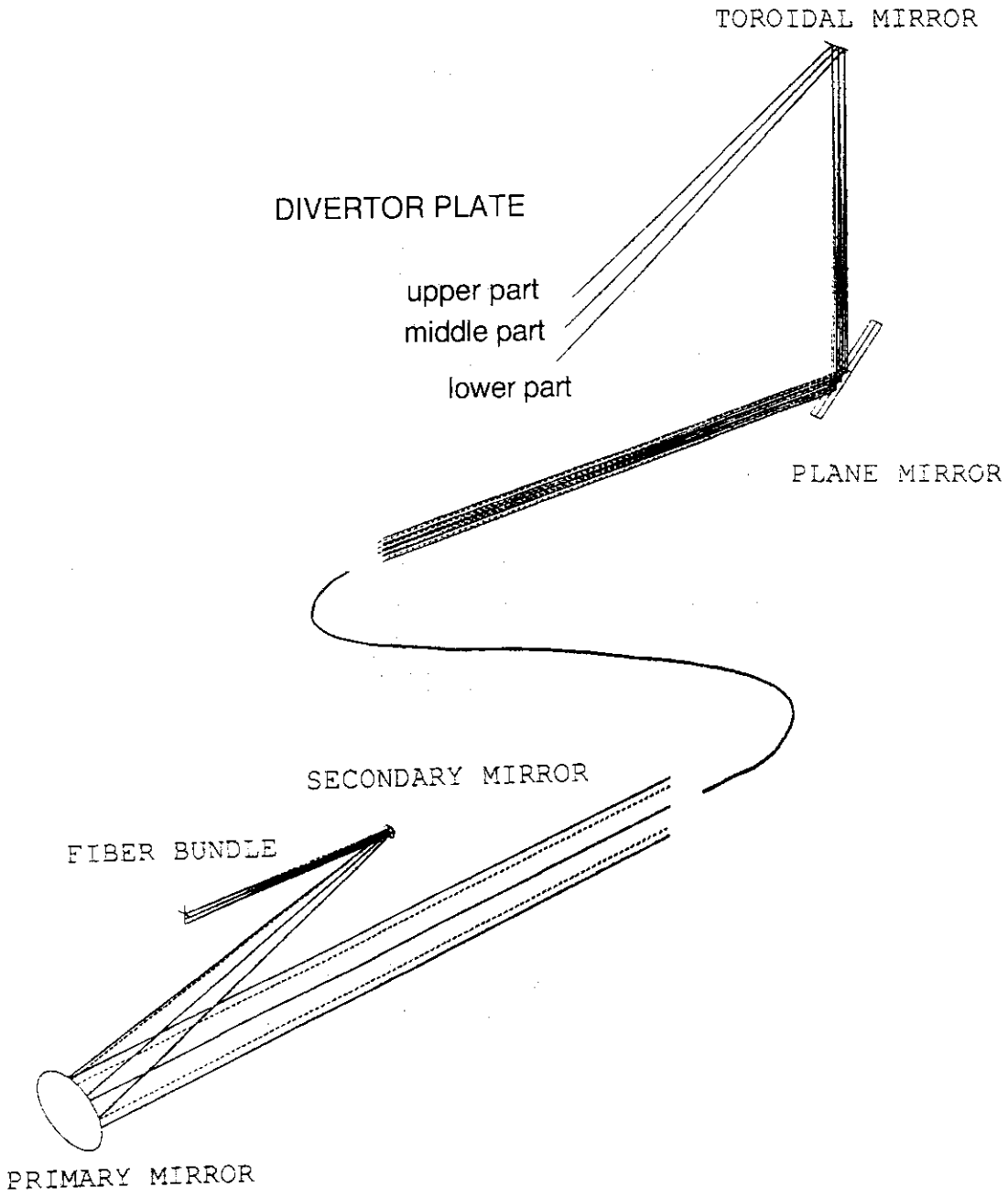

Fig.3.4-3(a) Ray trace for viewing fan OV (FINE): To simplify, rays started from only three deferent channels of the fiber array are drawn here. Those rays are focused on the upper, middle and lower part of the divertor plate.

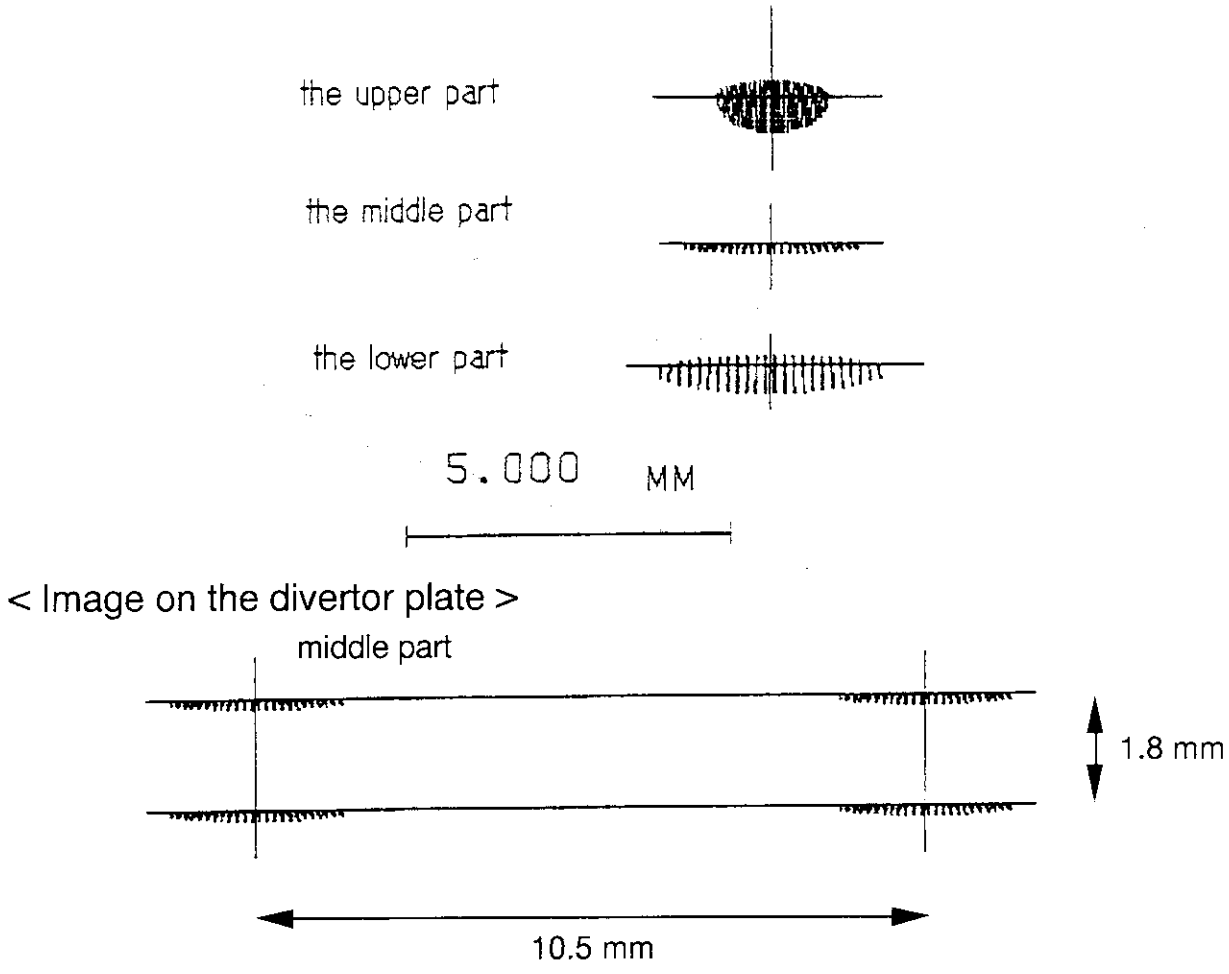

Fig.3.4-3(b) Spot diagrams for the viewing fan of OV (FINE): The rays are started from single point of each light guide and focused on the divertor plate. The 3-mm spatial resolution will be satisfied in this viewing fan.

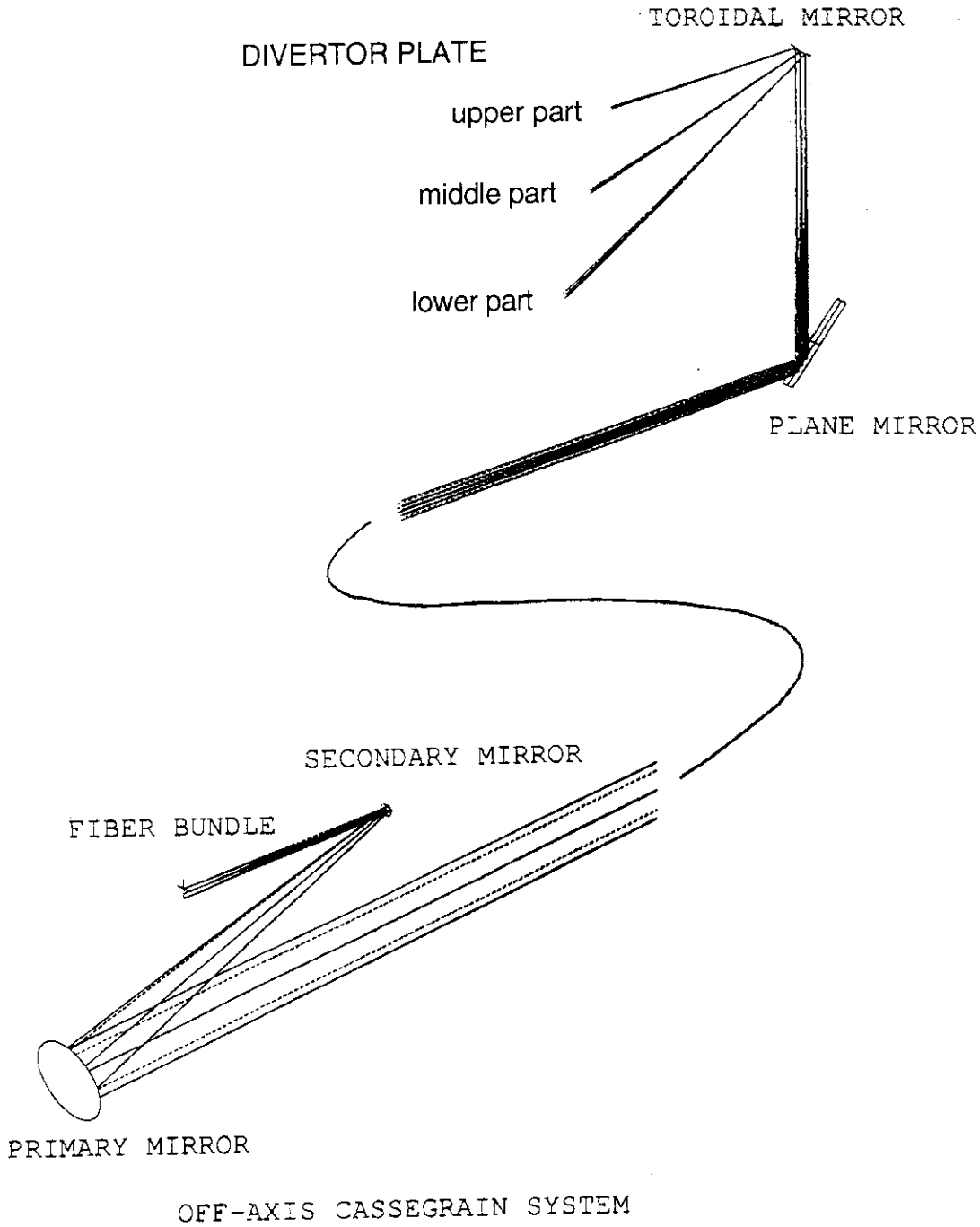

Fig.3.4-4(a) Ray trace for viewing fan OV (COARSE): To simplify, rays started from only three deferent channels of the fiber array are drawn here. Those rays are focused on the upper, middle and lower part of the divertor plate.

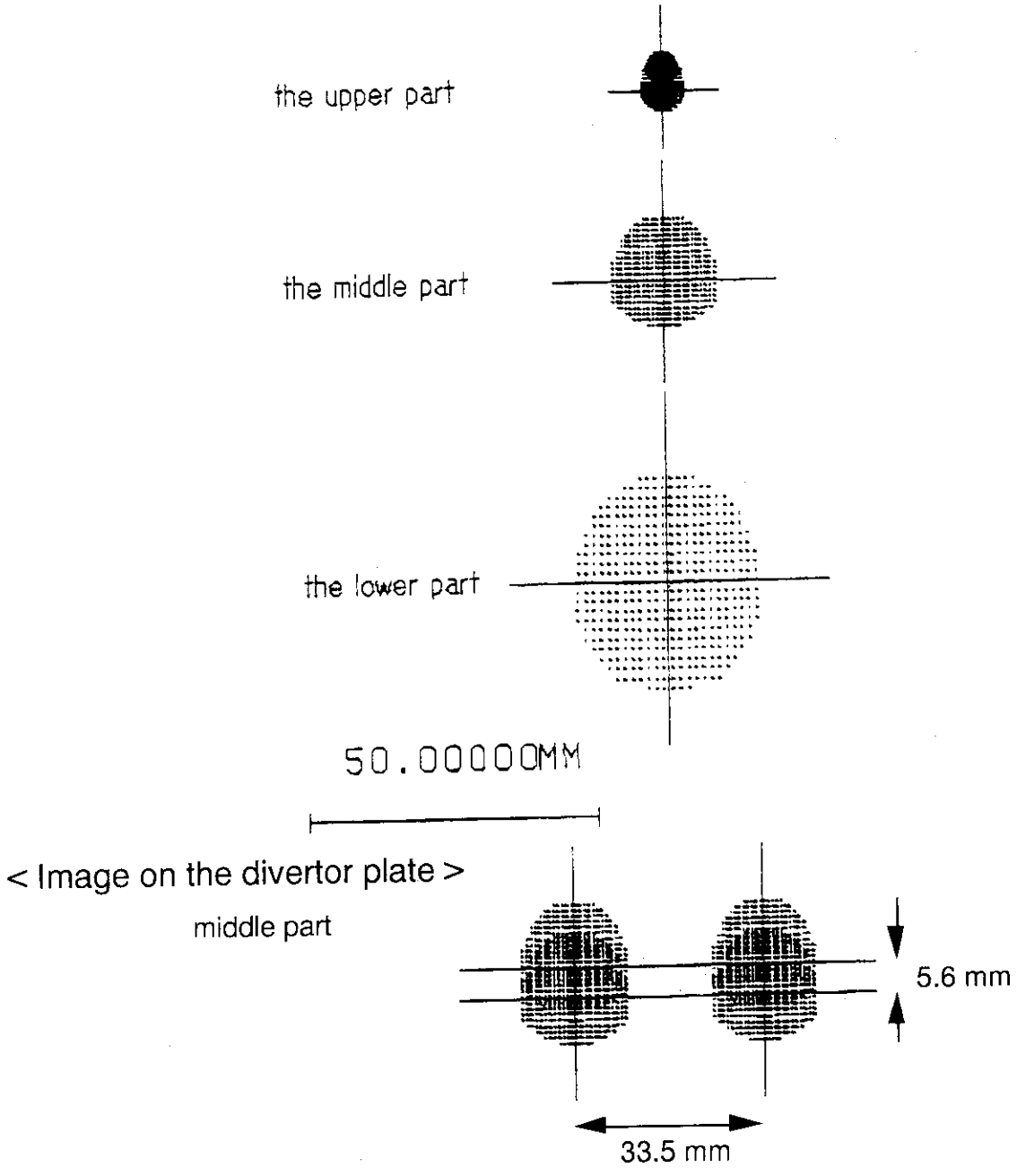

Fig.3.4-4(b) Spot diagrams for the viewing fan of OV (COARSE): The rays are started from single point of each light guide and focused on the divertor plate. The 10-mm spatial resolution will be satisfied in the upper part of the viewing fan.

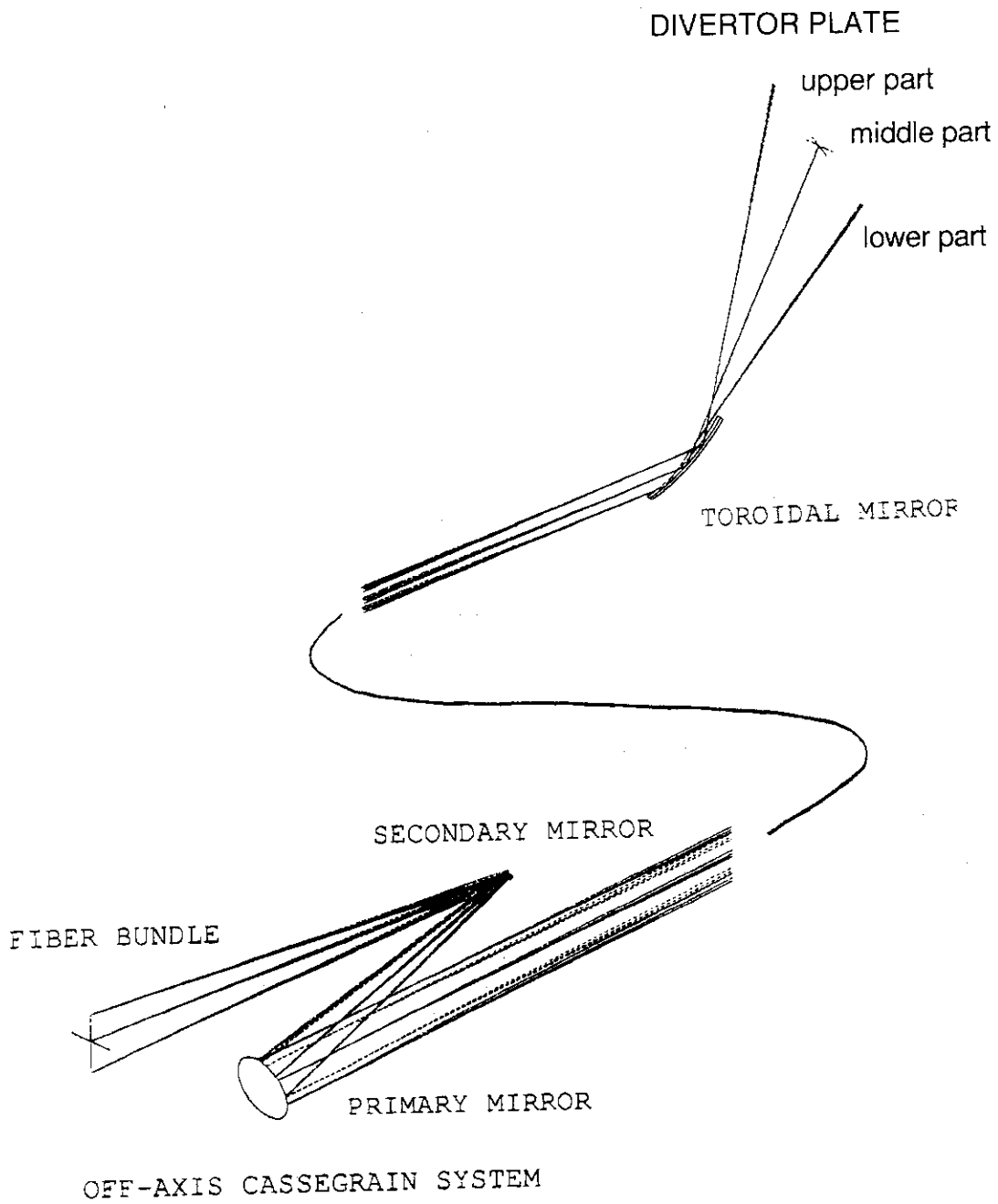

Fig.3.4-5(a) Ray trace for viewing fan IH: To simplify, rays started from only three deferent channels of the fiber array are drawn here. Those rays are focused on the upper, middle and lower part of the divertor plate.

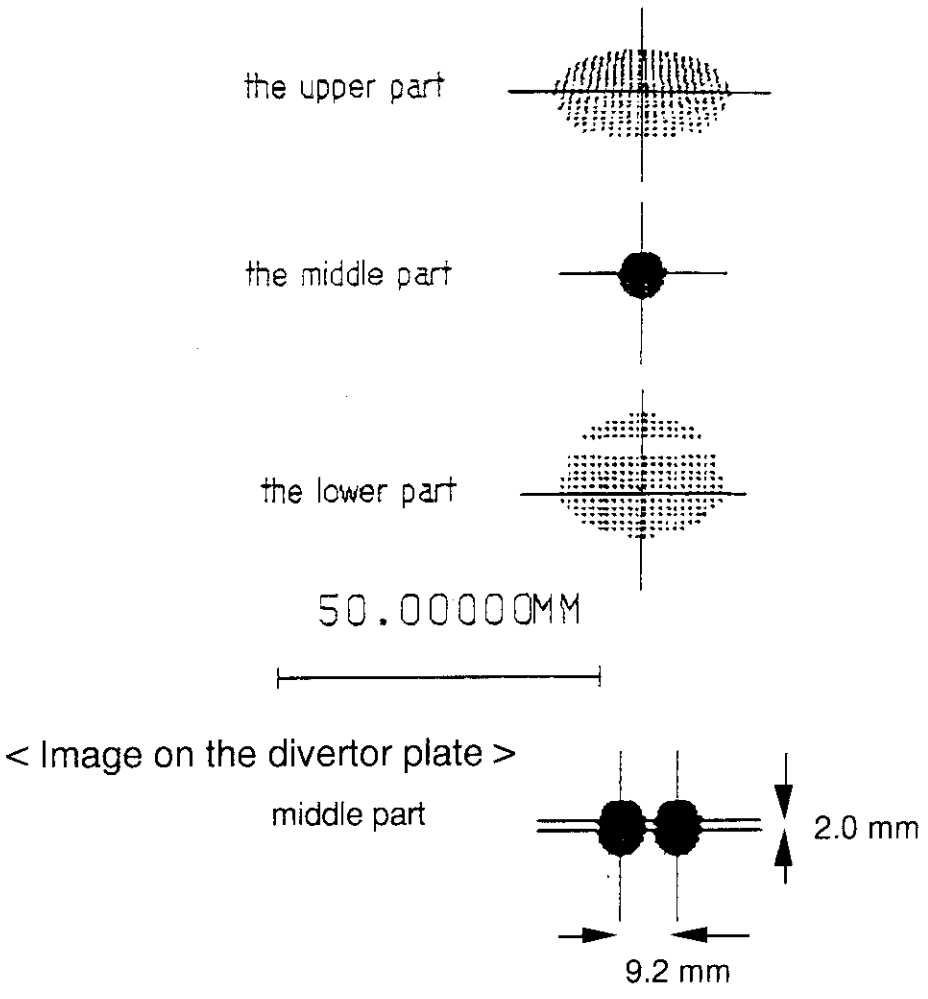

Fig.3.4-5(b) Spot diagrams for the viewing fan of IH: The rays are started from single point of each light guide and focused on the divertor plate. The 10-mm spatial resolution will be satisfied in the middle part of the viewing fan.

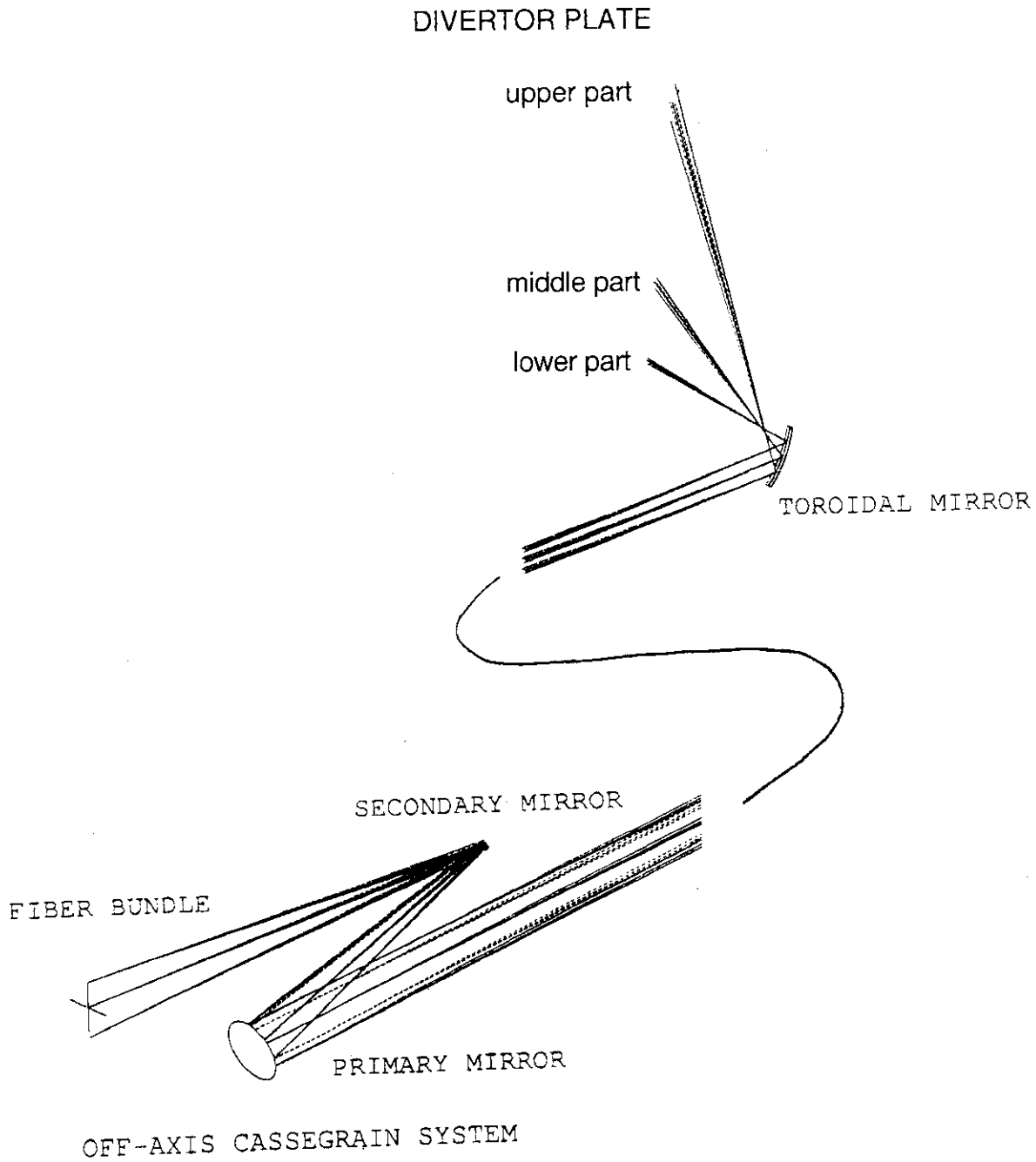

Fig.3.4-6(a) Ray trace for viewing fan OH: To simplify, rays started from only three deferent channels of the fiber array are drawn here. Those rays are focused on the upper, middle and lower part of the divertor plate.

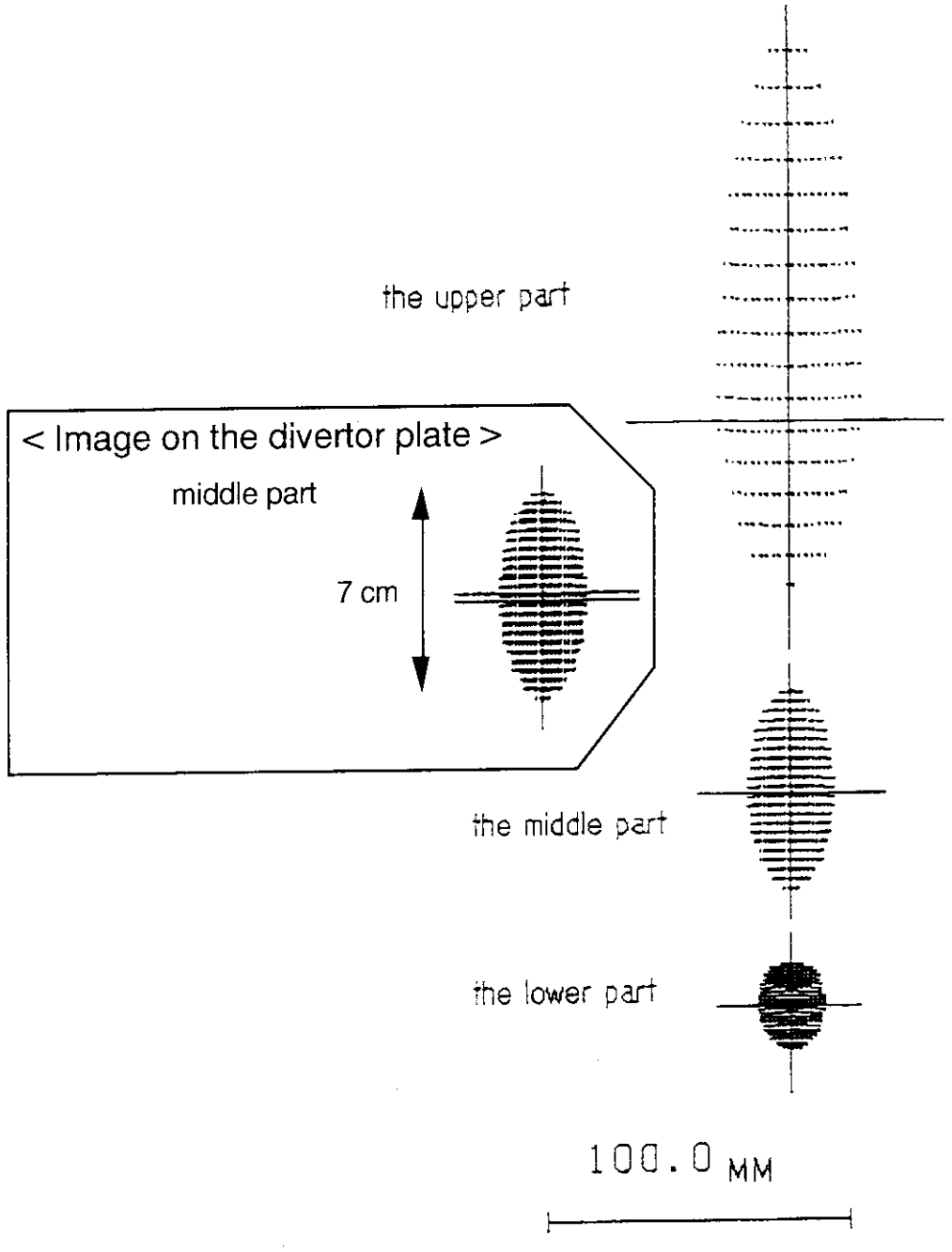

Fig.3.4-6(b) Spot diagrams for the viewing fan of OH: The rays are started from single point of each light guide and focused on the divertor plate. The 10-mm spatial resolution is difficult.

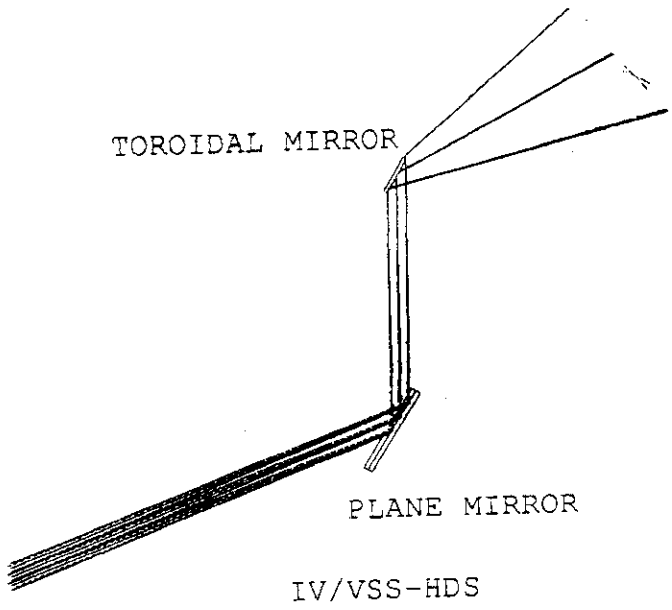

Fig.3.4-7 Ray trace for viewing fan IV of the visible survey spectrometer and the high dispersion spectrometer: To simplify, rays started from only three deferent channels of the fiber array are drawn here. Those rays are focused on the divertor plate.

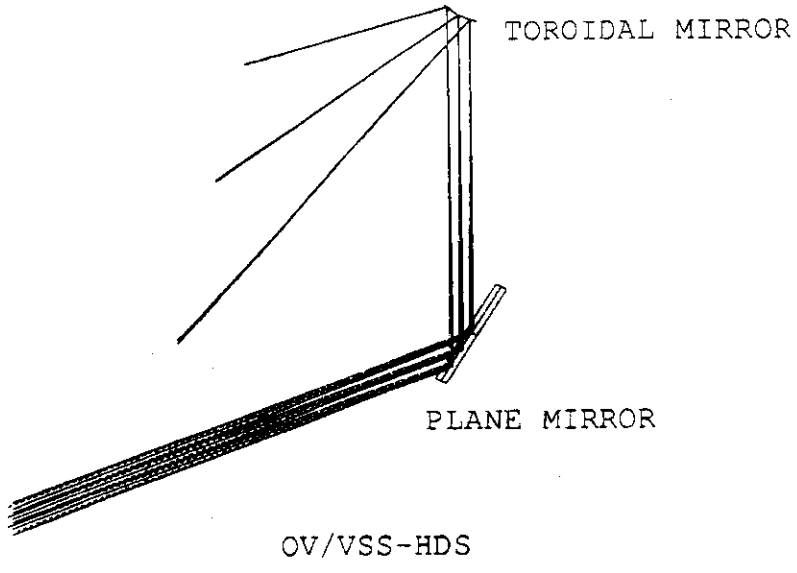

Fig.3.4-8 Ray trace for viewing fan OV of the visible survey spectrometer and the high dispersion spectrometer: To simplify, rays started from only three deferent channels of the fiber array are drawn here. Those rays are focused on the divertor plate.

3.5 Spectrometer

The conceptual design of three deferent kind of spectrometers described in section 2.1 has been carried out.

3.5.1 Spectrometer for species monitor (Visible survey spectrometer)

The object of this spectrometer is to survey impurity species in the divertor region with a spatial and a time resolution. The fundamental performance was decided as follows.

- Wavelength range : 200 - 1000 nm (simultaneously)
- Wavelength resolution : ~ 0.1 nm (1 Å)
- Time resolution : ~ 10 msec
- Spatial resolution : ~ 10 cm (on the divertor plate)

It is very difficult to observe spectral lines in the wavelength range of 200 - 1000 nm simultaneously. Therefor, we are planning to divide the light into four deferent wavelength region and to observe each region by one spectrometer respectively.

The light from the divertor region is divided into seven wavelength region by a pre-divider composed of six dichroic mirrors. The pre-divider is located on the transport cask in the pit. The divided lights enter the spectrometers as shown in Fig.3.5-1. The spectrometers for the wavelength region of 200 - 488 nm are set on the transport cask in the pit as described in section 2.3. The light over 488 nm is guided to the spectrometers in the diagnostic room by optical fibers.

The optical arrangement of the visible survey spectrometer is shown in Fig.3.5-2. The fiber bundle from the pre-divider is set just front of the entrance slit. The fiber arrangement along the slit length correspond to the viewing chord of the divertor. The light enters a collimator through the entrance slit and comes into a grating. The light dispersed by the grating is measured by a two dimensional detector through a camera optics.

The preliminary specifications for the visible survey spectrometer are listed in table 3.5-1.

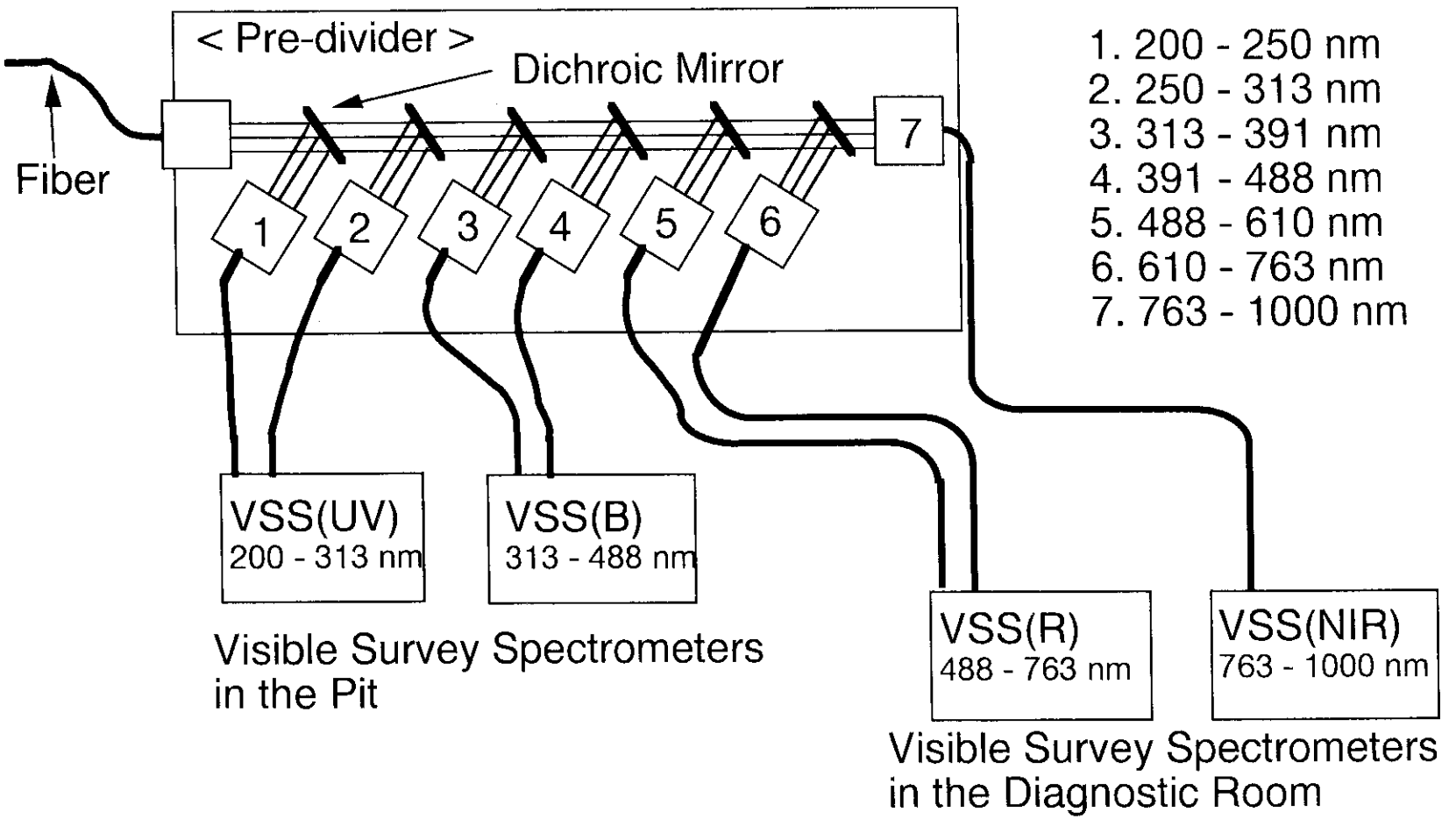

Fig. 3.5-1 The arrangement of the visible survey spectrometer.
The light from the divertor region is divided into seven wavelength region by a pre-divider composed of six dichroic mirrors. The pre-divider is located on the transport cask in the pit. The divided lights enter the spectrometers as shown in Fig.3.5-1. The spectrometers for the wavelength region of 200 - 488 nm are set on the transport cask in the pit as described in section 2.3. The light over 488 nm is guided to the spectrometers in the diagnostic room by optical fibers.

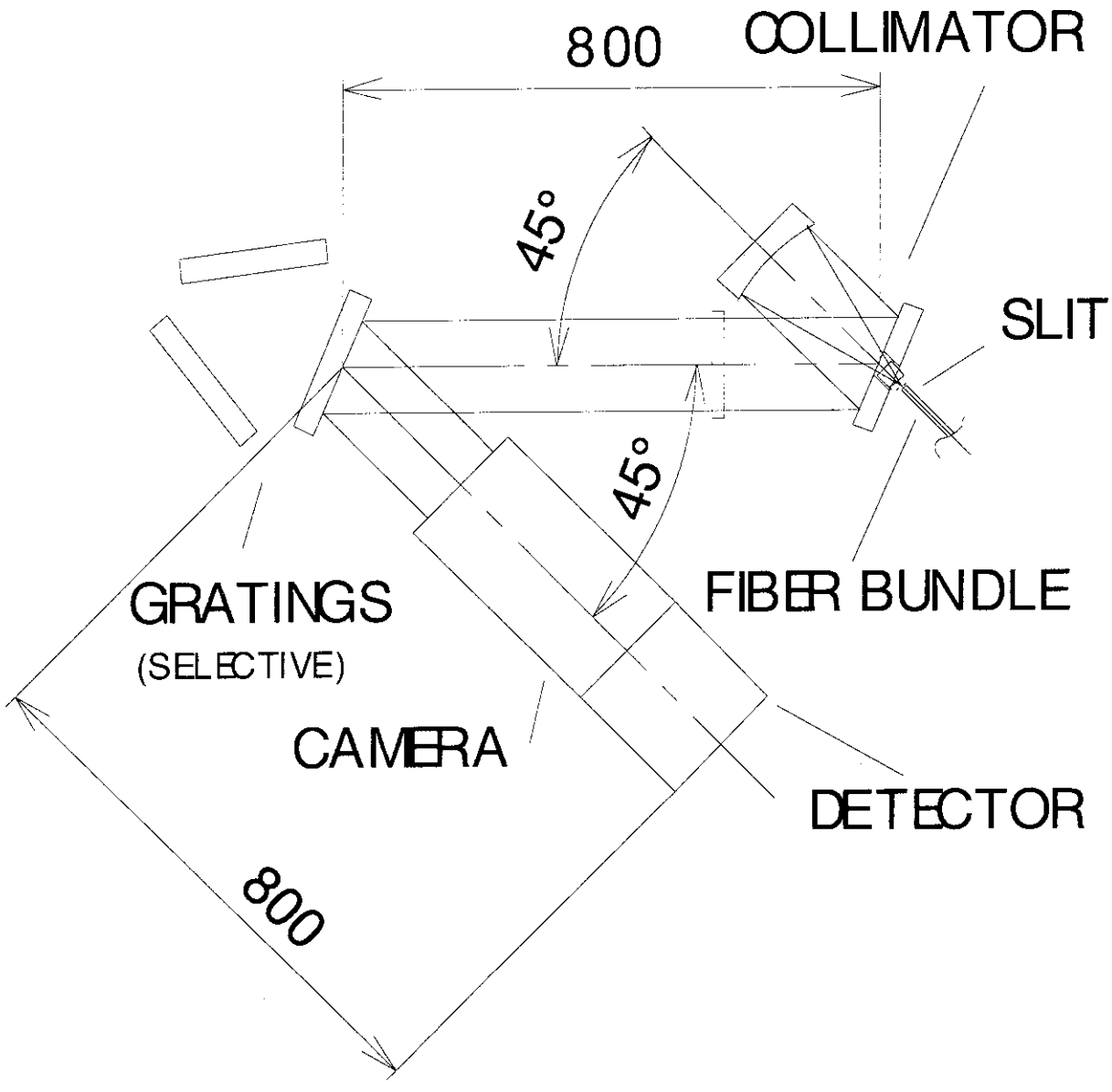

Fig. 3.5-2 Optical arrangement of visible survey spectrometer.

Table 3.5-1 Preliminary specifications for visible survey spectrometer.

	UV	B	R	NIR
Grating N [mm^{-1}]	600	600	600	270
θg	4.65636°	7.65075°	11.23483°	7.40068°
*Detector pixels 1 pixel=15μx15μ	2048 x 2048	4096 x 2048	4096 x 2048	4096 x 2048
size[mm]	30 x 30	60 x 30	60 x 30	60 x 30
Band width [nm]	190.9 ~307.9	294.0 ~520.8	488.0 ~706.2	663.8 ~1091.0
λc [nm]	250	410	600	881.5
Collimator f [mm]	225	225	225	225
Camera f [mm]	380	380	380	450
Magnification between slit and ditector	1.8068	1.8879	1.9917	2.2274
Appropriate slit width for 1 pixel [mm]	0.0083	0.0079	0.0075	0.0067

* Large area 2-D detector is a R & D item.

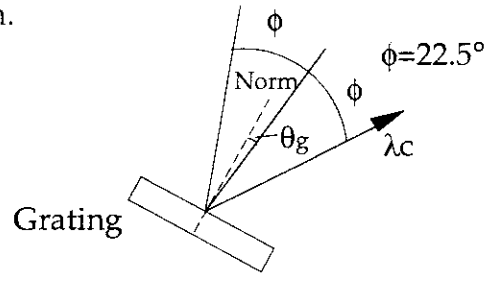

3.5.2 Filter optical system for influx measurement (Filter spectrometer)

The object of this spectrometer is influx measurements for impurity, deuterium and tritium particles in the divertor region with a spatial and a time resolution. The fundamental performance was decided as follows.

- Wavelength range : 200 - 1000 nm
- Number of spectral lines : 10 spectral lines simultaneously
- Wavelength resolution : ~ 1 nm (10 Å)
- Time resolution : ~ 1 msec
- Spatial resolution : 3~ 10 mm (on the divertor plate)

The number of viewing chord is very large (560 chords) and the time resolution is short. Therefore, it is better to use a filter optics.

The conceptual drawings of the filter spectrometers are shown in Fig. 3.5-3(a) and (b). We consider two type of spectrometer. One is composed of several sets of a multi-channel filter spectrometer (type 1) and the other has 560 sets of single channel filter spectrometer (type 2). Type 1 spectrometer has relay optics to avoid the divergence of each beam. On the other hand, type 2 spectrometer will not need the relay optics. Type 2 spectrometer has a simple structure but it will be very difficult to adjust the filter angles and so on because of the large number of sets.

<Type 1 spectrometer >
The lights from the viewing chords (100~200 chords) enter the spectrometer by a optical fiber bundle and the lights of a required wavelength band are reflected by a dichroic mirror . After that the lights are detected by a 2-D detector through a bandpass filter, if necessary, and focusing optics as shown in Fig. 3.5-3(a). The lights transmitted the dichroic mirror enter the next dichroic mirror. The dichroic mirrors for below 500 nm are in the pit and those over 500 nm are in the diagnostic room through optical fiber bundles.

< Type 2 spectrometer >
The light from the one viewing chord enter the spectrometer by a optical fiber and the light of required wavelength band is reflected by a dichroic mirror. After that, the light enter a optical fiber through bandpass filter, if necessary, and focusing optics. We need 560 sets of same spectrometers. The optical fibers corresponding to each spectral line are gathered to a optical fiber bundle as shown in Fig. 3.5-3(b). The image of the bundle focused on a 2-D detector by a relay optics for a spatial measurement. We nee 10 same set of the fiber bundle, the relay optics and the detector.

More detailed design is necessary for actual spectral lines to be measured.

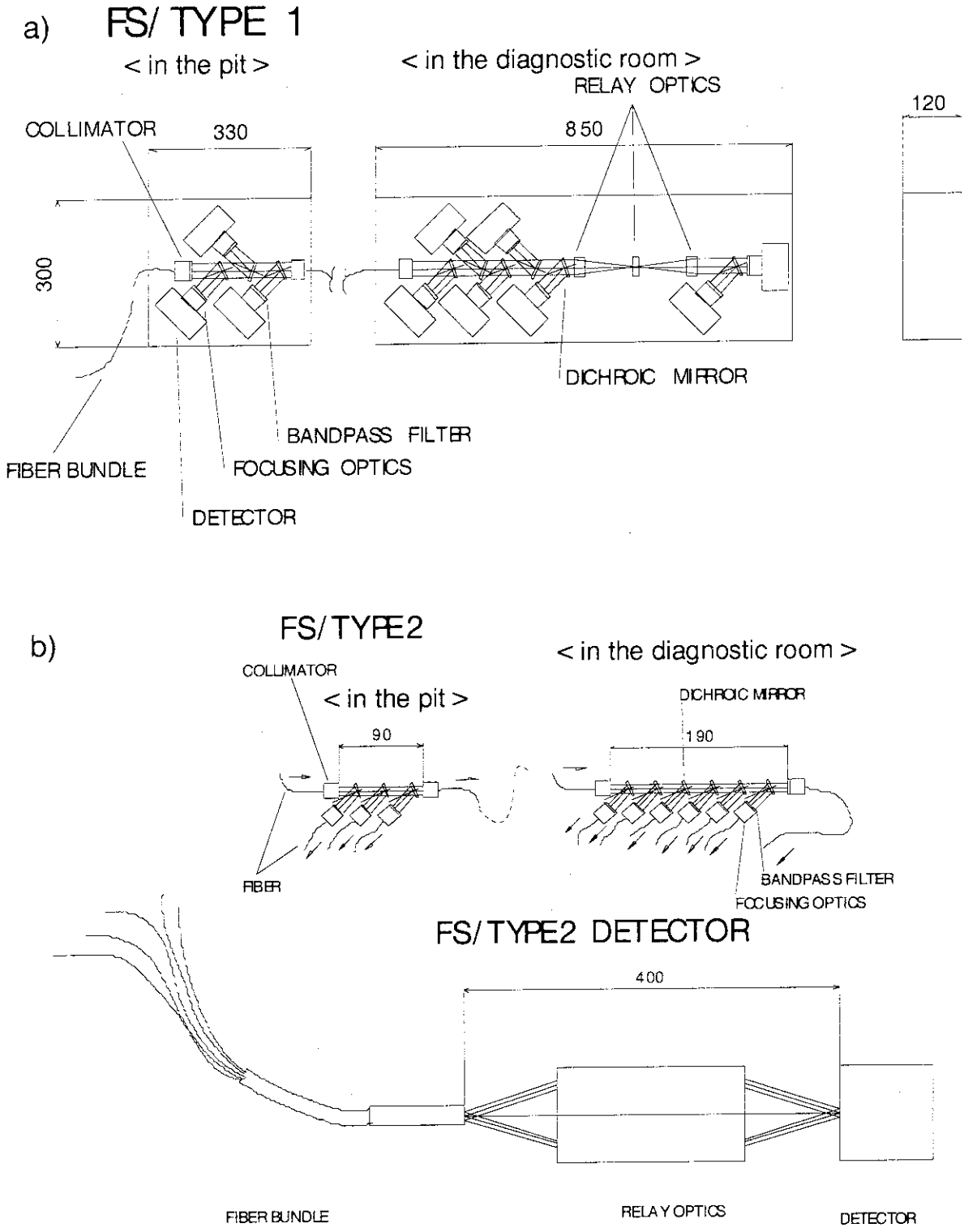

Fig. 3.5-3 Conceptual drawings of the filter spectrometers. (a) Type 1 spectrometer, (b) Type 2 spectrometer.

3.5.3 High dispersion spectrometer for line shape measurement

The object of this spectrometer is line shape measurements in order to get informations of ion temperature, particle energy distribution and so on in the divertor region with a spatial and a time resolution. The fundamental performance was decided as follows.

- Wavelength range : 200 - 1000 nm
- Wavelength resolution : ~ 0.01 nm (0.1 Å)
- Time resolution : ~ 10 msec
- Spatial resolution : ~ 10 cm (on the divertor plate)

Here, we are considering a Littrow type spectrometer with an echelle grating. The lights enter the spectrometers through pre-divider as shown in Fig. 3.5-4(a) and (b). The preliminary specifications are listed in table 3.5-2.

More detailed design is necessary for actual spectral lines to be measured.

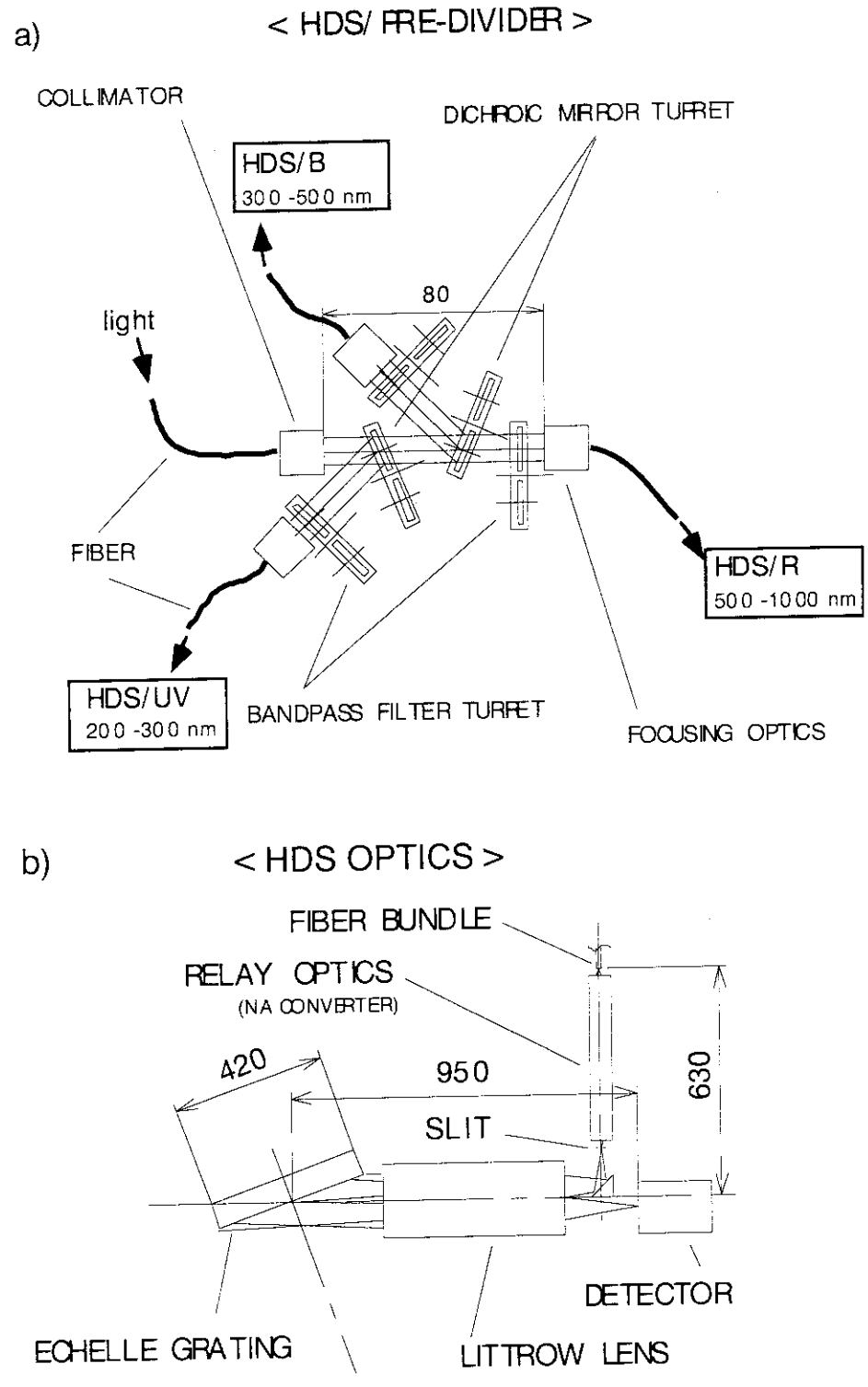

Fig. 3.5-4 (a) Pre-divider for high dispersion spectrometers. The light is divided into three wavelength ranges and enter the high dispersion spectrometer optics. (b) Optics of high dispersion spectrometer. We are considering a Littrow type spectrometer with an echelle grating.

Table 3.5-2 Preliminary specifications for high dispersion spectrometer.

		UV	B	R
Band width [nm]		200 ~ 300 nm	300~500 nm	500~1000 nm
Echelle grating	Grooves [mm^{-1}]	98.764	52.676	31.6
	Blaze angle [deg.]	63.433	70.5	75.07
Littrow optics f [mm]		500	500	500

3.6 Estimation of number of photons coming into the end of the optical fiber

The numbers of photons N_f coming into the end of the optical fiber located in the cryostat are estimated for Dα and CII lines. The number N_f is written by

$$N_f = P_c \times T \times I_{div}, \qquad (3.6\text{-}1)$$

where P_c is a collecting performance and T is a transmissivity of the penetration optics from the divertor to the end of the fiber, and I_{div} is a intensity of spectral line in the divertor.

3.6.1 Collecting performance and transmissivity of the penetration optics

The collecting performance P_c is defined as

$$P_c = \Omega_i \times M^2 \times S_f, \qquad (3.6\text{-}2)$$

where Ω_i is a input solid angle in the divertor, M is a magnification from the light guide in the cryostat to the image on the divertor plate and S_f is a area of the end of the light guide or the fiber. The relation is shown in Fig. 3.6-1. The calculated results for each viewing fan are listed in table 3.6-1.

Fig. 3.6-1 Ω_i, M and S_f

From the table, it is clear that the collecting performance is very low. This is due to observing wide area of the divertor through a narrow channel, which is come from the limitation of the penetration to the divertor.

The transmissivities T of the penetration optics from the divertor to the fiber in the cryostat are calculated for each viewing fan as shown in table 3.6-2. The optical system has 6 mirrors for the viewing fans of IV and OV, and 7 mirrors for the viewing fans of IH and OH. The transmissivities in case of using 6 Mo-mirrors, 6 Cu-mirrors, 2 Mo-mirrors + 4 Al-mirrors, and 2 Cu-mirrors + 4 Al-mirrors are listed for the IV and OV viewing fans. For the IH and OH viewing fans, the cases of 7 Mo-mirrors, 7 Cu-mirrors, 1 Mo-mirror + 6 Al-mirrors and 1 Cu-mirror + 6 Al-mirror are listed in the table.

From the table, it is better to use Al-mirrors for the penetration optics in this wavelength range . The Mo or Cu-mirror should be used for the first mirror in the divertor cassette. Irradiation tests of Al-mirror is necessary.

Table 3.6-1 Collecting performance of penetration optics.

	Solid Angle(sr)		M	Sf (m^2)		Pc (m^2•sr)	
	input Ωi	output		Fiber only	with Light guide	Fiber only	with Light guide
IV(FINE)	2.10E-06	1.70E-04	9.1	3.14E-08	3.00E-07	5.50E-12	5.20E-11
IV(COARSE)	3.90E-05	1.70E-04	2.1	3.14E-08	3.00E-07	5.40E-12	5.20E-11
IV(VSS/HDS)	6.90E-06	1.70E-04	5	-	1.50E-06	-	2.60E-10
OV(FINE)	4.40E-06	2.10E-04	7.1	3.14E-08	3.00E-07	7.00E-12	6.70E-11
OV(COARSE)	4.90E-05	1.70E-04	1.9	3.14E-08	3.00E-07	5.60E-12	5.30E-11
OV(VSS/HDS)	1.80E-06	1.70E-04	10	-	1.50E-06	-	2.70E-10
IH	9.90E-07	3.90E-05	6.3	3.14E-08	8.00E-07	1.20E-12	3.10E-11
OH	2.10E-04	3.90E-05	0.43	3.14E-08	8.00E-07	1.20E-12	3.10E-11

Table 3.6-2 Transmissivity of penetration optics.

	Wavelength	200 nm	300 nm	400 nm	500 nm	600 nm	700 nm	800 nm	900 nm	1000nm
IV and OV	Mo: 6surfaces	0.0650	0.0400	0.0240	0.037	0.030	0.030	0.024	0.041	0.250
	Cu: 6surfaces	0.0016	0.0013	0.0120	0.037	0.330	0.640	0.680	0.680	0.680
	Mo: 2, Al: 4	0.2700	0.2200	0.1900	0.220	0.200	0.190	0.150	0.200	0.450
	Cu: 2, Al: 4	0.0770	0.0730	0.1500	0.220	0.440	0.520	0.470	0.510	0.640
IH and OH	Mo: 7	0.0420	0.0240	0.0130	0.022	0.017	0.017	0.013	0.024	0.200
	Cu: 7	0.0006	0.0005	0.0059	0.022	0.280	0.610	0.650	0.650	0.650
	Mo: 1, Al: 6	0.3500	0.3200	0.3000	0.320	0.290	0.270	0.210	0.260	0.500
	Cu: 1, Al: 6	0.1900	0.1800	0.2600	0.320	0.440	0.450	0.370	0.420	0.590

3.6.2 Intensity estimation of spectral lines in the divertor

The electron density and temperature in the divertor are expected to be from $1x10^{19}$ to $1x10^{22}$ m^{-3} and from 1 to 50 eV respectively [1]. The requirement of influx measurement is given by the DDD [2] as shown in table 1-1. The particle influx Γ is written as

$$\Gamma = 4\pi \cdot K \cdot I \qquad (3.6\text{-}3)$$

where K is the number of ionization events per photon for the observed line with the intensity of I. We estimated the intensities of Dα, and carbon lines against the required influxes by equation (3.6-3).

< Intensity of Dα >

The required range of the deuterium total influx to the divertor is 10^{19} - 10^{25} at / sec as shown in table 1-1. On the other hand, if we assume the power deposition area on the divertor targets is about 10 m^2 as shown in the DDD[3], the deuterium influx density Γ to the divertor is 10^{18} - 10^{24} at / m^2·sec. The intensity of Dα line was estimated by using the equation (3.6-3) against the deuterium influx density Γ_D as shown in Fig.3.6-2. The value of K was estimated by the reference [4]. In this figure, the electron temperature range is 1 - 50 eV and the density range is 10^{10} -10^{22} m^{-3}.

< Intensity of CII >

The intensity of CII line is also calculated against the carbon influx density in case of the low electron density. We use the value of K in the reference [5]. The result is shown in table 3.6-3.

3.6.3 Measurable limit

If we assume the lower limit of number of photons is 100 (photon·$msec^{-1}$) at the fiber in the cryostat, the measurable intensity limit in the divertor is about $1x10^{16}$ (photon·m^{-2}·sr^{-1}·sec^{-1}) from the equation 3.6-1. This means it is difficult to measure the deuterium influx density of 10^{18} (at·m^{-2}·sec^{-1}) in a high electron density region as shown in Fig.3.6-2. More efficient optics is necessary.

Reference

[1] ITER Diagnostic Group, "ITER INFORMATION", S55 RE 1 95-07-11 F 1.
[2] Design Description Document 5.5 Diagnostics 5.5 E.04.
[3] Design Description Document 1.7 Divertor 2.1.1.1.
[4] L. C. Johnson and E. Hinnov, J. Quant. Spectrosc. Radiat. Transfer, **13**, (1973) 333.
[5] K. Behringer, et al., Plasma Phys. Cont. Fusion, **14**, (1989) 2059.

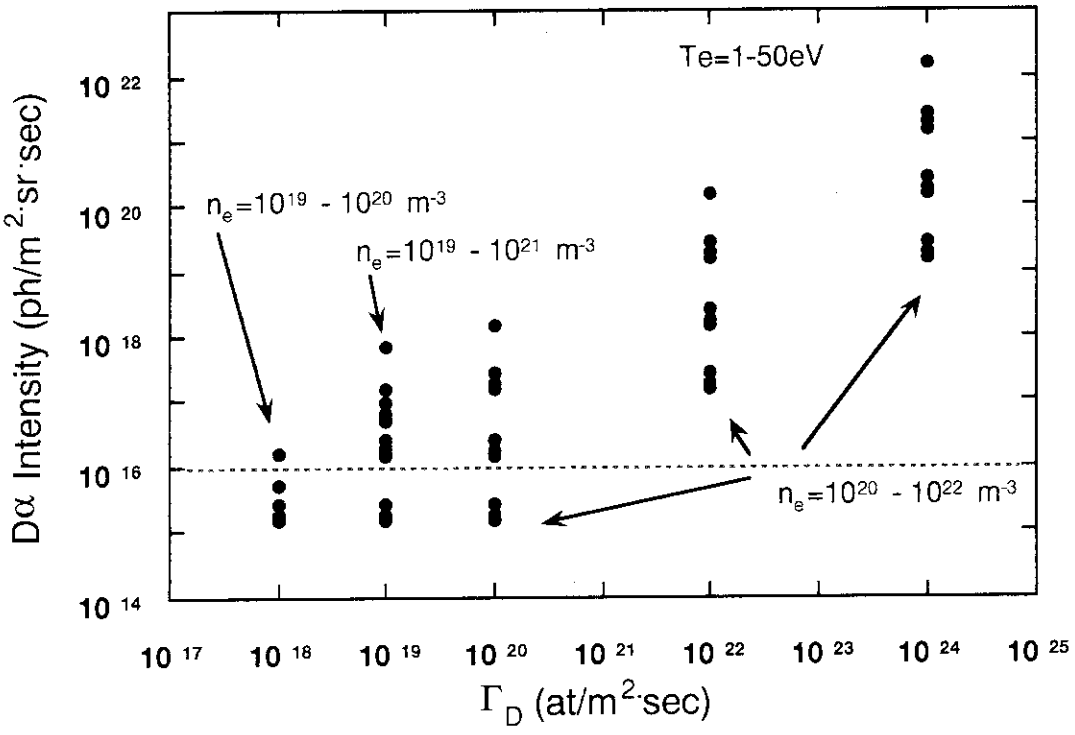

Fig.3.6-2 Dα intensities against influx densities of deuterium Γ_D for deferent electron densities.

Table 3.6-3 CII intensities against influx densities of carbon ion.

	wavelength (nm)	transition	influx (at / m2.sec)	ne (/m3)	Te (eV)	K S/XB	intensity (ph/m2.sr.sec)
CII	657.8	3s 2S-3p 2Po	1.00E+16		1		
			1.00E+16		5	1	7.95775E+14
			1.00E+16		10	4.2	1.8947E+14
			1.00E+16		50	25	3.1831E+13
			1.00E+18		1		
			1.00E+18		5	1	7.95775E+16
			1.00E+18		10	4.2	1.8947E+16
			1.00E+18		50	25	3.1831E+15
			1.00E+20		1		
			1.00E+20		5	1	7.95775E+18
			1.00E+20		10	4.2	1.8947E+18
			1.00E+20		50	25	3.1831E+17
			1.00E+21		1		
			1.00E+21		5	1	7.95775E+19
			1.00E+21		10	4.2	1.8947E+19
			1.00E+21		50	25	3.1831E+18

3.7 Neutron and γ-ray irradiation effect on the optical fiber

The neutron and γ-ray flux during the operation are described in the memorandum [1]. In the memorandum, the total (fast + thermal) neutron flux is 5.5×10^{11} ($m^{-2} \cdot s^{-1}$) and the γ-ray flux is 6.4×10^{11} ($m^{-2} \cdot s^{-1}$) just behind the vacuum vessel. These are very optimistic values, because this calculation dose not assume a hole on the vacuum vessel. At the divertor port, there are some holes. Therefor, the values will be higher than these ones. But, we use these values, because of no calculation at the divertor port.

The neutron and γ-ray irradiation effect on the optical fiber is investigated as shown in Fig.3.7-1 and 2 with JMTR and FSN in JAERI under the ITER EDA task number of T246. [2], [3] From these figures, the optical absorption intensity is plotted against the neutron fluence as shown in Fig. 3.7-3.

The length of the optical fiber inside the biological shield will be about 3 m. Therefore, if we allow optical absorption intensity of 3 dB/3m (1dB/m), the neutron fluence of 3×10^{14} n/cm^2 will be acceptable. This means the optical fiber just behind the vacuum vessel will survive ~5×10^6 sec (~ 5000 shots).

The estimation here is very optimistic and preliminary. More detailed and actual estimation will be necessary.

Reference

[1] S, Mori, S 82 MD 05 95-03-17 W3; San Diego JCT Interoffice Memorandum.
[2] T. Kakuta, et al., Sci. Rep. RIT **A40** (1994)153.
[3]T. Kakuta, et al., Proc. 9th Workshop on Radiation Detectors and Their Uses, 17-18 Jan. (1995) KEK, Tsukuba, Japan

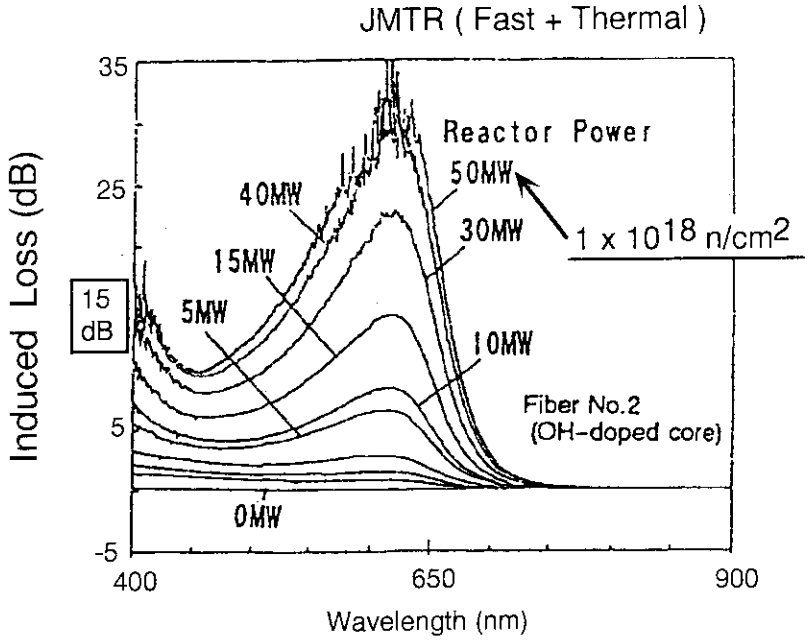

Fig. 3.7-1 Spectral absorption loss of OH-doped fiber. [2]

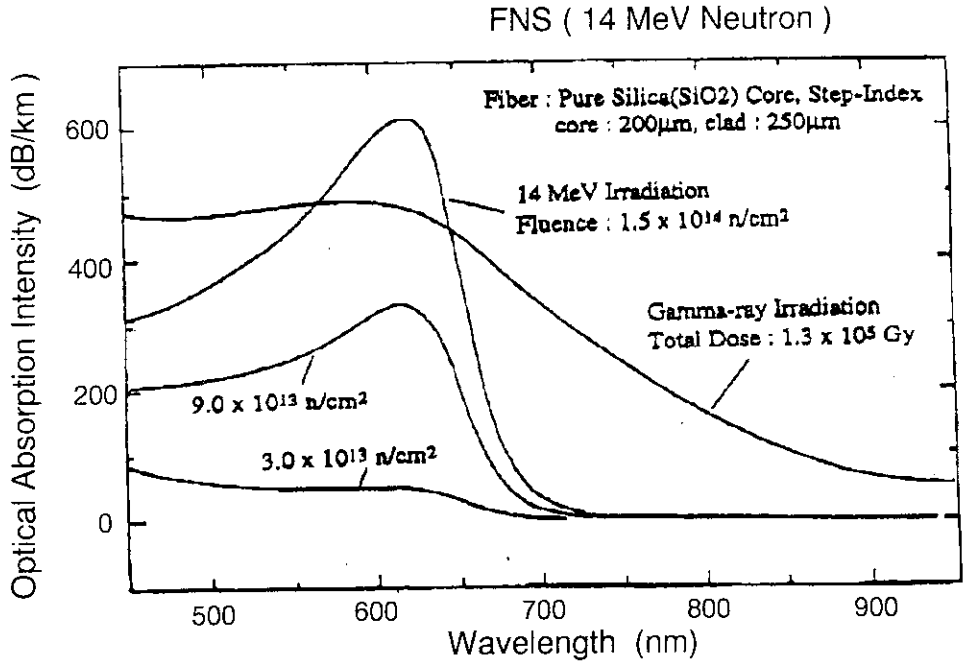

Fig. 3.7-2 Spectral induced absorption of pure silica core fiber during 14 MeV fast neutron irradiation as compared with Co-60 gammaray. [3]

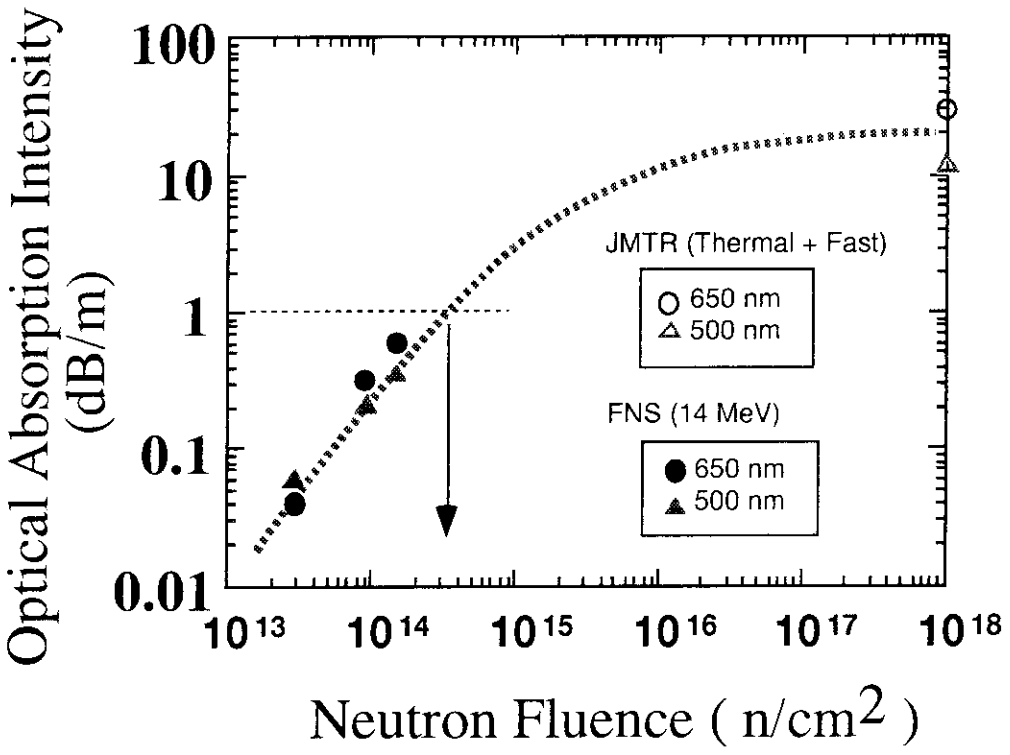

Fig. 3.7-3 Optical absorption intensity against neutron fluence.

4. Mechanical design

4.1 Main concept of mechanical design

According to the optical design and the design of the divertor diagnostic cassette, the mechanical system was designed under the following main concept.

(1) In order to absorb the movement and vibration of the optical axis, the fiber coupled optical system is introduced to the light transmission from the out of the vacuum vessel to the spectrometers.

(2) In order to prevent the independent movement of the optical axis, all of optical components are adjusted before the operation and fixed tightly on the divertor cassette and the diagnostic port. After the operation, the optical axis can not be adjusted.

4.2 Optical arrangement

The arrangement of the optical components is shown in Fig. 4.2-1 and Fig. 4.2-2. The light emitted at the divertor region is collected and reflected at the first mirrors made of molybdenum which are mounted on the divertor cassette and transported through the bottom of divertor cassette to the diagnostic port. The light is reflected by two plane mirrors to make a dog-leg optical pass for the neutron shield. The vacuum window is located between these mirrors. The light is focused on the optical fiber bundle by using the Cassegraine optics located just after the dog-leg optics. After that, the light is transmitted to the spectrometer by the fiber bundle through the wall of the cryostat using the optical feed through. In the pit area, optical components such as a spectrometer and a pre-divider are mounted on the transport cask owing to the easy remote handling. Cables and fibers are connected to the terminal boxes and laid to the diagnostic room. Other optical components and a data acquisition system are located in the diagnostic room.

4.3 Details of optical component

4.3.1 Optical component in the divertor cassette

Figure 4.3-1 shows the schematic view of the optical component in the divertor cassette. Details of the optical arrangement in the divertor cassette are shown in Fig. 4.3-2. The two mirror units are installed on the divertor cassette. One is located on the divertor dome and the other is located on the bottom of the divertor cassette. The mirror units 1 shown in Fig. 4.3-3 consists of four toroidal mirrors made of molybdenum. Two of them are used for the filter spectrometer (FS) of IV and OV chords. And the others are used for the visible survey spectrometer (VSS) and the high dispersion spectrometer (HDS) of IV and OV chords. The space resolution of the viewing fans of IV and OV for FS is changed

by using the different curvature of the toroidal mirrors. The size of this mirror unit is 280x96x263 mm.

The mirror unit 2 shown in Fig. 4.3-4 and Fig. 4.3-5 consists of two toroidal mirrors for OH and IH chords of FS and two plane mirrors for reflecting the light from viewing fans of IV and OV. These mirrors are also made of molybdenum. The size of mirror unit 2 is 593x230x170 mm. The cross section of the light path is about 150 x 150 mm.

These two mirror units are mounted at the time of the installation of the diagnostic divertor cassette. This mirror units are adjusted before the pumping and fixed tightly. After that, we will not be able to adjust those units.

4.3.2 Windows and fiber interface optics

The light passed through near the bottom of the divertor cassette and the diagnostic port is reflected by two plane mirrors to make a dog-leg optical path for the neutron shielding as shown in Fig. 4.3-6. These two mirrors are mounted on the mirror folder which are also adjusted before the pumping. The size of mirrors in the divertor port including the neutron shielding are 1500 mm x 1404 mm x 963 mm. The vacuum window made of quartz glass is located between them. The effective diameter of the window is 150 mm. The window is a very important R & D item in ITER. The light from the divertor is focused on the fiber bundle of each optical path by using the off-axis Cassegraine optics. The first and the second Cassegraine mirrors are also mounted on the mirror folders which are fixed on the same optical base as shown in Fig. 4.3-7. As a difference of the focal points for each of viewing fans, the lights from the different viewing fans are focused on the surface of the fiber bundles which are located on the different position as shown in Fig. 4.3-8. The size of this optical system in the cryostat is 2300 mm x 450 mm x 963 mm.

4.3.3 Optical feed through

It is obvious that the multichannel optical feed through is one of the most important R&D item. Figure 4.3-9 shows one example of the possible systems. The collimators and receivers, which consist of achromatic lenses, are located on the same optical axis. In this example, the size of the window is 337mm diameter for 645 channels. It is necessary to carry out more details design and also to consider other possible optical methods such as a multi-channel fiber feed through.

4.3.4 Optical component in the pit area

Figures 4.3-10 and 4.3-11 shows the schematic view of the optical component in the pit area. The optical fibers from the optical feed through are connected with

the push-on optical connectors for the easy maintenance and then transported to the pre-divider (PD) for VSS and HDS system and FS which are mounted on the moving cask. Spectrometers for the wavelength region of below 500 nm are mounted in this area. Other spectrometers and the data acquisition systems are located on the diagnostic room. The schematic view of the spectrometers and the pre-dividers are shown from Fig. 4.3-12 to Fig. 4.3-17. The sizes of each optical equipments are shown in Table 4.3-1. In this design, the pre-divider and FS are prepared for each of optical fibers. So, 560 sets of FS and 40 sets of pre-dividers were located in this area. The size of the optical system on the transport cask is 5300mm x 2400mm x 2600mm.

We are also considering a multi-channel filter spectrometer (type 1) as described in section 3.5.2.

Table 4.3-1 The size and number of each spectrometers used in this system

	size (W x L x H mm)	Number of Spectrometer
HDS	1000 x 1600 x 450	3
VSS	1300 x 1500 x 450	4
FS	365 x 90 x 60	560
PD/HDS	170 x 200 x 60	20
PD/VSS	285 x 100 x 60	20

The optical fibers and wire cables are terminated at the fiber box and the wire box just beside the transport cask and laid to the diagnostic room. The sizes of each boxes are 700 mm x 800 mm x 1750 mm for the wire box and 900 mm x 1000 mm x 2950 mm for the fiber box. These boxes are fixed on the floor of the pit area.

4.3.5 Optical component in the diagnostic room

Figures 4.3-18 and 4.3-19 show the schematic view of the optical components in the diagnostic room. The fibers from the fiber boxes are transported to the each spectrometers sitting in the racks. The output signals from the detectors are transported to the local data acquisition system. The occupied area of the optical components and the data acquisition system in this room is estimated to be 10050 mm x 3289 mm on the floor.

4.4 Calibration system

Figure 4.4-1 shows the schematic view of the calibration system for monitoring the transmission of the optical path. As a light source, the monochromator is used to make the monochromatic light. The light is divided into two beams by a half mirror before the entrance of the optical fiber. The one of them is a reference and the other is a probe light beam. The optical fiber is

prepared for each optical path (one for each viewing fan). The four light beams are transported through the same optical path for measurement and reflected by the corner cube mirrors installed on the divertor cassette and returned to the diagnostic room. The advantage of this system is easy to measure the wavelength dependence of the transmission rate but the measured transmission rate includes the change of the reflectivity of the corner cube mirrors. The corner cube mirrors will be degraded by irradiation, particle spattering and so on. Therefore the corner cube mirrors must be mounted on the area in which the degradation is small to change the reflectivity. The choice of the material is also important.

4.5 Remote handling

For the avoidance of the reduction of the transmission rate, the optical fibers and the optical components in the cryostat and the diagnostic divertor cassette must be changed at the same time of the change of the divertor cassette it self. Figure 4.5-1 shows the concept of the remote handling maintenance system schematically. All of the optical component except for the wire box and fiber box are mounted on the transport cask (Fig. 4.5-1(a)). At that time the fibers are removed from the fiber connector in the pit area by using a pusher and then the double doors are closed in order to avoid the contamination(Fig. 4.5-1(b)). The transport cask are transported to the maintenance area (Fig. 4.5-1(c)). After that, the remote handling cask comes to the pit and opens the double door and removed all of the optical components in the cryostat and installed new optical component by the remote handling equipment(Fig. 4.5-1(d)). Details must be discussed with the remote handling group.

4.6 Analysis of the electro-magnetic stress during disruption

Rapid decay of the plasma current during the disruption affected the large stress on the optical component. Therefore this effect on the Cassegraine optical base were roughly estimated. In this estimation, followings are assumed;

(1) Because the Cassegraine optics are located out of the toroidal coils, only poloidal field (B_p) is considered for the estimation.
(2) The strength of B_p is about 0.5 T as shown in Fig.2.2-2 and is constant during the disruption.
(3) The decay rate of the plasma current including the skin effect of the vacuum vessel is 24 MA/s.
(4) The size of the Cassegraine optical base is 500 x 2300 x 20 mm which is made of the stainless steel.

The basic equations are as follows;

$$F = I \times l_2 \times B_p \qquad (4.6\text{-}1)$$

where F is the electromagnetic force, I is the current induced by the disruption, l_2 is the length of the base and B_p is the external poloidal field. I is expressed as follows;

$$I=[l_1 l_2 d/8\rho(l_1+l_2)](\mu_0/2\pi r_0)\partial I_p/\partial t \qquad (4.6\text{-}2)$$

where l_1, l_2 and d are geometry of the base shown in Fig. 4.6-1, $\partial I_p/\partial t$ is the decay rate of the plasma current during the disruption, ρ is the resistivity of the base, and r_0 is the distance from the plasma center.

By using the equation and above-mentioned parameters ($\partial I_p/\partial t$=24MA/s, B_p=0.5T, r_0=10.36m, l_1=0.5m, l_2=2.3m and d=0.02m), F=37 kgf is obtained.

As the result, the electromagnetic stress on the Cassegraine optical base is not serious during the disruption. But detailed analysis should be necessary for the stress on the optical component in the divertor cassette because of the large toroidal field.

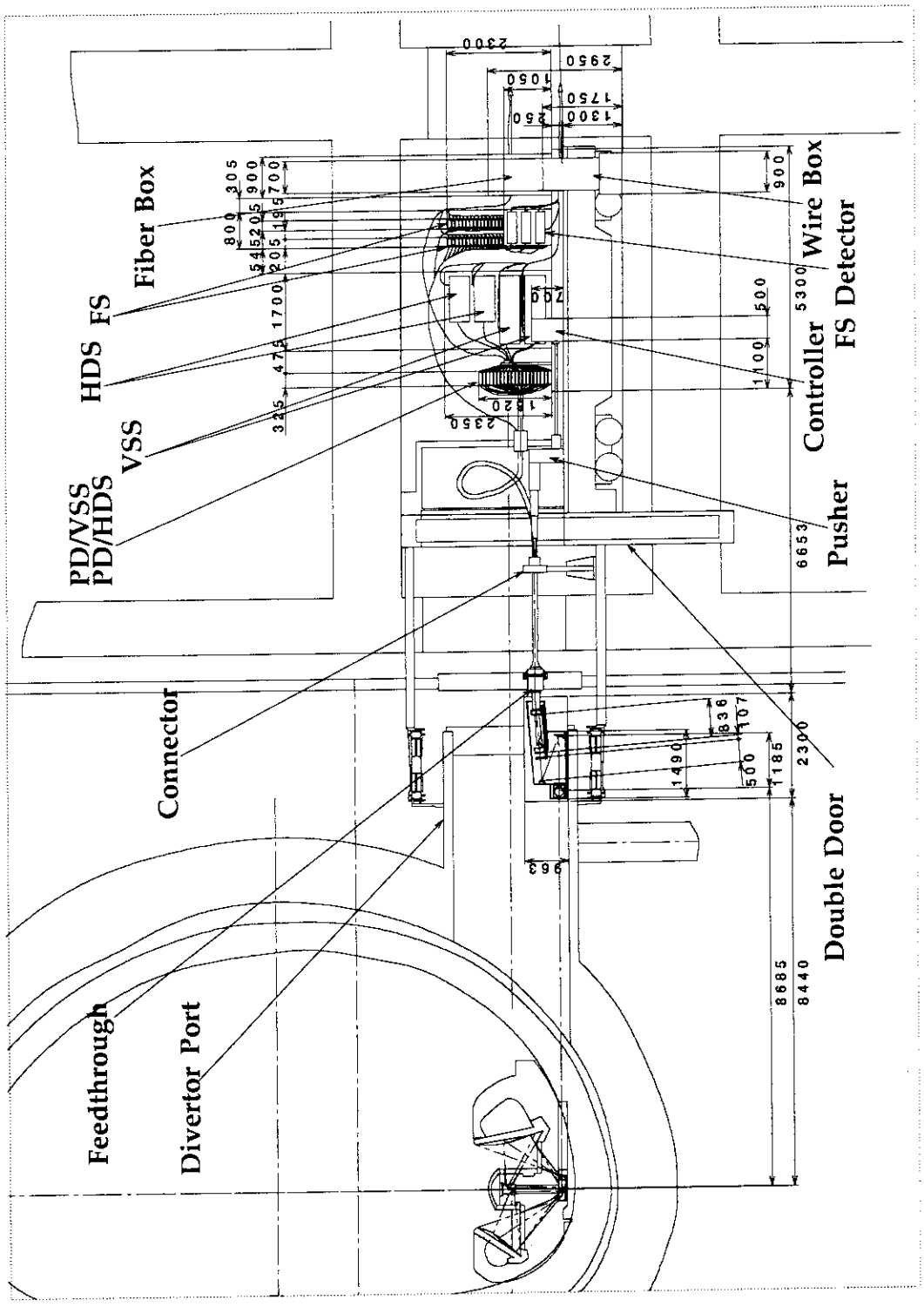

Fig.4.2-1 Side View of Divertor Impurity Monitoring System

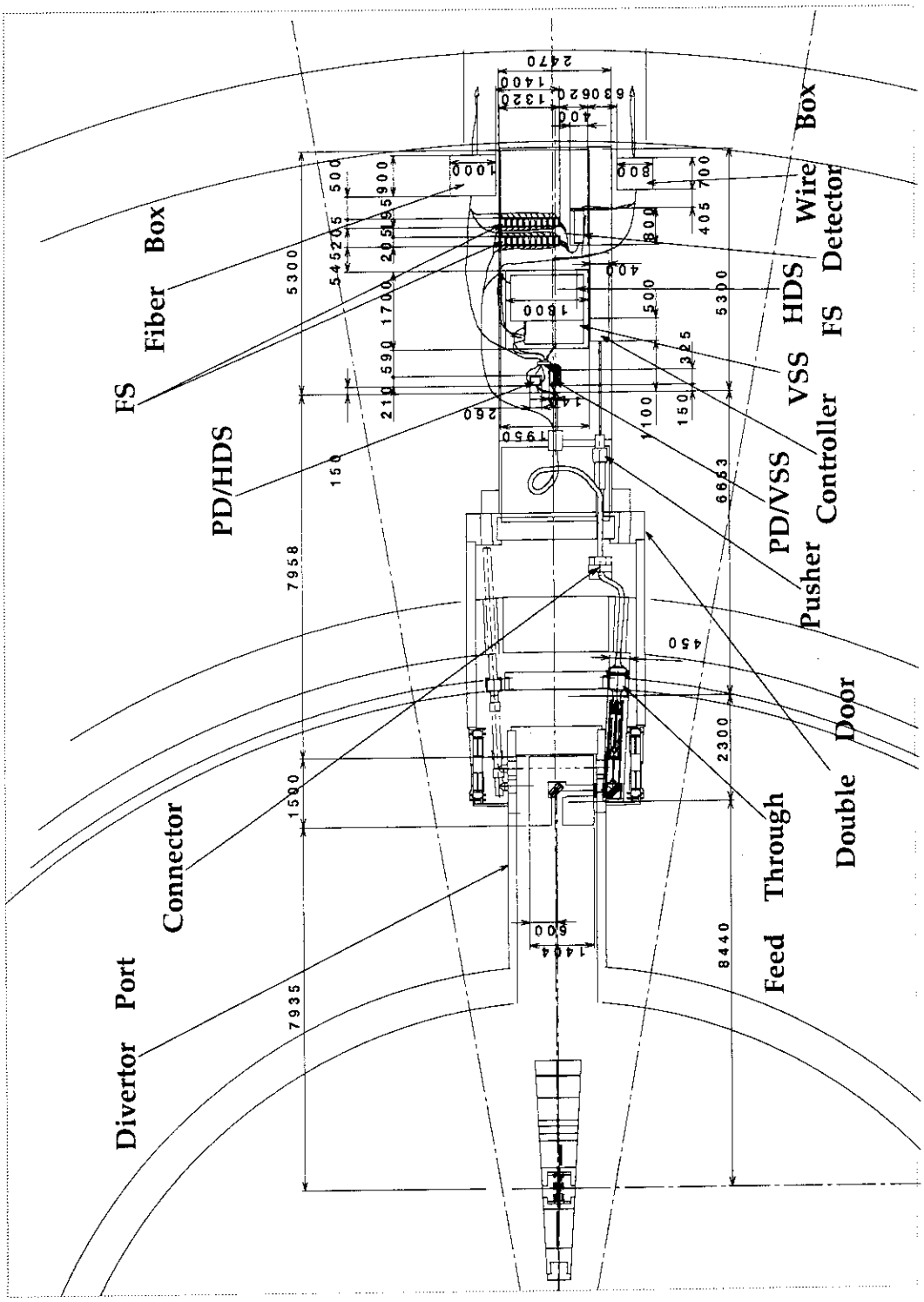

Fig.4.2-2 Top View of the Divertor Impurity Monitoring System

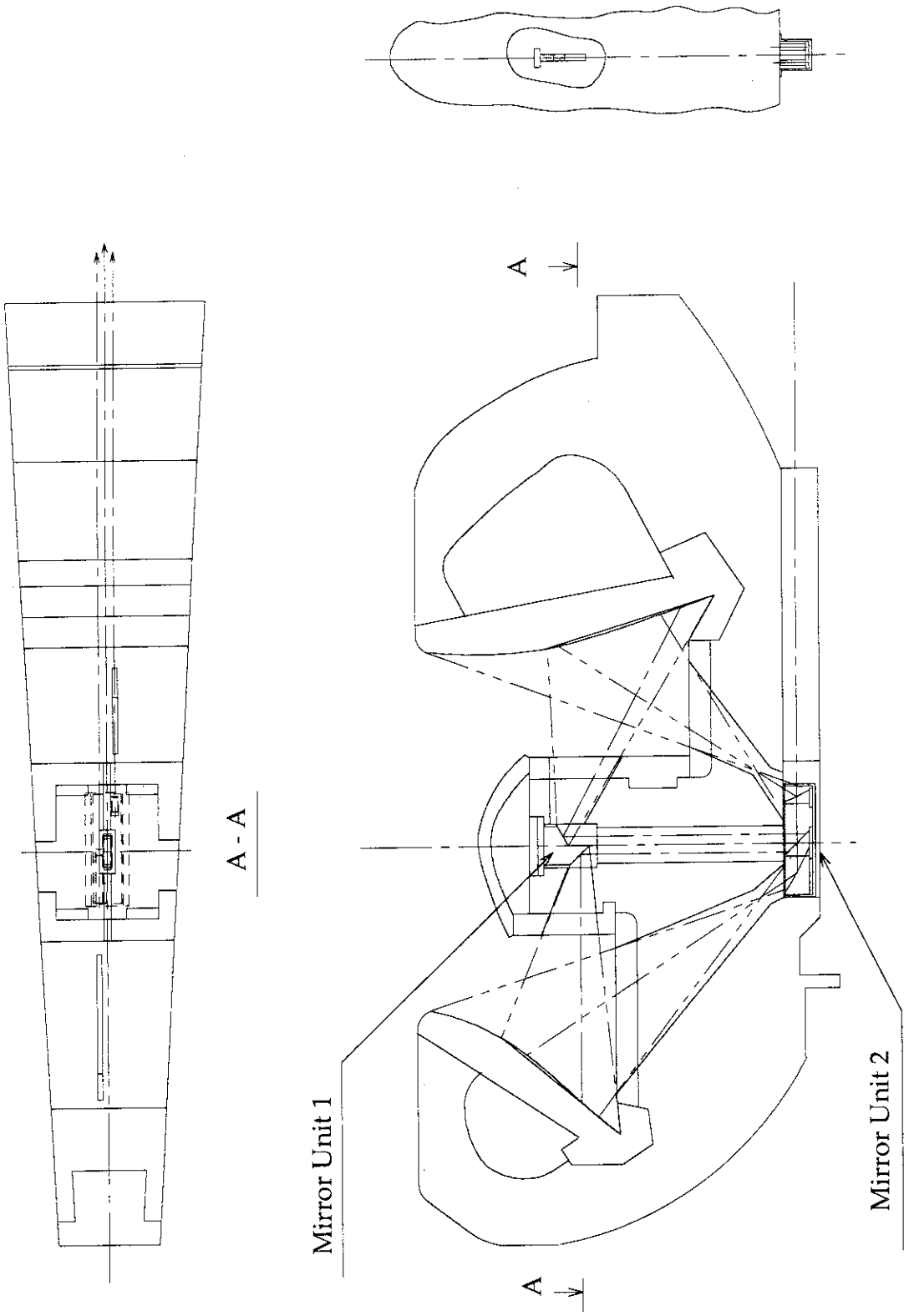

Fig.4.3-1 Optical Components in Divertor Cassette

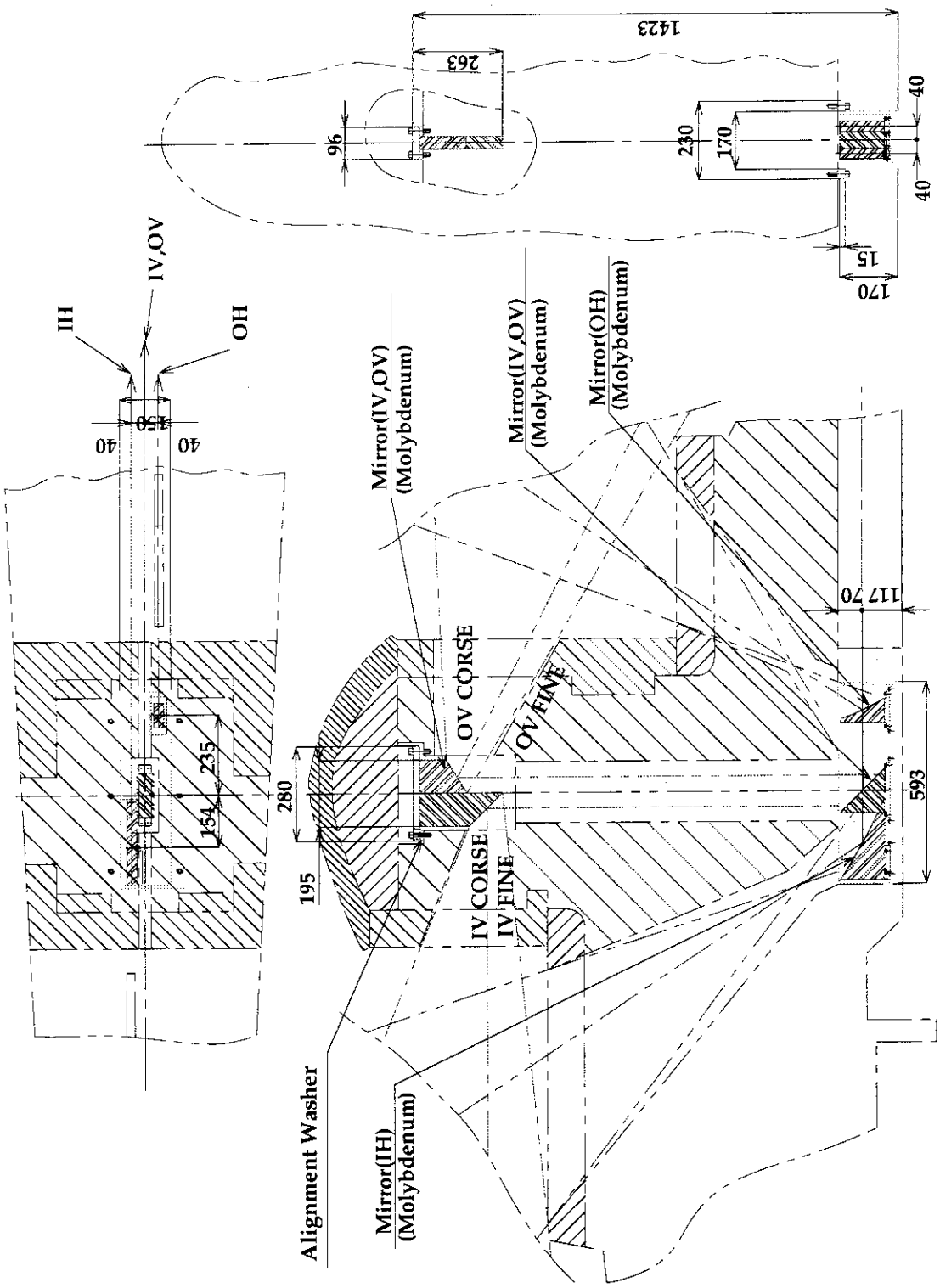

Fig.4.3-2 Detailes of Optical Arrangement in Divertor Cassette

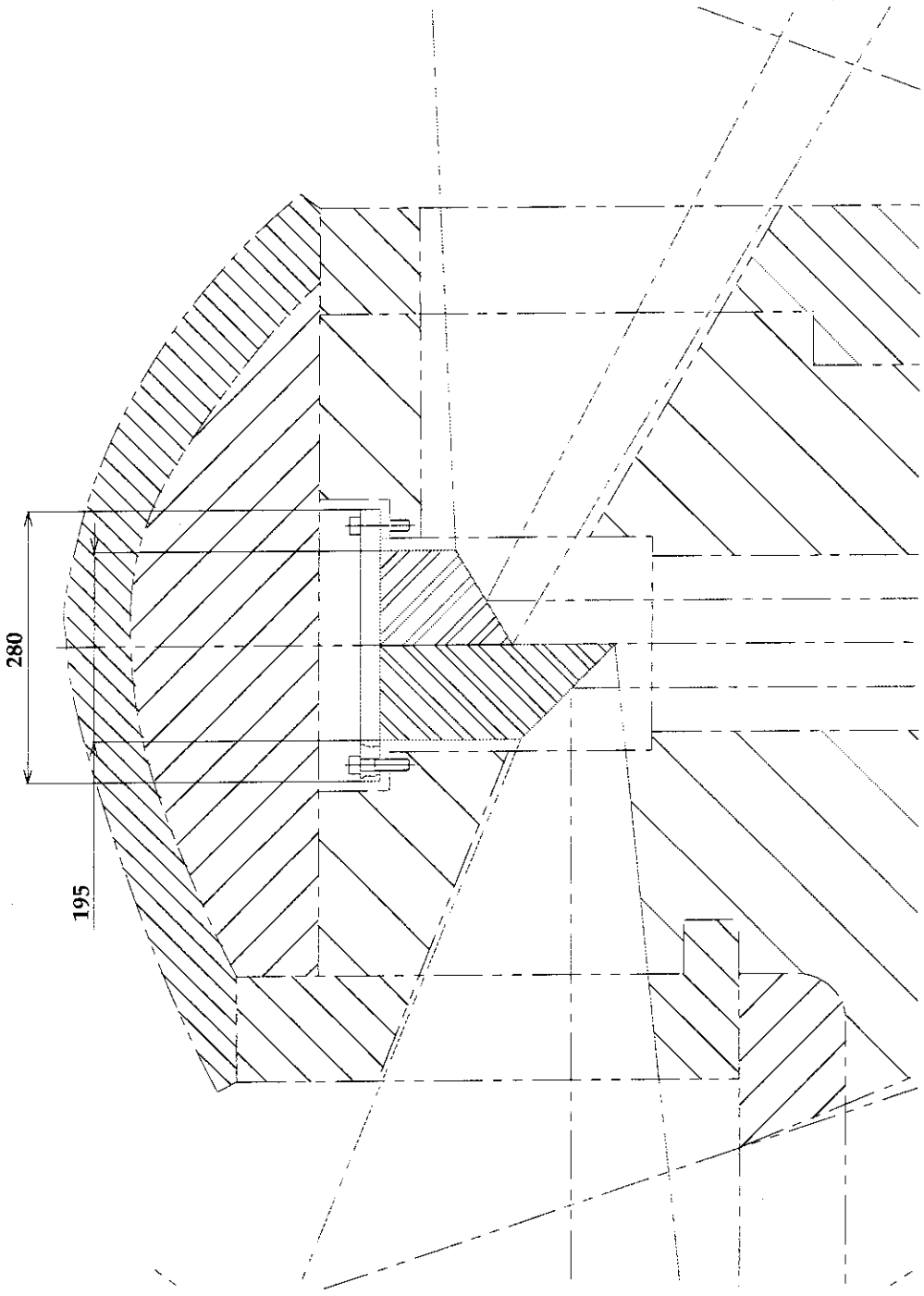

Fig.4.3-3 Side View of Mirror Unit 1

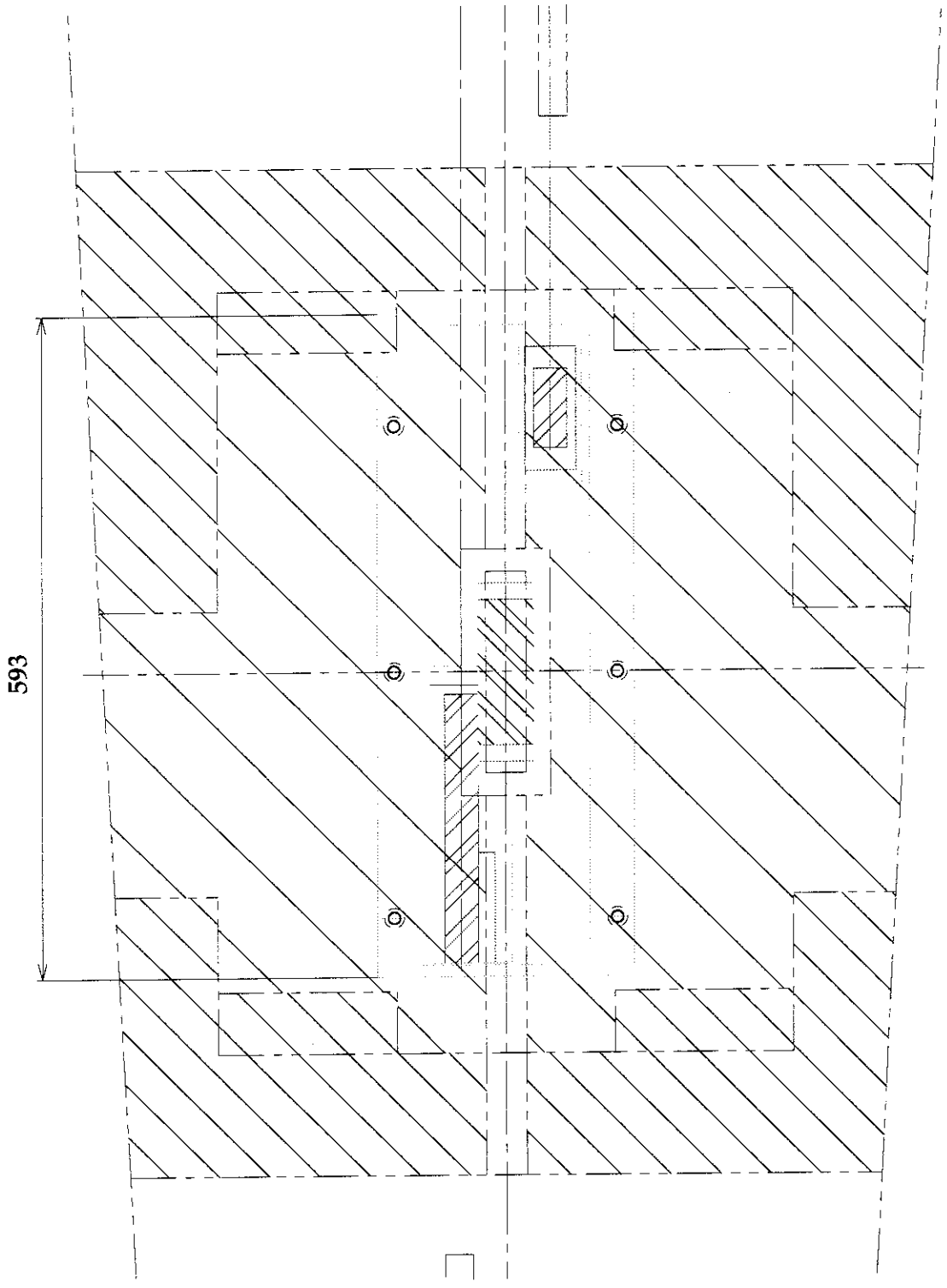

Fig.4.3-4 View of Optical Arrangement of Mirror Unit 2

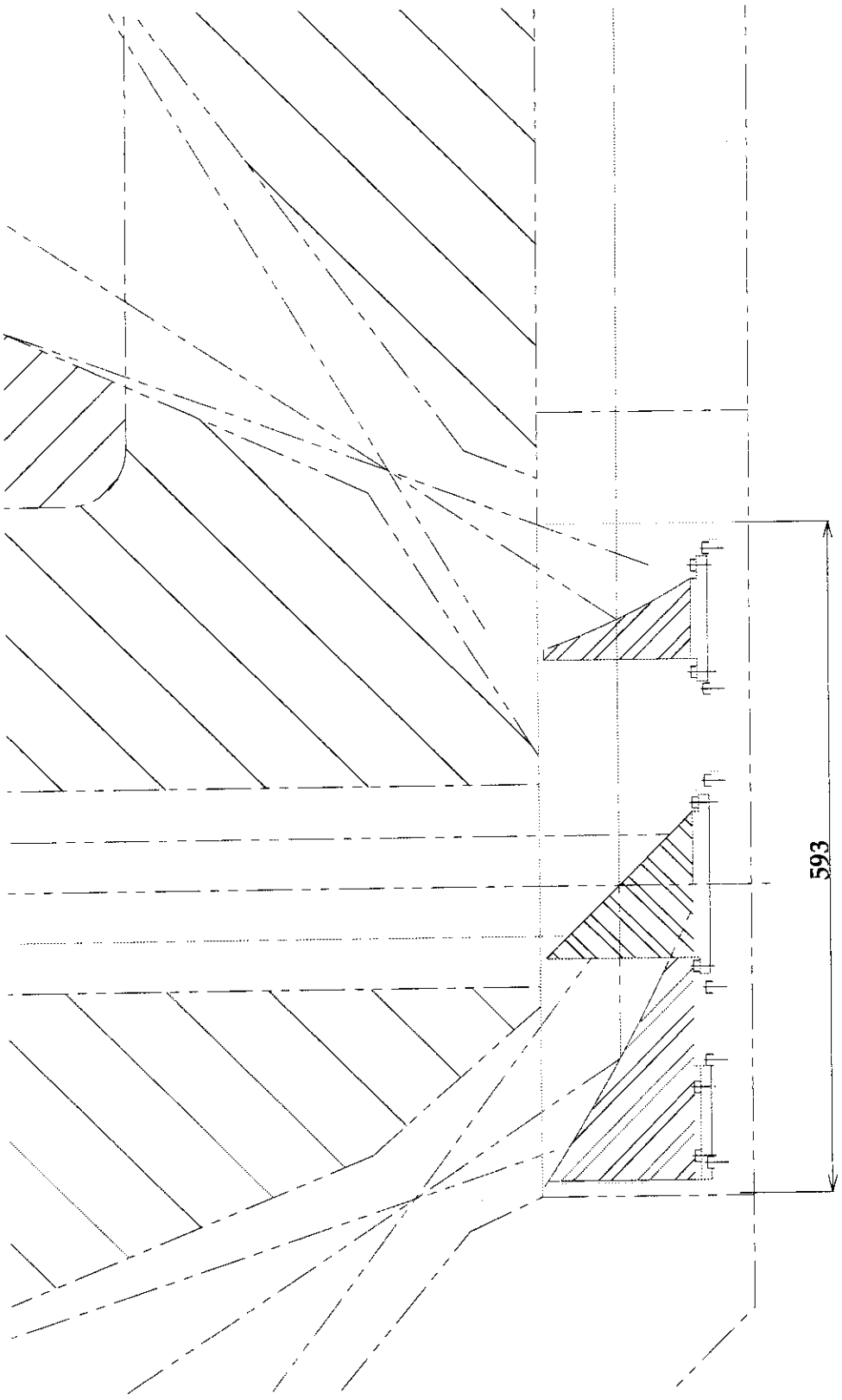

Fig.4.3-5 Side View of Optical Arrangement of Mirror Unit 2

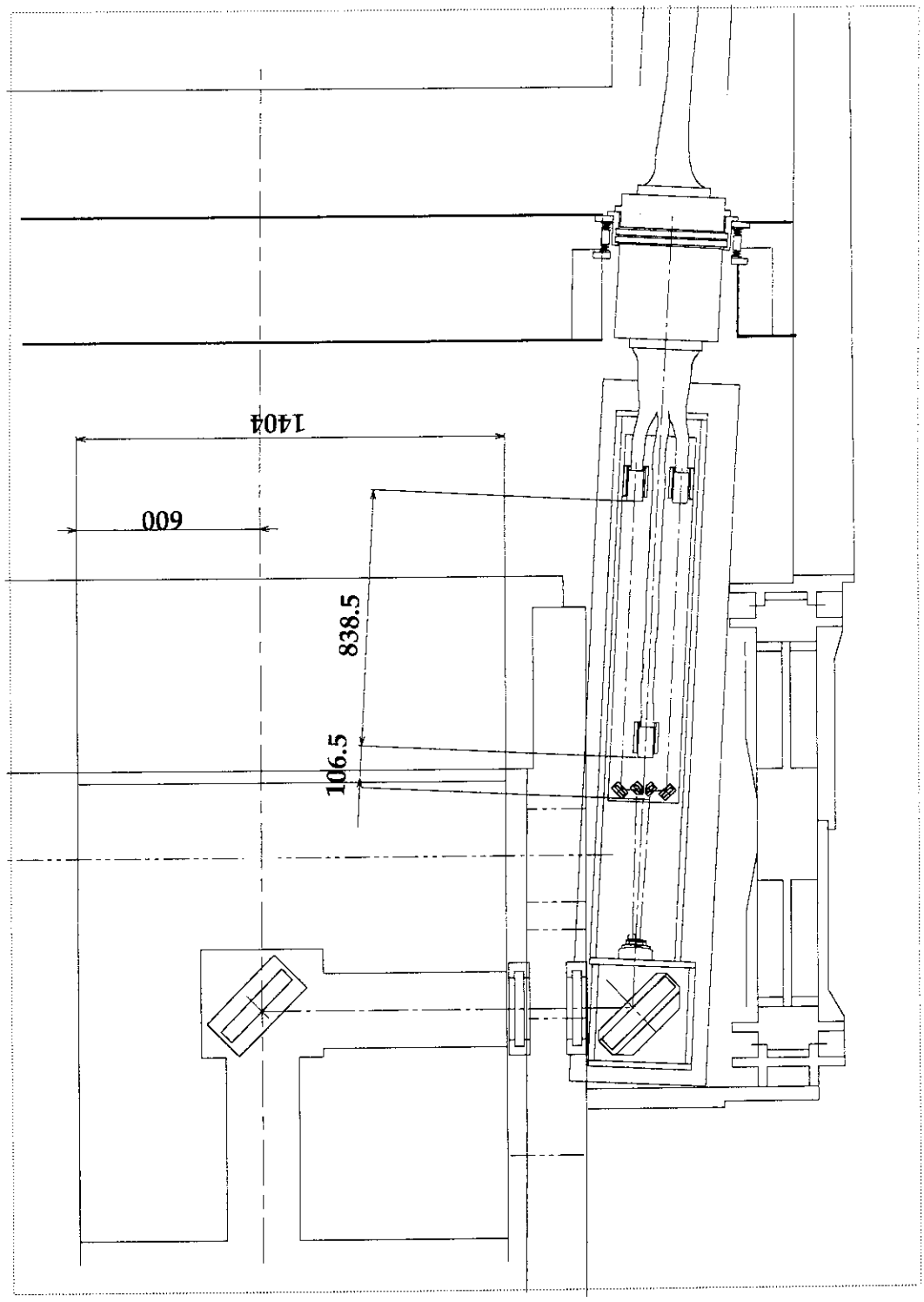

Fig.4.3-6 Top View of Fiber Coupling Optics

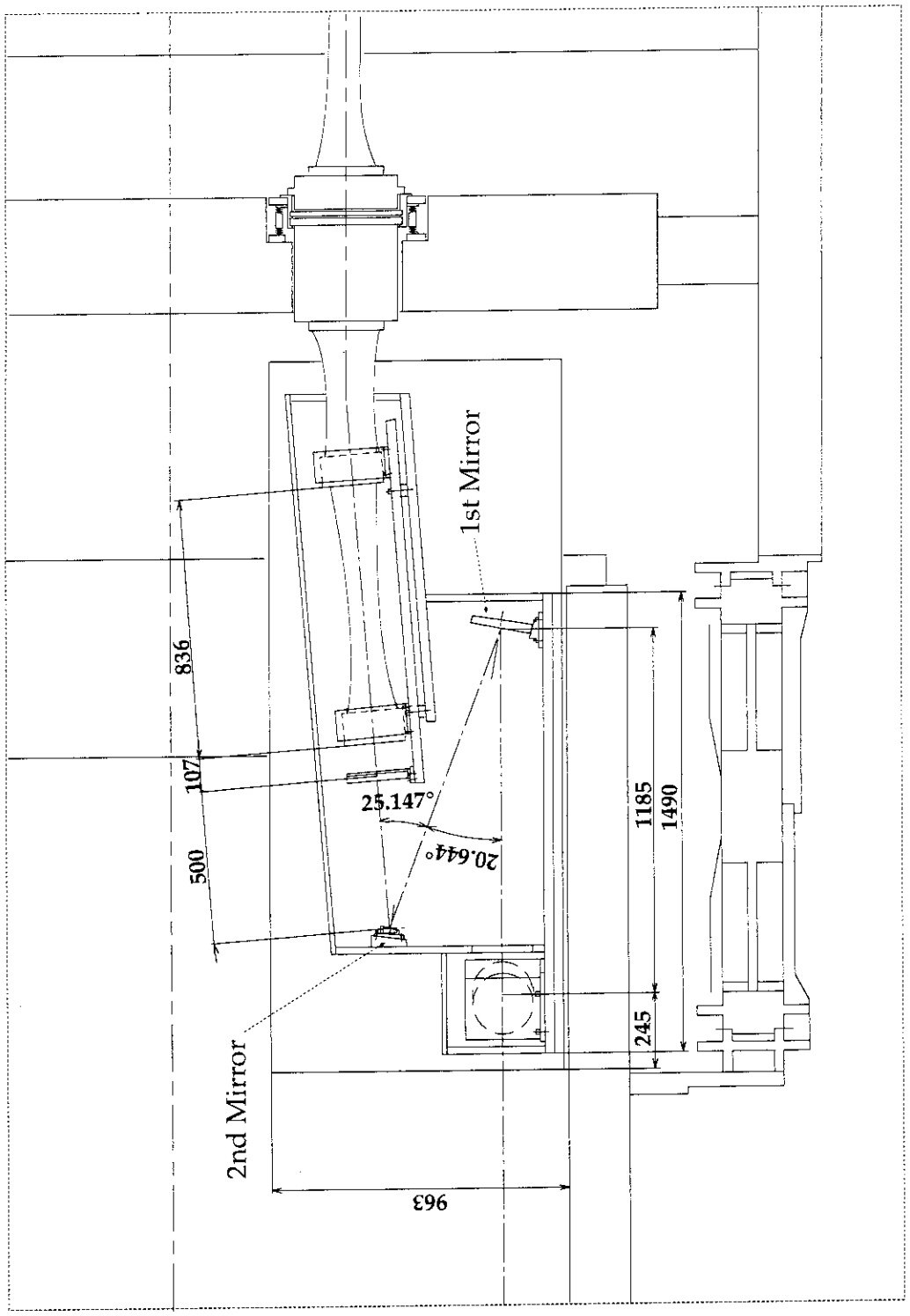

Fig.4.3-7 Side View of Fiber Coupling Optics (off-axis Cassegraine optics).

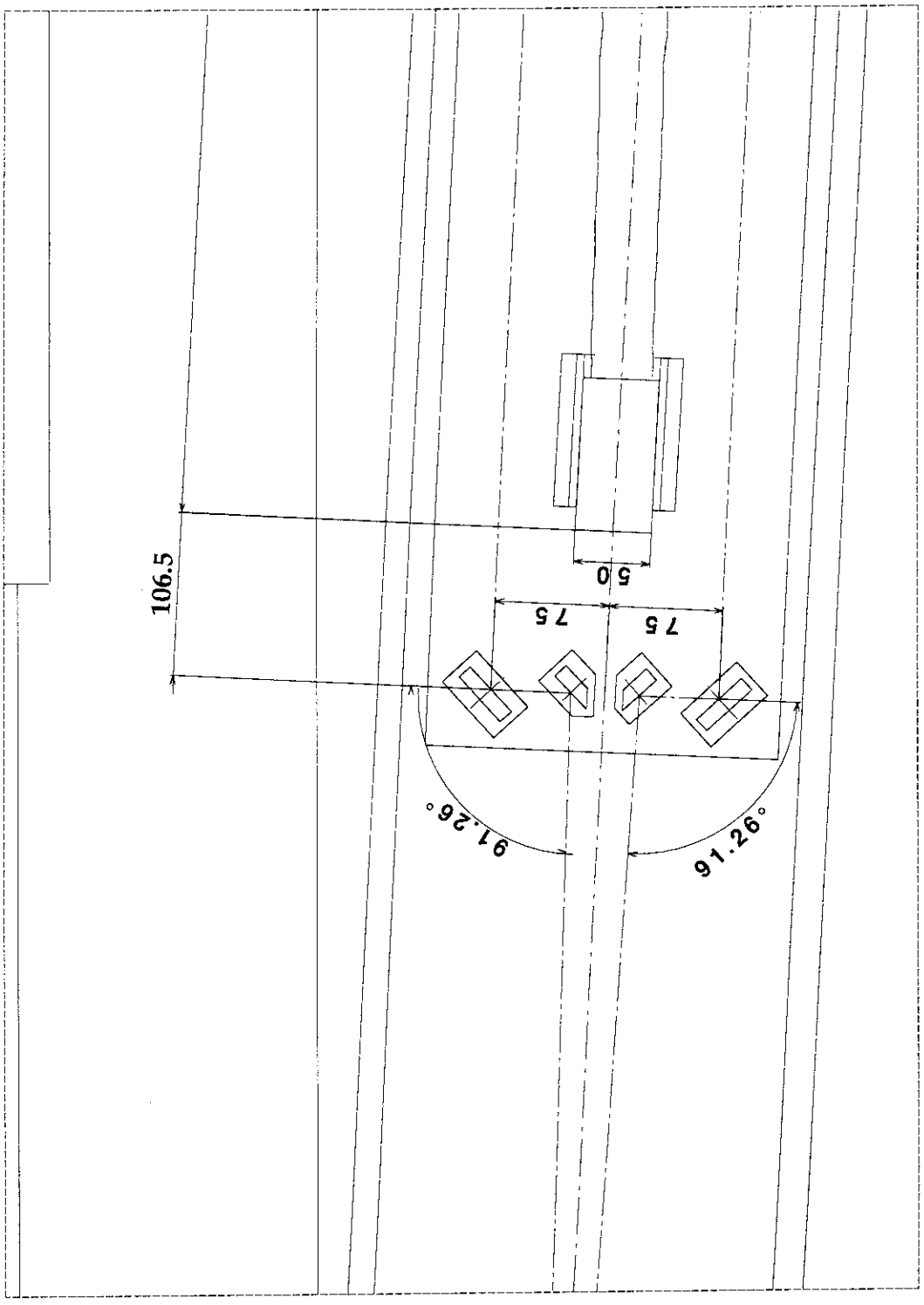

Fig.4.3-8 Detailes of Fiber Coupling

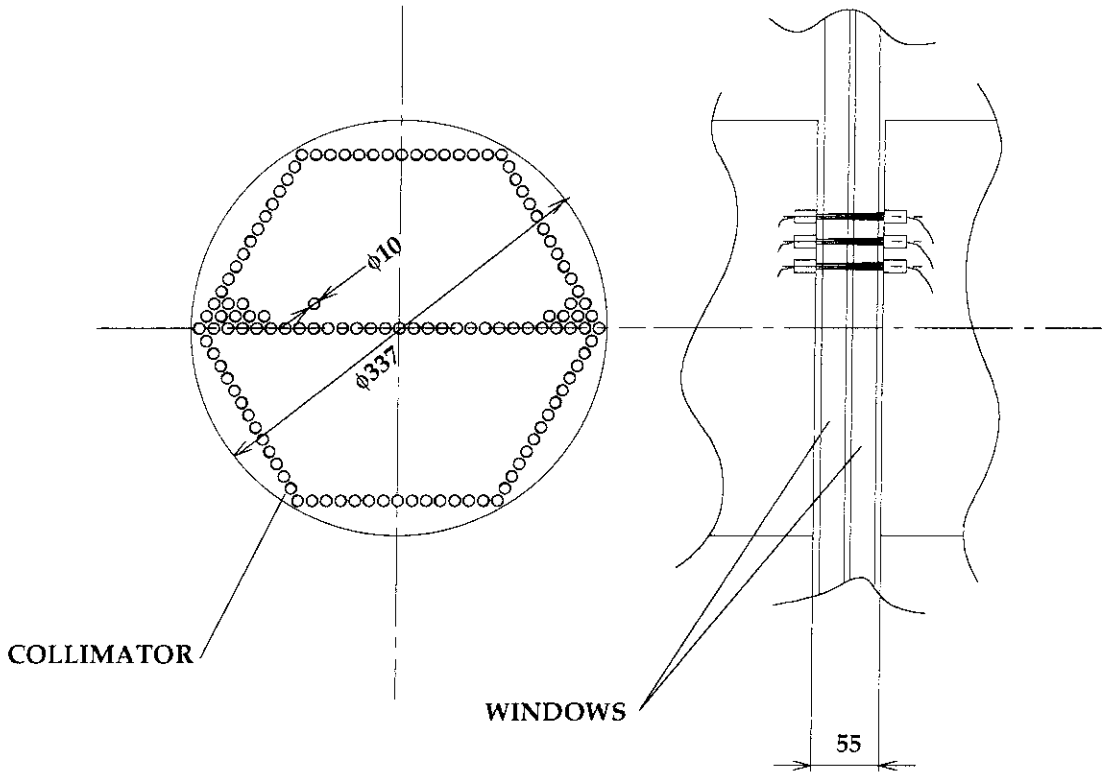

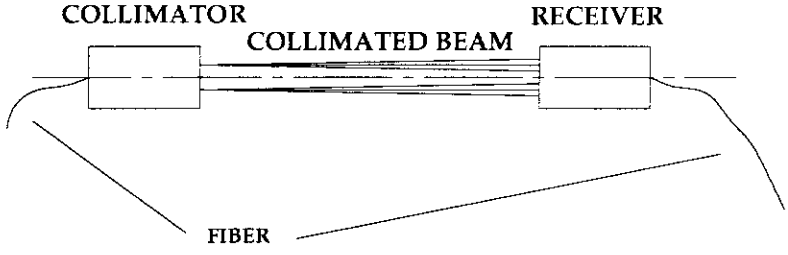

NUMBER OF FIBERS

	IH	OH	IV	OV
FS	140	140	140	140
VSS	0	0	10	10
HDS	0	0	10	10
CAL	1	1	1	1
ALI	1	1	1	1

TOTAL 608

Fig.4.3-9 Optical Arrangement of Fiber Feedthrough

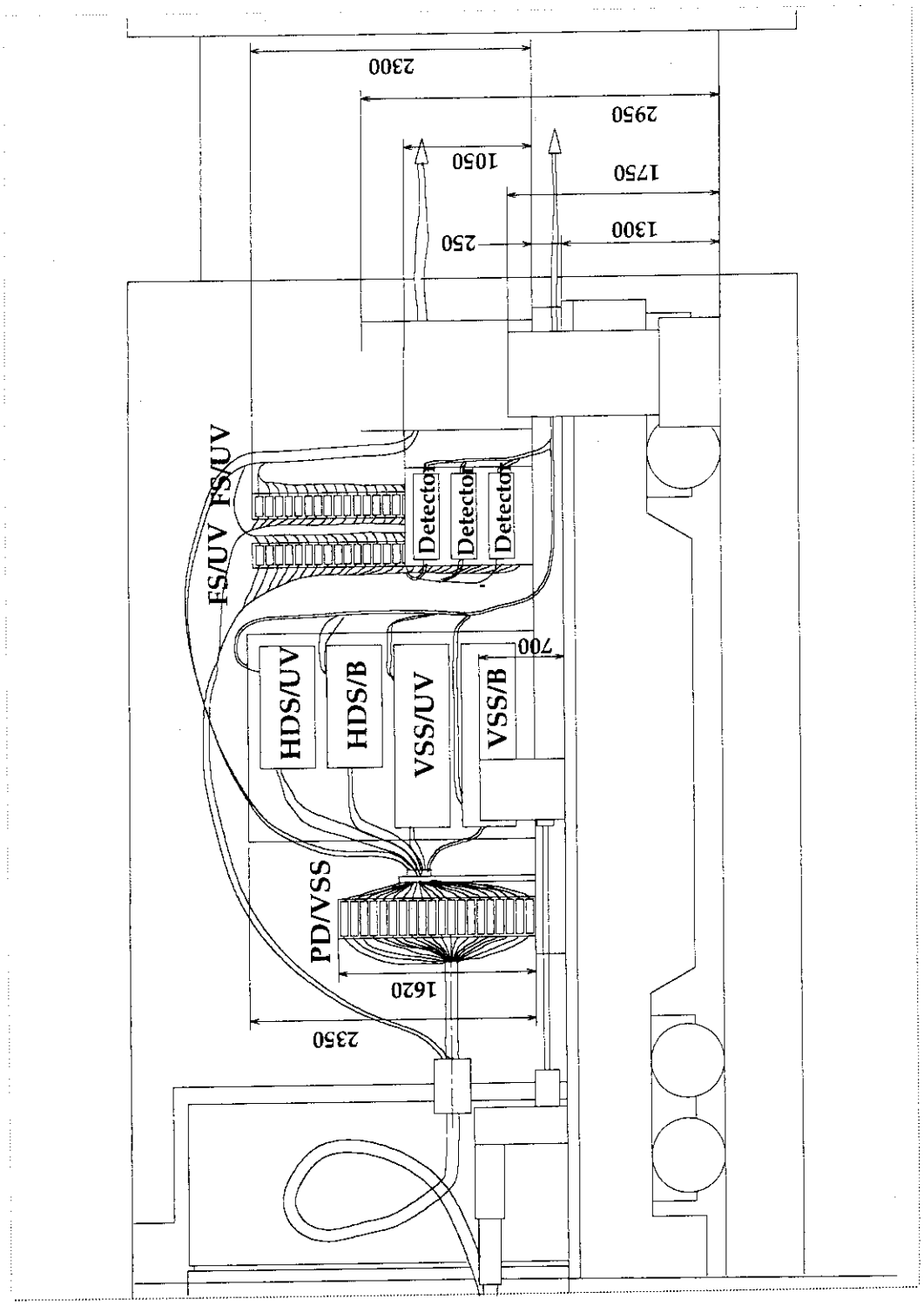

Fig.4.3-10 Side View of Optical Arrangement in the Pit Area

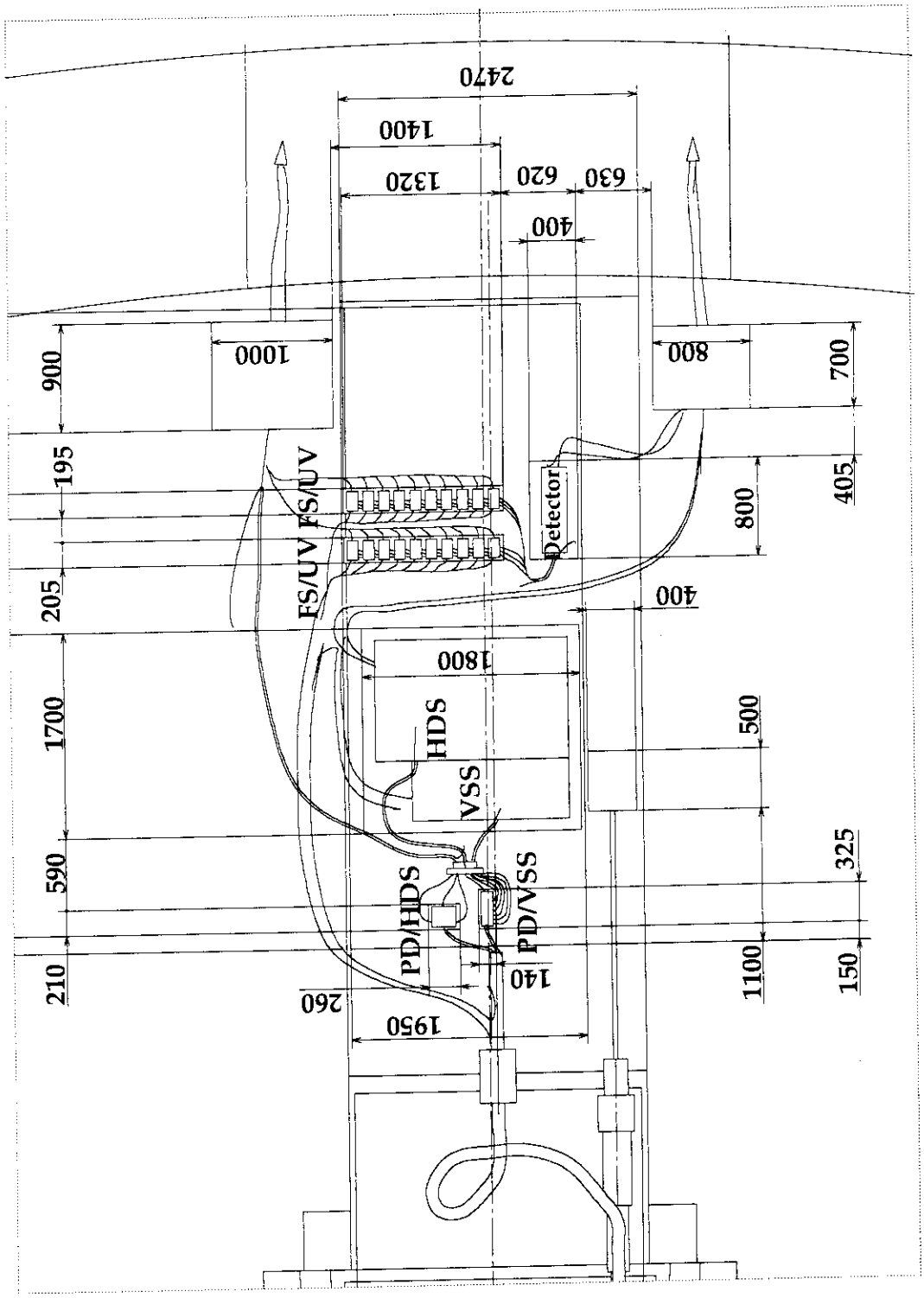

Fig.4.3-11 Top View of Optical Arrangement in the Pit Area

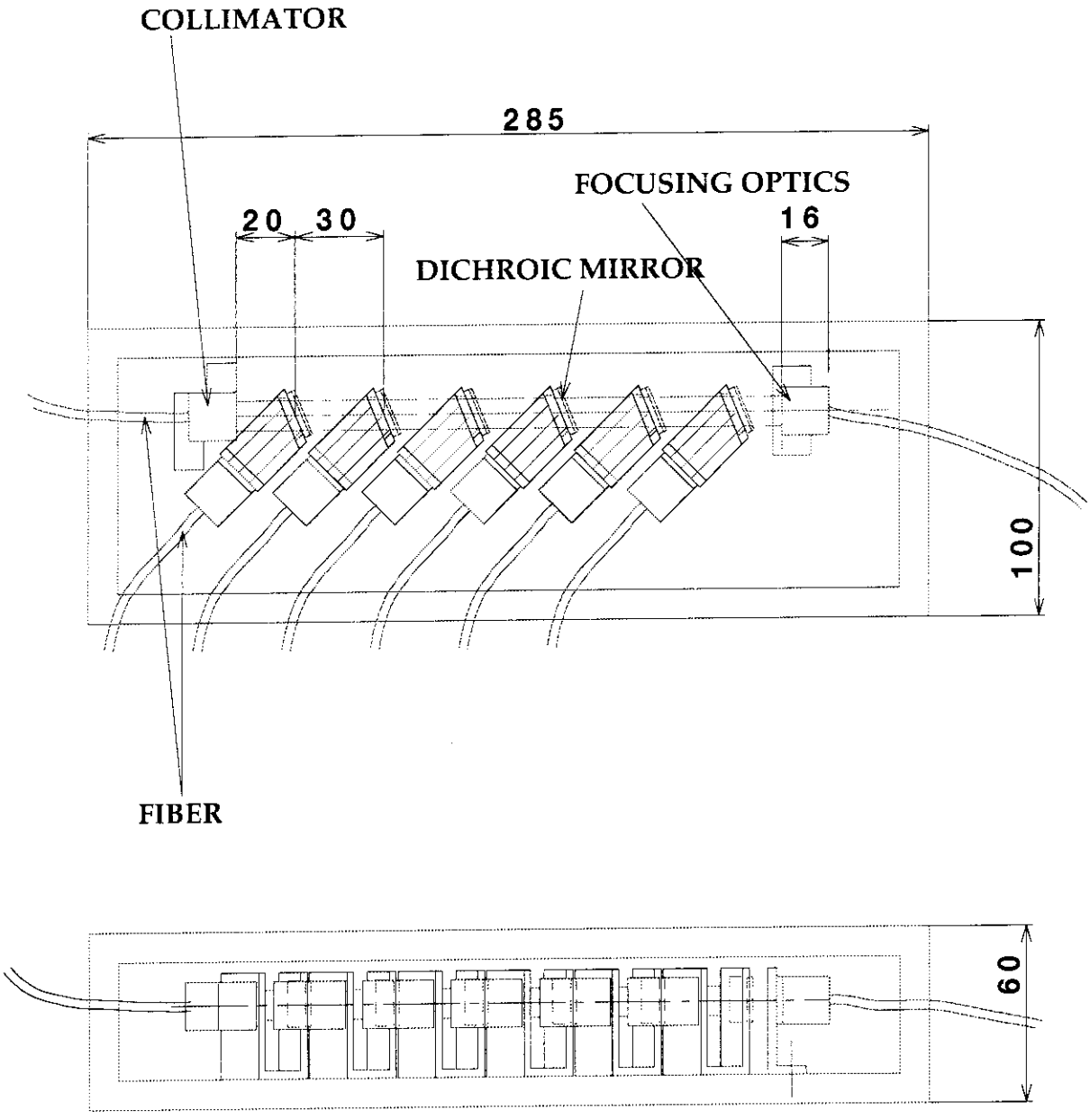

Fig.4.3-12 Optical Arrangement of Pre-Divider for Visible Survay Spectrometer

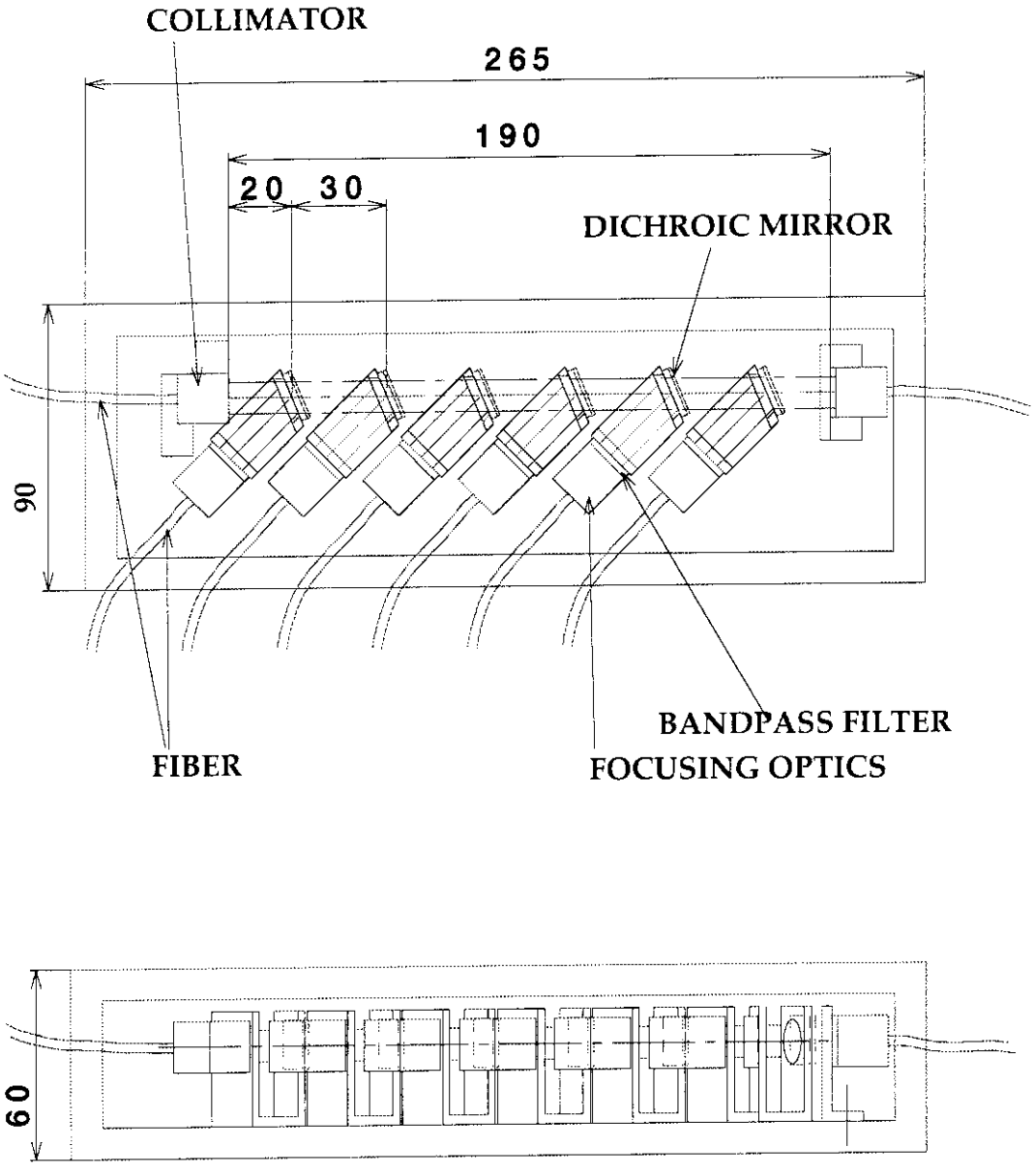

Fig.4.3-13 Optical Arrangement of Filter Spectrometer

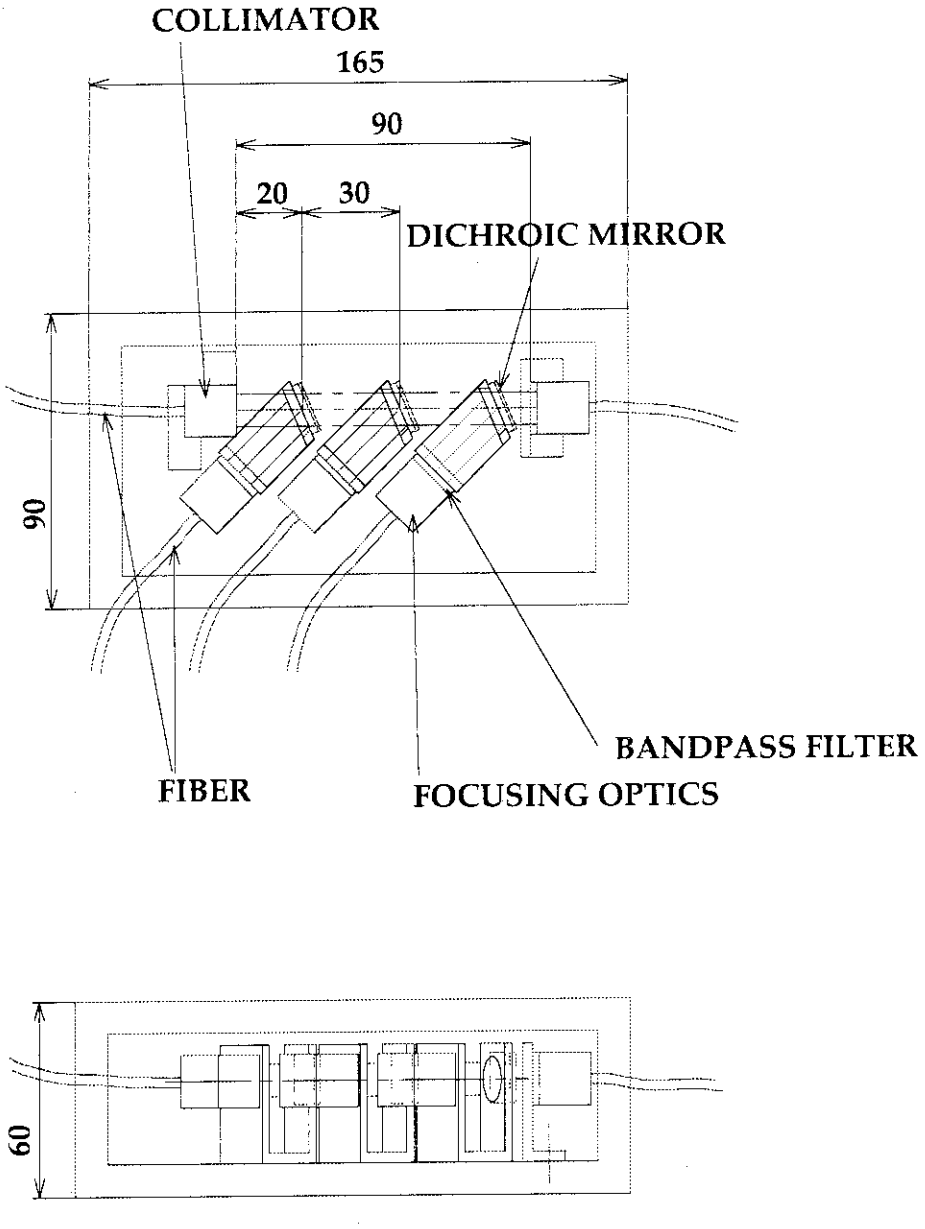

Fig. 4.3-14 Optical Arrangement of Filter Spectrometer for UV Region

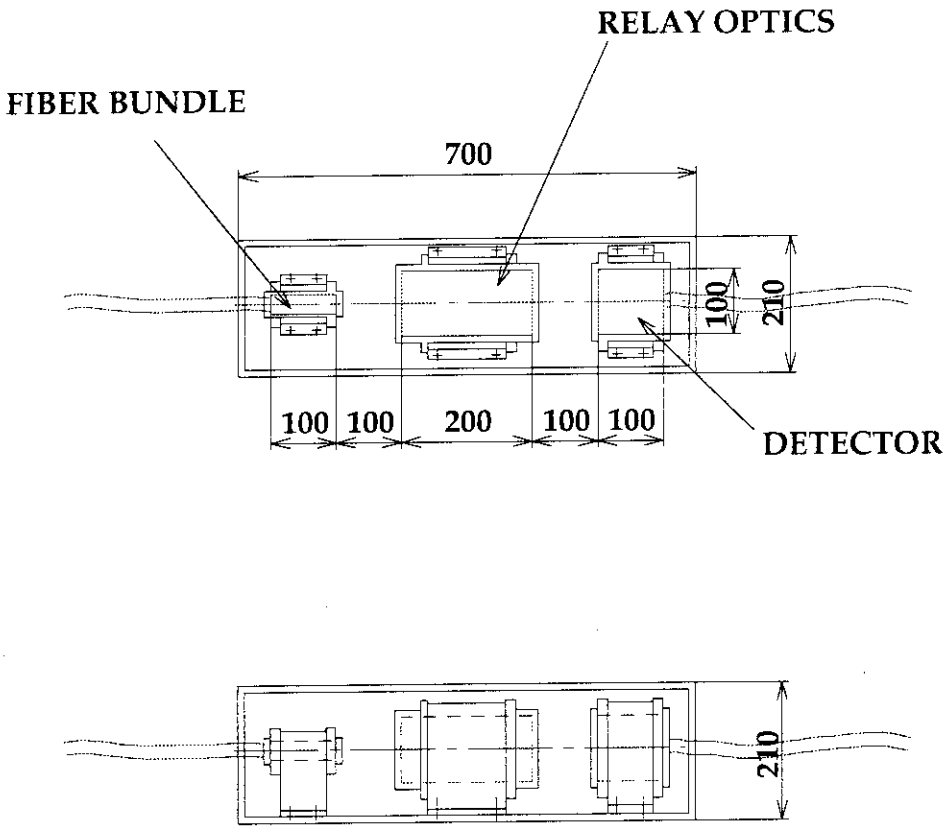

Fig4.3-15 Optical Arrangement of Detector System of Filter Spectrometer

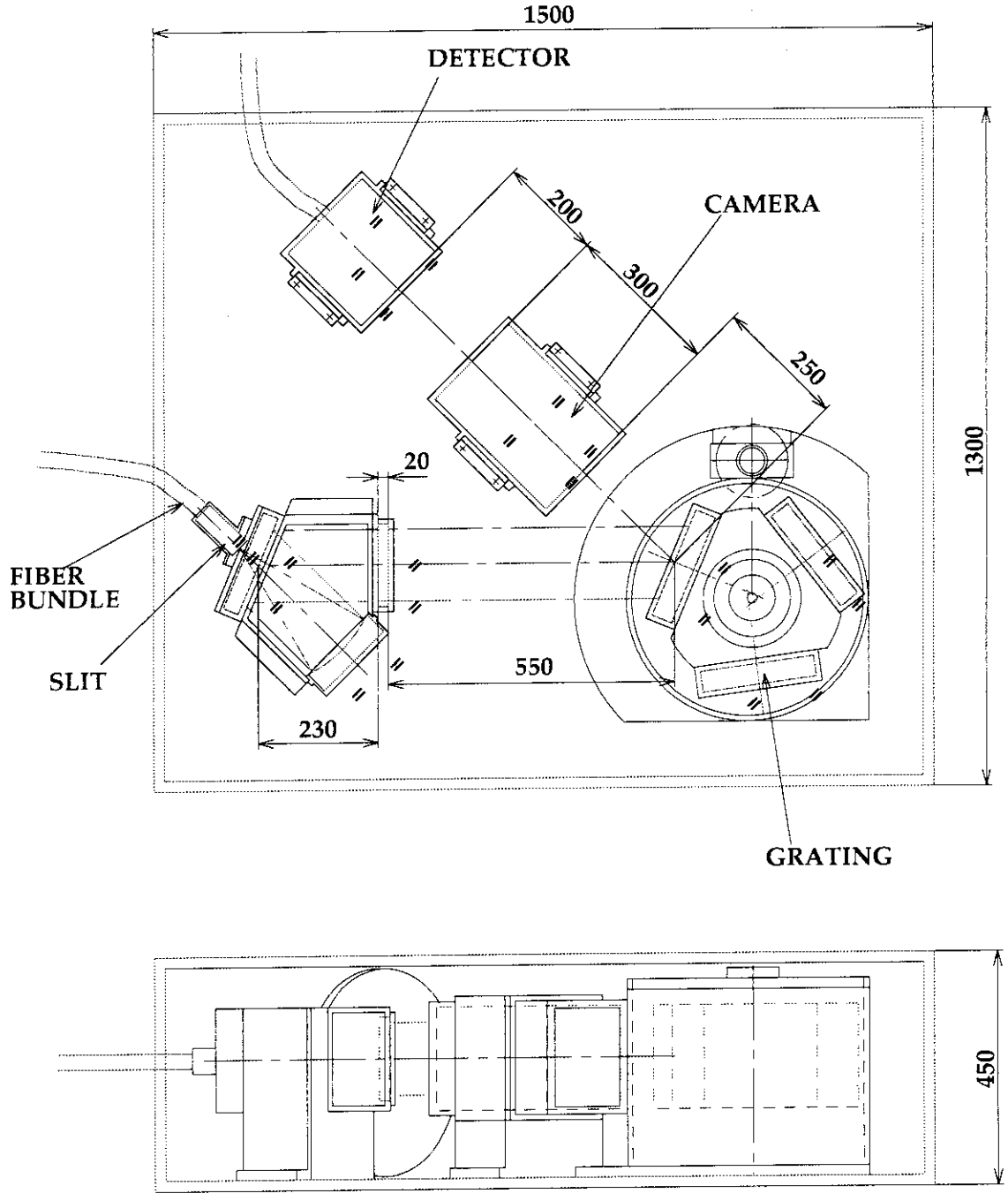

Fig.4.3-16 Optical Arrangement of Visible Survay Spectrometer

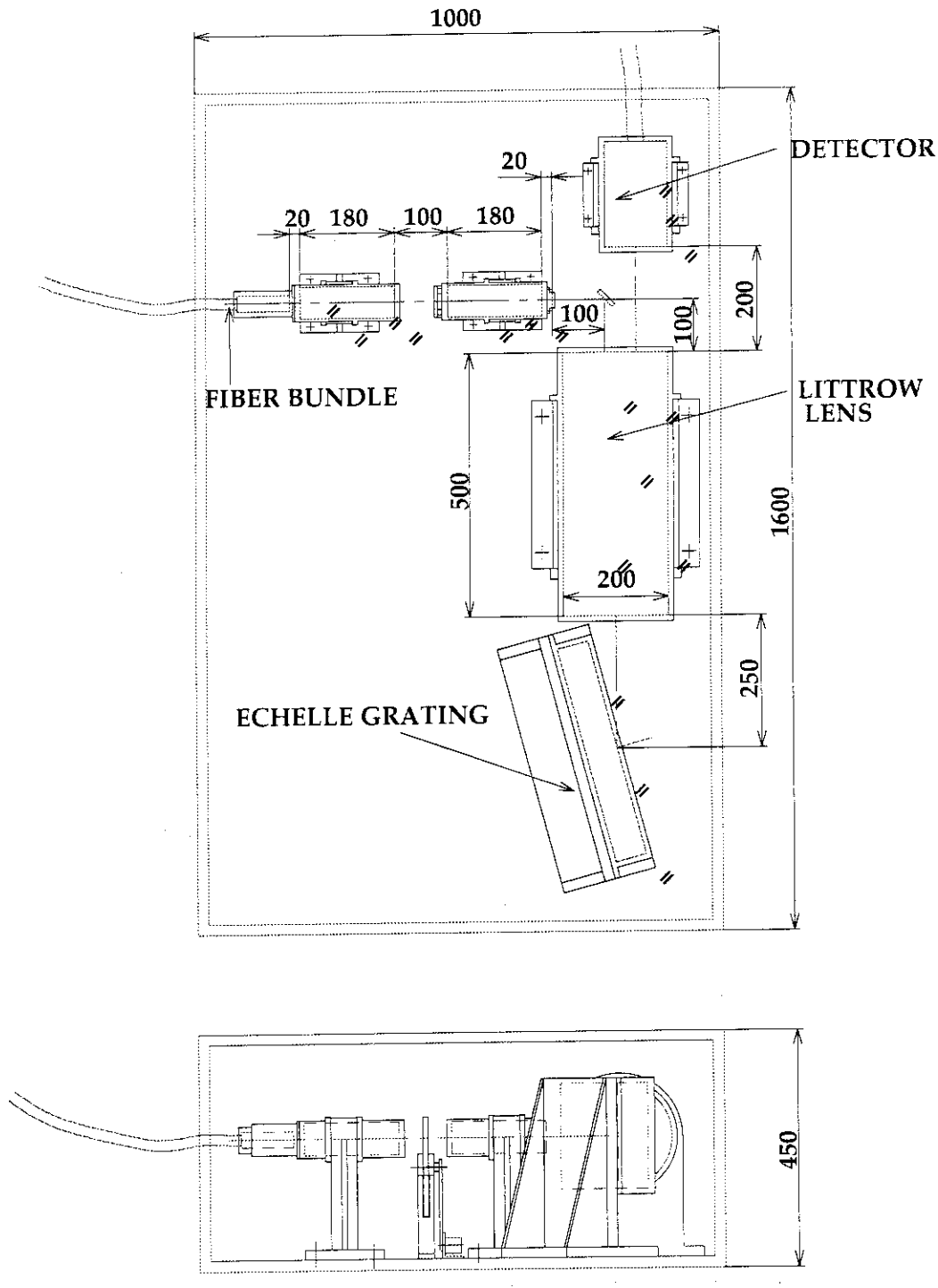

Fig.4..3-17 Optical Arrangement of High Dispersion Spectrometer

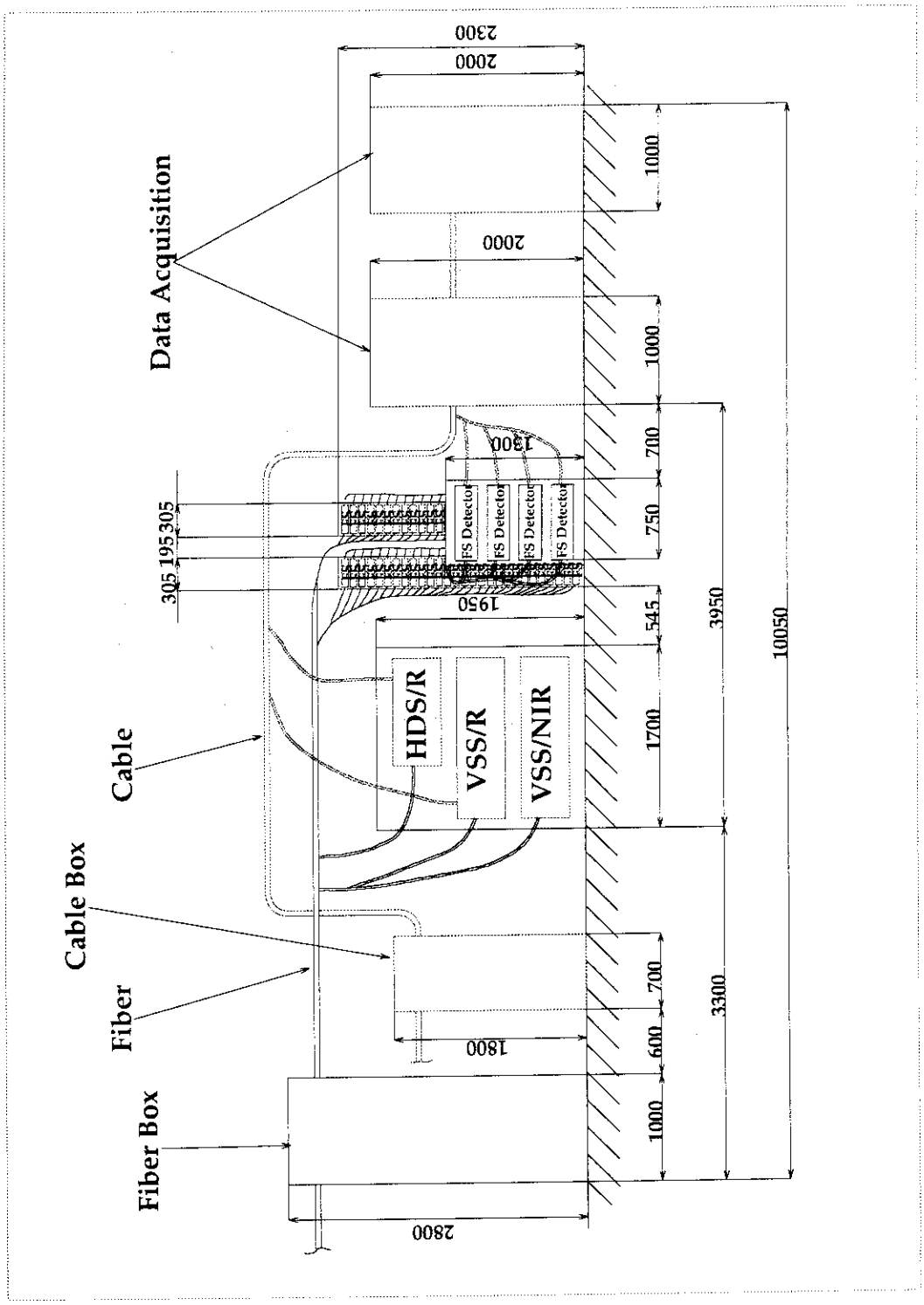

Fig.4.3-18 Side View of Optical Arrangement in Diagnostic Room

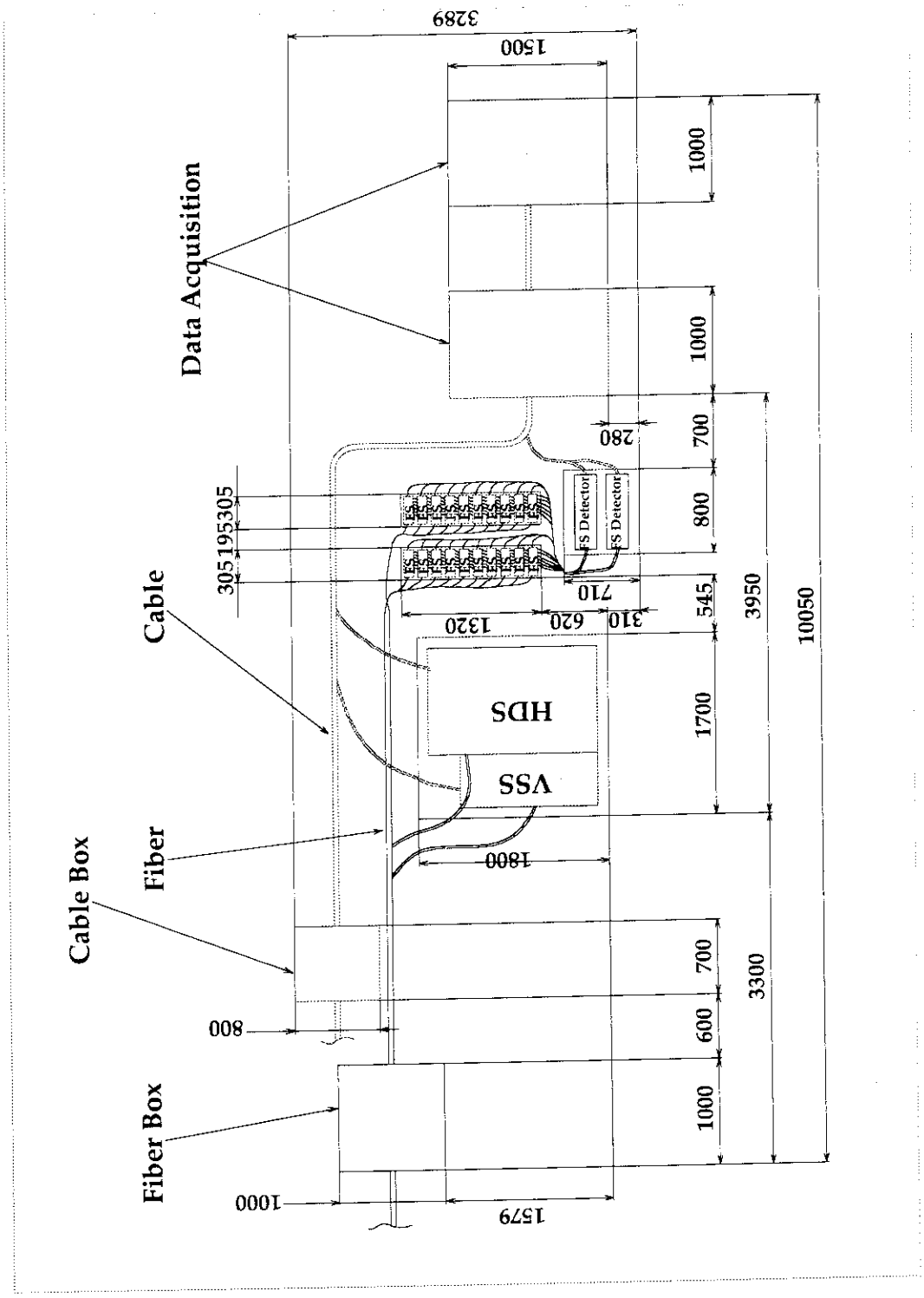

Fig.4.3-19 Top View of Optical Arrangement in Diagnostic Room

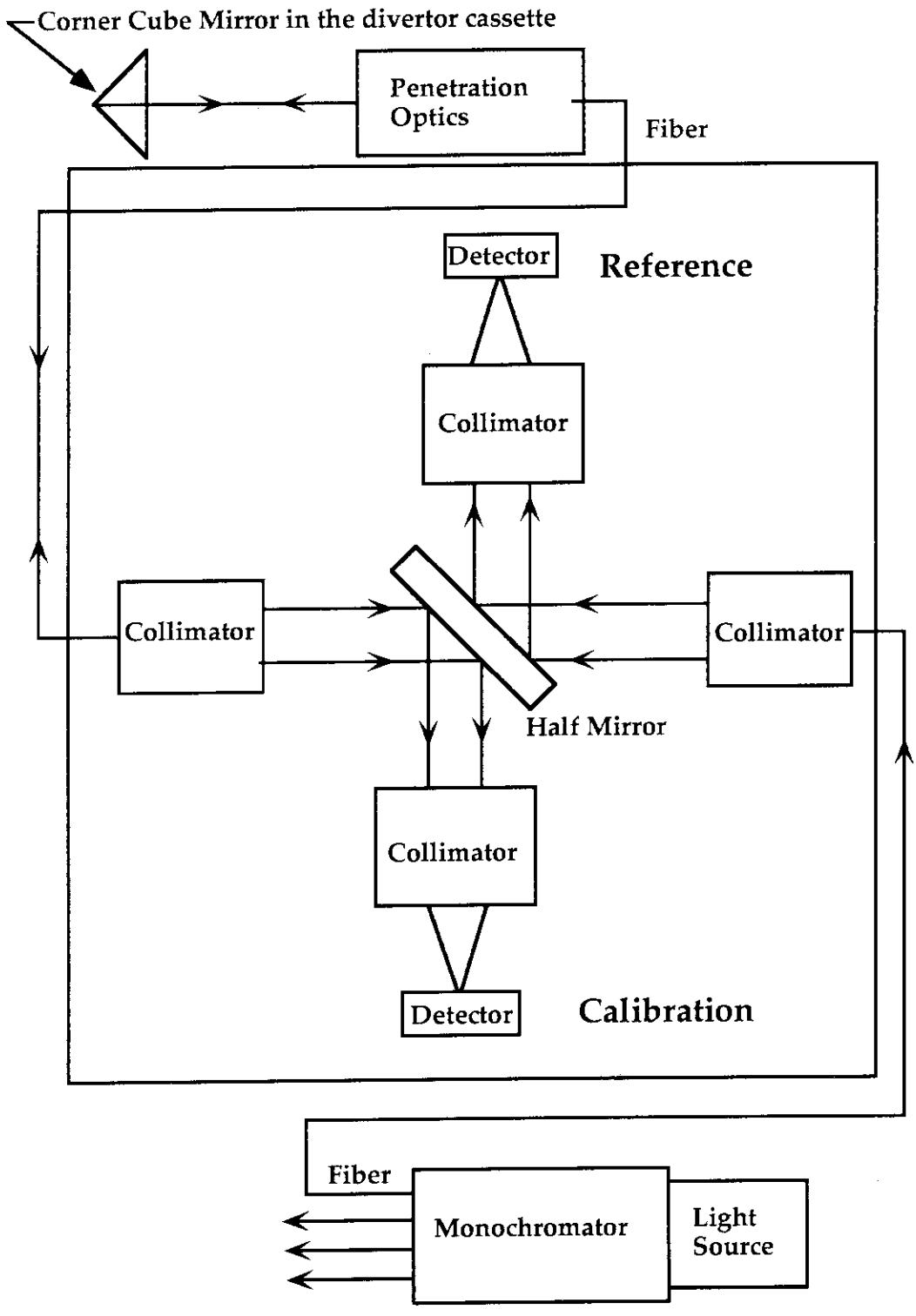

Fig. 4.4-1 Concept of Calibration System

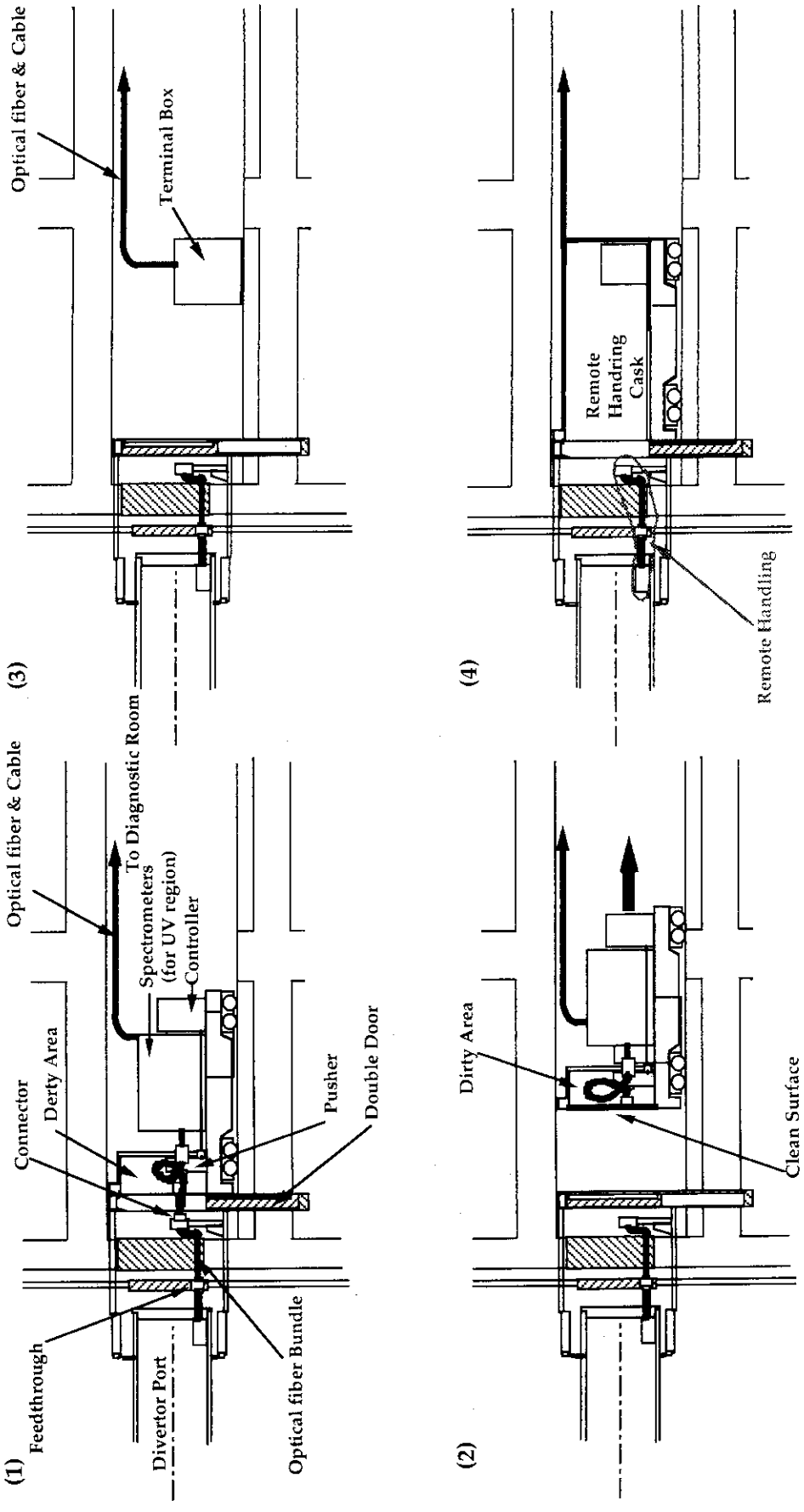

Fig.4.5-1 Concept of Remote Handling

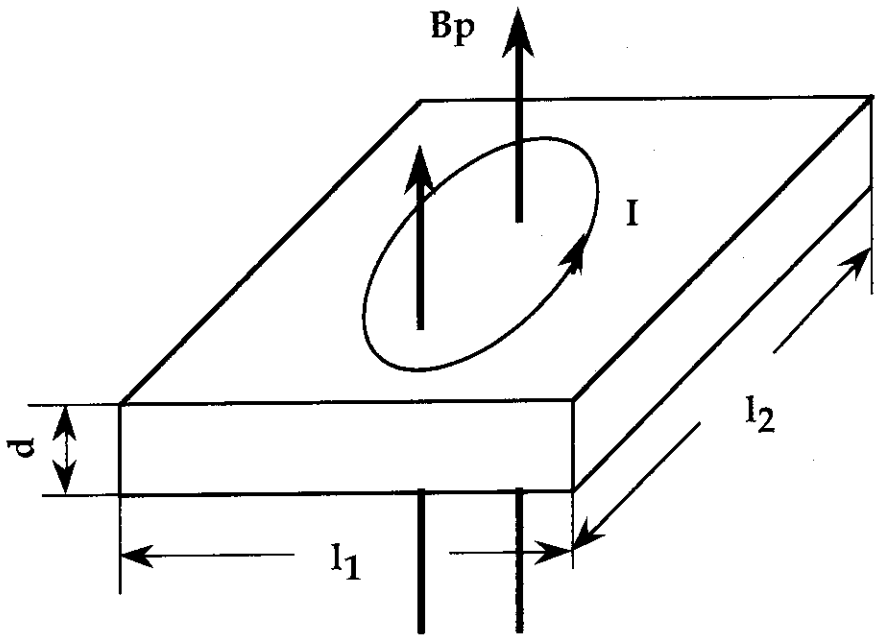

Fig. 4.6-1 Geometry of the Optical Base

5. Space requirement

The space requirement of this system is summarized as follows.

- In Diagnostic Divertor Cassette:
  (1) in Divertor Dome: 280 x 96 x 263 mm
  (2) in Bottom of Divertor: 593 x 230 x 170 mm
- In Diagnostic Port: 1500 x 1404 x 963 mm
- Cassegraine Optics: 2300 x 450 x 963 mm
- Pit Area:
  (1) on Transport Cask: 5300 x 2400 x 2600 mm
  (2) Wire Box: 700 x 900 x 1750 mm
  (3) Fiber Box: 900 x 1000 x 2950 mm
- In Diagnostic Room: 10050 x 3289 x 2800 mm

6. Necessary design work during EDA, and necessary R & D

From the design work here, we conclude that the following design works and R & D will be necessary during EDA.

< Necessary design work >

1) Exact calculation for the neutron and γ-ray shield
2) Detailed design for the optical and mechanical systems.
   - Calibration system
   - Adjustment system of optical axes
   - Heat transfer analysis
   - Nuclear heating analysis
   - Electromagnetic analysis
   - Distortion analysis
   - Interface with other systems
3) Evaluation of the degradation of the first mirror
4) Remote handling interface
5) Control and data acquisition equipment
6) Assembly process
7) Maintenance plan

< R & D items >

1) Window
2) Multi-channel fiber feed through
3) Multi-channel fiber connector
4) Large area 2-D detector

5. Space requirement

The space requirement of this system is summarized as follows.

- In Diagnostic Divertor Cassette:
  (1) in Divertor Dome: 280 x 96 x 263 mm
  (2) in Bottom of Divertor: 593 x 230 x 170 mm
- In Diagnostic Port: 1500 x 1404 x 963 mm
- Cassegraine Optics: 2300 x 450 x 963 mm
- Pit Area:
  (1) on Transport Cask: 5300 x 2400 x 2600 mm
  (2) Wire Box: 700 x 900 x 1750 mm
  (3) Fiber Box: 900 x 1000 x 2950 mm
- In Diagnostic Room: 10050 x 3289 x 2800 mm

6. Necessary design work during EDA, and necessary R & D

From the design work here, we conclude that the following design works and R & D will be necessary during EDA.

< Necessary design work >

1) Exact calculation for the neutron and γ-ray shield
2) Detailed design for the optical and mechanical systems.
   - Calibration system
   - Adjustment system of optical axes
   - Heat transfer analysis
   - Nuclear heating analysis
   - Electromagnetic analysis
   - Distortion analysis
   - Interface with other systems
3) Evaluation of the degradation of the first mirror
4) Remote handling interface
5) Control and data acquisition equipment
6) Assembly process
7) Maintenance plan

< R & D items >

1) Window
2) Multi-channel fiber feed through
3) Multi-channel fiber connector
4) Large area 2-D detector

7. Conclusion

The Divertor Impurity Monitoring System has been designed here in the wave length region of 200 - 1000 nm in accordance with the work order and the requirements of the design description document (DDD). The conceptual design, the optical design and the mechanical design of this system have been mainly carried out here. In addition, the measurable limit, the neutron and γ-ray irradiation effect on the optical fiber, the remote handling concept and the space requirement were considered preliminary. The necessary design works during EDA, and necessary R & D were also listed.

Main results are as follows.

1) System should be composed of three kind of spectrometers such as a visible survey spectrometer, a filter spectrometer and a high dispersion spectrometer.

2) Spectrometers should be located outside the cryostat from the magnetic shield point of view.
   - Spectrometers for the wavelength range of 200 - 500 nm should be sit on a transport cask in the pit.
   - Spectrometers for over 500 nm should be set in the diagnostic room from the accessibility and flexibility point of view.

3) In order to realize 2D measurements on the poloidal plane both in outer and inner divertor region, four viewing fans are proposed with mirror optics in the divertor cassette.

4) Optical fiber bundles are considered for the penetration optics from the divertor port to the spectrometers to evade the displacement of the optical axes due to the movement of the divertor port.

5) The ray trace analysis shows that the 3-mm spatial resolution in the all region of the divertor is difficult.

6) Spectrometers are designed preliminary.

7) It is difficult to measure deuterium influx lower than 10^{19} (at/$\cdot m^{-2} \cdot sec^{-1}$) in a high electron density region. More efficient optics will be necessary.

8) Neutron and γ-ray irradiation effect on the optical fiber is considered preliminary.

9) Mechanical designs have been carried out for the optical penetration system, spectrometers, remote handling concept and so on.

10) Space requirements are listed preliminary.

11) Necessary design works during EDA, and necessary R & D are listed.

Acknowledgment

This paper has been prepared as an account of work assigned to the Japanese Home Team under Task Agreement number S 91 TD21 95-01-20 FJ within the Agreement among the European Atomic Energy Community, the Government of Japan, the Government of the Russian Federation, and the Government of the United States of America on Cooperation in the Engineering Design Activities for the International Thermonuclear Experimental Reactor ("ITER EDA Agreement") under the auspices of the International Atomic Energy Agency (IAEA).

The authors are grateful to Drs. A. Costley, S. Yamamoto, L. de Kock, C. Walker, V. Mukhovatov, S. Mori, H. Nakamura and the members of ITER EDA Joint Central Team for their fruitful discussions and cooperations. We also greatly appreciate fruitful comments concerning the irradiation effect on the optical fiber by Dr. T. Kakuta. We would like to express our gratitude to Drs. T. Tsunematsu and S. Matsuda for thier continuous encouragement to this work.